3 00372

# Un Cúmulo Obscurecido de Galaxias en la Región del Gran Atractor



TESIS: Que para Obtener el Grado Académico de
MAESTRO EN CIENCIAS (ASTRONOMIA)
en el Instituto de Astronomía
Facultad de Ciencias
**Universidad Nacional Autónoma de México**
Presenta:



**Manuel Ochoa Silva**

Directores de Tesis: Dra. Renée C. Kraan-Korteweg y Dr. Heinz J. Andernach

*A mis padres*

# Índice General

# Sinopsis



El Gran Atractor (GA) es un exceso en densidad de masa dinámicamente importante, el cuál fue puesto en evidencia por el flujo sistemático a gran escala de galaxias en el Universo local. Las reconstrucciones teóricas del campo de densidad de masa, usando velocidades peculiares, predicen que el pico del GA se ubica detrás de la Vía Láctea, $(\ell, b, v) \sim (320°, 0°, 4000 \text{ km s}^{-1})$ (Kolatt et al. 1995). La naturaleza y extensión del GA han sido tema de mucho debate, en buena parte debido a que está obscurecido por la Vía Láctea. La mayor concentración de masa detectada en la región central del GA es el cúmulo de Norma (ACO 3627). Norma constituye aproximadamente el 10% de la masa predicha para el GA. ¿Es Norma el único cúmulo masivo detrás de la Galaxia en la región del GA? Hasta ahora, otros cúmulos masivos de galaxias no han sido identificados en la región central del GA y es posible que una gran parte de la masa del GA puede estar aún obscurecida por nuestra Galaxia.

Muchos cúmulos ricos de galaxias, como el cúmulo de Norma, son fuertes emisores de rayos X y exhiben emisión de radio que proviene de su galaxia central, como en el caso de la radio galaxia PKS 1610−608 en el cúmulo de Norma. El hecho de que la segunda fuente de radio más brillante del hemisferio sur ($f_{20cm} = 79$ Jy, McAdam 1991, y referencias en este trabajo), PKS 1343−601 con $(\ell, b, v, A_I) \sim (309.^\circ7, 1.^\circ8, 3872 \text{ km s}^{-1}, 4.5^{\text{m}})$ (West & Tarengi 1989, Woudt 1998, Kraan-Korteweg & Woudt 1999) se ubique cerca del centro del GA, sugiere que esta radio galaxia puede marcar el centro de otro cúmulo rico y masivo de galaxias en el GA.

En esta tesis, se analizan imágenes profundas en la banda $I$ de la vecindad de la radio galaxia PKS 1343−601. Un campo de $2^\circ \times 2^\circ$ alrededor de PKS 1343−601 fue observado con exposiciones de hasta 600 segundos con un "*seeing*" de $0.5''$. Una búsqueda mediante inspección visual meticulosa de galaxias detectó 49 candidatos en estas observaciones. En esta búsqueda se detectaron galaxias con niveles de extinción de $A_I = 5.^{\text{m}}5$ y con una distribución modulada por el gradiente de extinción en esta región. Por lo tanto, la concentración de galaxias alrededor PKS 1343−601 no era esperada y no es observada. Simulaciónes muestran cómo la distribución de las

galaxias del cúmulo de Coma, en la posición y con los mismos niveles de extinción en PKS 1343−601, es muy semejante a la distribución de galaxias encontradas en la vecindad de PKS 1343−601. De esta manera, la distribución de galaxias encontradas alrededor de PKS 1343−601 es consistente con la presencia de un cúmulo rico de galaxias como el cúmulo de Coma.

# Reconocimientos

Primeramente quiero agradecer a mis padres: su apoyo ha sido muy importante y fundamental para my carrera.

Es un gusto para mi agradecer el apoyo, motivación, y dirección que he recibido de mis dos directores de tesis: la Dra. Renée Kraan-Korteweg y el Dr. Heinz J. Andernach. No me es fácil expresar en palabras mi agradecimiento por dedicarme su tiempo y estar siempre disponibles cuando los necesité. Los resultados que se presentan en esta tesis no hubieran sido posible sin su dirección y contribución.

También quiero reconocer y agradecer a las siguientes personas:

P. Woudt por las imágenes en la banda-$I$ y su apoyo en la reducción de ellas.

A. Schröder por proporcionarme parte de sus resultados de DENIS antes de su publicación.

R. Coziol por su ayuda computacional durante mi tesis y consejos.

Yo hice uso de la base de datos CATS (Verkhodanov et al. 1997) de el *Special Astrophysical Observatory, Russia*. Además, también de la base de datos *NASA/IPAC Extragalactic Database*(NED) la cuál es operada por el *Jet Propulsion Laboratory, California Institute of Technology*, bajo contrato con la *National Aeronautics and Space Administration*.

Finalmente quiero agradecer a la UNAM y al posgrado en astronomía por su apoyo durante mis estudios y el trabajo de esta tesis.

# Capítulo 1

# Introducción

## 1.1 Preámbulo

Las galaxias estan distribuidas en el espacio de tal manera que forman estructuras a gran escala (EGE) como filamentos, grandes paredes, vacíos y cúmulos. Estas estructuras gigantescas son observadas en casi todo el cielo, excepto en un área muy específica que coincide con el disco de nuestra Galaxia. Por nuestra posición en la Vía Láctea, el disco Galáctico, donde el polvo se encuentra más concentrado, obscurece una parte del cielo en la cual aparentemente no existen galaxias dado que se observan muy pocas. La Vía Láctea obscurece aproximadamente hasta el 25% de la emisión óptica del cielo extragaláctico, creando así un área aparentemente vacía de galaxias conocida como la "Zona de Obscurecimiento" (ZOA[1]). Por tal motivo los mapas de distribución de galaxias se encuentran incompletos limitando así los estudios de formación de EGE y la dinámica del Universo cercano.

La distribución de la masa del Universo cercano dentro de una distancia de corrimiento al rojo de 6000 km $s^{-1}$ detrás de la ZOA es dinámicamente relevante por su contribución al movimiento gravitatorio del Grupo Local (GL) de galaxias. Interpolaciones basadas en POTENT (Dekel 1994; Kolatt, Dekel & Lahav 1995), ver Capítulo 2, muestran que la dirección del vector de velocidad peculiar del GL puede cambiar hasta 35° si se incluye la masa conocida dentro de $b \sim \pm 20°$ (Kolatt et al. 1995).

El estudio de las velocidades peculiares de galaxias en el Universo cercano[2] sugiere la existencia de una gran concentración de masa conocida como el Gran Atractor (GA)

[1] *Zone of Avoidance* (ZOA, por sus siglas en inglés)

[2] En terminos de corrimiento al rojo, el Universo cercano se toma hasta 10, 000 km $s^{-1}$, 150 Mpc (Fairall 1998).

que está oculta por la sección de la Vía Láctea que es vista desde el hemisferio sur. El GA parece ser responsable, en parte, del movimiento a gran escala del Universo cercano, incluyendo al Grupo Local (GL). La masa de las EGE ocultadas por la ZOA afectan la estimación de parámetros cosmológicos como el de la densidad ( $\Omega_o$) y del *bias* ($b$) El pico de densidad de masa del GA se sugiere que está en $\ell = 320°$, $b = 0°$, y a una velocidad radial de $cz = 4500$ km s$^{-1}$ (Burstein et al. 1990, Kolatt et al. 1995). Tal concentración de masa no ha sido observada completamente debido a que una gran parte de la región del GA se encuentra detrás del disco Galáctico.

Búsquedas profundas en el óptico dentro de la región del GA han descubierto que el cúmulo ACO 3627 es la concentración de galaxias más prominente conocida hasta hoy dia dentro del GA. ACO 3627 es un cúmulo rico de galaxias en la región central del GA. Se cree que la radio fuente PKS 1343−601 en $\ell = 309.^{\circ}7$ y $b = 1.^{\circ}8$, la más fuerte en radio en el hemisferio sur, posiblemente marca el centro de otro cúmulo rico de galaxias en la región del GA. Por lo tanto, el propósito científico de este proyecto es investigar si tal cúmulo rico de galaxias existe o no.

## 1.2 Estructuras a Gran Escala y la ZOA: una perspectiva histórica

La presencia de la Zona de Obscurecimiento (ZOA) fue notada por primera vez por Proctor (1878) como la "Zona de muy pocas nebulosas". En una distribución de nebulosas basada en los datos del "Catálogo General de Nebulosas"del John Herschel (1864), Proctor observó una banda libre de nebulosas. Este catálogo de nebulosas fue publicado en 1864 e incluía todas las 4,630 nebulosas conocidas en aquella época. Más adelante, John Herschel reconoció por primera vez el Supercúmulo Local (SCL), al cual describió como un sistema aproximadamente esférico centrado en Virgo. El también notó que nuestro sistema estelar, la Galaxia, se encuentra lejos de la parte más densa de este sistema. Su descripción del SCL concuerda sorprendentemente con las observaciones de hoy en dia. Herschel llegó a este descubrimiento simplemente contando nebulosas en el cielo. Los primeros diagramas de la distribución de nebulosas en el cielo fueron hechos por Proctor y basados en los datos del "Catalogo General"de Herschel. La Figura 1.1 de esta tesis muestra uno de los diagramas de Proctor.

En aquel tiempo la naturaleza de las nebulosas era desconocida y fue tema de debate por mucho tiempo. Fue hasta la década de los años veinte del siglo pasado cuando se comprobó la teoría de los "Universos Islas"del filósofo Emmanuel Kant

con las observaciones de Edwin Hubble. Usando el telescopio más poderoso de aquel tiempo, el reflector Hocker de 100 pulgadas de Mount Wilson en California y las variables Cefeidas, Hubble comprobó la naturaleza extragaláctica de la nebulosa espiral de Andromeda. Hubble abrió el estudio de las EGE en el Universo con un muestreo de 44,000 galaxias. Este muestreo reveló más claramente la existencia de la "Zona de Obscurecimiento", asi como la exitencia de grupos y cúmulos de galaxias. Posteriormente, el muestreo *National Geographic Palomar Observatory Sky Survey* (POSS) de la década de los años cincuenta del siglo pasado reveló la existencia de miles de cúmulos ricos de galaxias. En 1958, George Abell publicó un catálogo de cúmulos ricos de galaxias basado en las placas fotográficas del POSS.

## 1.3 La Distribución de Galaxias en Mapas de Todo el Cielo

Un catálogo de "todo" el cielo se puede construir usando los siguientes tres catálogos de galaxias existentes: el *Uppsala General Catalogue* (UGC) para la parte norte que cubre $\delta \geq -2.^\circ5$ (Nilson 1973), el *ESO Uppsala Catalogue* para el sur $\delta \leq -17^\circ$ (Lauberts 1982), y el *Morphological Catalogue of Galaxies* (MCG) para la región $-17.^\circ5 < \delta < -2.^\circ5$ (Vorontsov-Velyaminov & Archipova 1963-74). El conjunto de datos de estos tres catálogos puede ser homogenizado aplicando los ajustes de diámetros de galaxias propuestos por Lahav: $D = 1.15D_{UGC}$, $D = 0.96D_{ESO}$, y $D = 1.29D_{MCG}$ (Lahav 1987). De esta manera se tiene un catálogo de todo el cielo completo para galaxias con diámetros más grandes que $D = 1.'3$ (Hudson & Lynden-Bell 1991). La distribución de galaxias como producto de la unión de estos tres catálogos es mostrada en la Fig. 1.2 de esta tesis en coordenadas Galácticas.

En la distribución prensentada en la Fig. 1.2 se pueden observar varias estructuras a gran escala. El supercúmulo local se observa como un gran círculo, el Plano Supergaláctico. La Pared de Centauro se ve como una estructura continua que cruza la Galaxia en dirección de la posición sugerida para el Gran Atractor, $\ell = 320^\circ$ and $b = 0^\circ$ (Kolatt et al. 1995). El cúmulo de Pavo $(332^\circ, -24^\circ)$, Centauro $(302^\circ, 22^\circ)$, e Hydra $(270^\circ, 27^\circ)$ se ven como parte de la Pared de Centauro. Otra estructura a gran escala que se puede reconocer es la cadena Perseo-Piscis curveándose hacia la ZOA entre $\ell = 95^\circ$ y $\ell = 165^\circ$. Otros cúmulos visibles son los de Antlia $(273^\circ, 19^\circ)$, Indus y Fornax. En la Fig. 1.2, la ZOA aparece como una banda vacia de galaxias de aproximadamente $20^\circ$ de ancho en medio de la distribución

En la década pasada se han conducido varios muestreos sistemáticos de galaxias en el óptico, cercano infrarrojo, infrarrojo, HI y rayos X para reducir el ancho de la ZOA. A pesar de ser fuertemente afectadas por la extinción, las búsquedas en el óptico han resultado ser más eficientes para revelar la existencia de cúmulos ricos en galaxias E y S0. Una búsqueda profunda en el óptico descubrió que el cúmulo ACO 3627 (el cúmulo de Norma) en $\ell = 325.^{\circ}3$, $b = -7.^{\circ}2$ y $v = 4844$ km s$^{-1}$ es un cúmulo rico de galaxias muy obscurecido por la Vía Láctea (Kraan-Korteweg et al. 1996; Woudt et al. 2000a; 2000b). El cúmulo de Norma es la concentración más prominente de galaxias conocida dentro del Gran Atractor.

La existencia de otros cúmulos ricos de galaxias en el GA es altamente probable ya que ACO 3627 contiene sólo una pequeña fracción de la masa sugerida para el GA. Por ejemplo, la radio fuente PKS 1343−601 es uno de los emisores más fuertes en radio del hemisferio sur. Esta radio fuente se encuentra dentro de la región central del GA. Su posición es: $\ell = 309.^{\circ}7$ y $b = 1.^{\circ}8$ con $v = 3800$ km s$^{-1}$. Sabiendo que esta radio fuente tiene una extinción de $A_B = 12^{\rm m}$ en el óptico y que la radio galaxia central de un cúmulo rico de galaxias es frecuentemente un emisor fuerte de radio, PKS 1343−601 podría ser el centro de otro cúmulo rico de galaxias en la región del GA. La motivación científica de esta tesis es comprobar la existencia de tal cúmulo rico de galaxias.

## 1.4 Bosquejo de esta Tesis

Esta tesis es presentada en 6 capítulos. Una perspectiva histórica como introducción a las EGE conocidas en el Universo cercano es presentada en el Capítulo 1. El segundo capítulo cubre en detalle las búsquedas profundas de galaxias en la "Zona de Vacio" (ZOA), particularmente en el óptico. El proceso de reducción de 128 imágenes que corresponden a 16 campos en la banda $I$ del "WFI"es descrito en el Capítulo 3. El resultado de una búsqueda meticulosa de candidatos a galaxias en las 128 imágenes en la banda $I$ es mostrado en el Capítulo 4. El análisis de la distribución de los candidatos a galaxias encontrados es presentado en el Capítulo 5. Finalmente, el Capítulo 6 es dedicado a las conclusiones y al trabajo futuro.

# Capítulo 2

# Búsquedas Profundas y Acumulación de Galaxias detrás de la ZOA

## 2.1 Introducción

Las estrellas y el polvo de la Vía Láctea nos impiden ver aproximadamente el 25% del cielo extragaláctico en el óptico y 10% del cielo extragaláctico visto por el satélite IRAS creando así una "Zona de Obscurecimiento" en los mapas de distribución de galaxias detectadas en el óptico e infrarrojo. Harlow Shapley propuso definir la ZOA como la región delimitada por "el *isopleth* de cinco galaxias por grado cuadrado de los muestreos de los observatorios Lick y Harvard" (Shapley 1961). En estos dos muestreos, una tasa promedio de 54 galaxias por grado cuadrado se obtuvo para regiones del cielo fuera del plano Galáctico (Shane & Wirtanen 1967). Por el poco número de galaxias encontrado en la ZOA, astrónomos interesados en estudios extragalácticos evitaban observar esta región del cielo. Sin embargo, ahora es necesario conocer las estructuras a gran escala que están detrás del disco Galáctico para estudios dinámicos del Universo, por ejemplo para la determinación de ciertos parámetros cosmológicos, como $\Omega_o$, y para saber el origen del dipolo de radiación cósmica de fondo. Por lo tanto, la ZOA ha sido explorada en varias longitudes de onda por diversos grupos de astrónomos interesados en revelar la EGE que existe detrás de la Zona de Obscurecimiento. Este capítulo da una visión en general de los resultados de los muestreos ópticos más recientes realizados para revelar la EGE que existe detrás de la ZOA.

## 2.2 Búsquedas Profundas de Galaxias en el Optico detrás de la ZOA

Varios grupos de astrónomos han conducido búsquedas sistemáticas profundas en el óptico para descubrir galaxias obscurecidas en los muestreos del *Palomar Observatory Sky Surveys* (POSS I y POSS II) en el norte y en el *ESO-SRC (UK Science Research Council) Southern Sky Atlas.* Miles de galaxias parcialmente obscurecidas con diámetros D$\geq$ 0$'$.1 han sido detectadas en estas búsquedas. La búsqueda de galaxias débiles y con diámetros pequeños se suele hacer a ojo. Dada la cantidad de estrellas presentes del disco Galáctico, la búsqueda a ojo a latitudes $|b| \leq 15°$ es mucho más efectiva que la extracción de galaxias vía procesos automatizados como COSMOS[1] (Drinkwater et al. 1995), APM[2] (Lewis et al. 1996) o la aplicación de *Artificial Neural Networks* (ANN).

A partir de búsquedas profundas en el óptico de galaxias han encontrado más de 50,000 galaxias nuevas en la ZOA. La Figura 2.1 de esta tesis muestra los diferentes muestreos conducidos en la ZOA (Kraan-Korteweg 2000b). Para detalles y resultados de estas búsquedas consultar Kraan-Korteweg (2000b). Estas búsquedas sistemáticas en el óptico cubren toda la Zona de Obscurecimiento definida como el área del cielo delimitada por el contorno de extinción de frente de $A_B = 1\overset{m}{.}0$ dado por los mapas de extición de DIRBE (Schlegel et al 1998), ver Capítulo 2. La Fig. 2.2 es un ejemplo de estas búsquedas sistemáticas de galaxias en el óptico, y muestra la región $D_1$-$D_5$ donde se cree que está ubicada la región central del GA. Los puntos pequeños representan nuevas galaxias, mientras que los puntos más grandes corresponden a galaxias previamente conocidas. Los tres contornos corresponden a los niveles de extinción de $A_B$ =$1\overset{m}{.}0$, $3\overset{m}{.}0$ y $5\overset{m}{.}0$ de acuerdo con los mapas de DIRBE (Schlegel et al. 1998).

La extinción hace que las galaxias aparezcan más débiles y pequeñas. La reducción de diámetros de galaxias por extinción fue investigada por Cameron (1990). El obtuvo una relación entre la reducción del diámetro como función de la extinción en la banda B (óptico), $A_B$:

$f(\text{Diam}) = 10^{0.10A_B^{1.7}}$ para galaxias espirales
$f(\text{Diam}) = 10^{0.13A_B^{1.3}}$ para galaxias elípticas y S0

[1] COSMOS (por sus siglas en inglés; COordinates, Sizes, Magnitudes, Orientations, and Shapes) es una maquina para escanear placas fotográficas.

[2] *Automated Plate Measuring Machine* (APM, por sus siglas en inglés).

Aqui $f$(Diam) es la proporción por la cual los diámetros son reducidos en función de la extinción. Aplicando estas correcciones a galaxias obscurecidas se obtiene que las búsquedas profundas en el óptico son completas para galaxias con diámetros intrínsecos D° $\geq$ 1.'0 con niveles de extinción $A_B \leq 3.^{\rm m}0$.

Los resultados de las búsquedas profundas en el óptico complementan los tres catálogos UGC, ESO-Uppsala, y MCG para tener un catálogo de "todo" el cielo con una ZOA reducida. Así se obtiene un catálogo completo para galaxias con diámetros corregidos por extinción de D° = 1.'3 para niveles de extinción $A_B \leq 3.^{\rm m}0$. Una proyección Aitoff[3] de todo el cielo mejorada con una ZOA reducida es mostrada en la Fig. 2.3 de esta tesis, para más detalles leer la versión en inglés de esta tesis.

## 2.3 Acumulación de Galaxias dentro del GA

La naturaleza y la extensión de la sobredensidad de masa, la cual ha sido denominada como el Gran Atractor (GA) por Alan Dressler, ha sido bastante controversial debido a su ubicación detrás del Plano Galáctico (PG). Lynden-Bell et al. (1988) descubrieron una sobredensidad de masa enorme en el Universo cercano aplicando la relación Faber-Jackson[4] a cerca de 400 galaxias elípticas distribuidas sobre todo el cielo. Basados en este estudio, ellos concluyeron que una enorme concentración de masa en $(\ell, b) \sim (307°, 9°)$ y a una distancia de 4,500 km s$^{-1}$ es la causa del movimiento peculiar del Grupo Local (GL) de galaxias, es decir del flujo cósmico del Universo local. Ellos propusieron un modelo para esta enorme concentración de masa (GA) que explicaría el origen del flujo cósmico observado (Dressler 1991) con las siguientes predicciones:

1. La existencia de una gran sobredensidad de masa.
2. Su centro en el espacio de corrimientos al rojo debe ubicarse a 4,000 km s$^{-1}$.
3. Las velocidades peculiares deben declinar al aproximarse a su centro e invertirse una vez atravesado.

Estas tres predicciones han sido parcialmente confirmadas (Dressler y Faber 1990a,b; Dressler 1991). Si la luz traza la materia, una gran concentración de masa debería haber sido observada en la dirección del GA, pero no ha sido así.

[3]Es una proyección de todo el cielo en una elipse, de áreas iguales, creada por David Aitoff en 1889.

[4]La correlación entre la luminosidad de una galaxia elíptica y su dispersión de velocidades de las estrellas en su región central.

La confirmación de la existencia del GA tiene importantes implicaciones cosmológicas, por ejemplo, para el modelo de "materia obscura fría" (CDM, por sus siglas en inglés). Una concentración de masa como el GA es excesivamente rara o ausente en el marco del modelo de CDM. La masa estimada para el GA es del orden de $\sim$ 5.4 x $10^{16}$ masas solares (Lynden-Bell et al. 1988).

Los métodos matemáticos han sido usados como una alternativa estadística para reconstruir la distribución de galaxias obscurecidas por la Vía Láctea. Uno de estos métodos es POTENT, el cual reconstruye el campo del potencial a partir de las velocidades peculiares de galaxias disponibles en una región (Bertschinger y Dekel 1989). Kolatt et al. (1995) usaron velocidades peculiares de galaxias en ambos lados de la ZOA para trazar la disribución de masa detrás de esta región. Los contornos de fluctuaciones de densidad de masa para "todo" el cielo hasta 4,000 km $s^{-1}$ obtenidos por POTENT son mostrados en la Fig. 2.4 de esta tesis. El análisis de los resultados de POTENT indica que el pico del GA está en $(\ell, b)) \sim (320°, 0°)$ a una "distancia" de 4,000 km $s^{-1}$. La Fig. 2.5 muestra el campo de velocidades y de fluctuaciones de densidad de masa obtenidos con POTENT, usando las velocidades de aproximadamente 3,000 galaxias (Dekel 1994, 1995). En ambos diagramas las principales estructuras del Universo local son visibles y el GA aparece en el lado izquierdo.

## 2.4 ACO 3627: El Cúmulo de Norma

ACO 3627 es un cúmulo de galaxias que se encuentra dentro de la región del Gran Atractor y es más masivo y conocido hasta hoy dia dentro de la región central del GA (Kraan-Korteweg et al. 1996 y Woudt 1998). ACO 3627 es conocido también como el cúmulo de Norma por estar en la constelación de Norma. ACO 3627 tiene las coordenadas Galácticas $(\ell, b) = (325.^{\circ}3, -7.^{\circ}2)$, a sólo 9° de la posición sugerida para el centro del GA; este cúmulo tiene una velocidad de recesión de 4,882 km $s^{-1}$ (Kraan-Korteweg et al. 1996) situándolo a la distancia del GA. Tiene una dispersión de velocidades de 897 km $s^{-1}$, lo cual implica que es muy masivo. Una masa de aproximadamente 5.1 x $10^{15} h_{50}^{-1} M_{\odot}$ se ha determinado para este cúmulo. Esta masa constituye sólo el 10% de la masa sugerida para el GA, la cual es del orden de $\sim 10^{16}$ masas solares. Los cúmulos ricos de galaxias en general son fuertes emisores en rayos X y de radio; además suelen presentar galaxias tipo cD en sus centros. Norma al igual que Coma está dominado por dos galaxias cD centrales que son fuertes emisores de radio.

## 2.5 Un Cúmulo de Galaxias Cercano, no Catalogado

Los mapas de flujo de velocidades y de fluctuaciones de densidad de masa, como los mostrados en Fig. 2.4 y 2.5, nos indican que el GA es una concentración muy grande y extendida de materia, pero hasta ahora se ha detectado solamente un cúmulo rico de galaxias (ACO 3627) en esta región, con una masa del 10% de la sugerida para el GA. Por lo tanto, es muy posible que existan otros cúmulos ricos de galaxias dentro de la región del GA, los cuales están muy probablemente obscurecidos por la Vía Láctea.

Es posible que la segunda fuente extragaláctica de radio más brillante del hemisferio sur, PKS 1343−601, $f_{20cm} = 79$ Jy (ver McAdam 1991), sea el centro de otro cúmulo rico de galaxias. Dado que esta radio galaxia se encuentra detrás del disco Galáctico, $(\ell, b, v) \sim (309.^{\circ}7, 1.^{\circ}8, 3872$ km s$^{-1})$, está muy obscurecida con 12 magnitudes de extinción en la banda B. La contraparte óptica de PKS 1343−601 es una radio galaxia gigante con una velocidad de recesión de $cz = 3{,}872$ km s$^{-1}$ (West & Tarenghi 1989). Esta radio galaxia también exhibe gran emisión de rayos X (McAdam 1991, Tashiro et al. 1998).

La extinción es tan severa en la dirección de PKS 1343−601 que las galaxias más brillantes de un supuesto cúmulo rico no serían visibles. La Fig. 2.6 muestra un cúmulo rico de galaxias (A3627) y el probable cúmulo centrado en PKS 1343−601, los dos se encuentran dentro de la región del GA. Esta figura muestra en el lado izquierdo la distribución casi simétrica de las galaxias del cúmulo de Norma (Woudt & Kraan-Korteweg 2001), mientras que en el lado derecho presenta el probable cúmulo exhibiendo un gradiente en la distribución de galaxias. A mayor extinción, menos galaxias son visibles. Observaciones en longitudes de onda donde la extinción es menos severa son necesarias para determinar si PKS 1343−601 marca la posición de un cúmulo no conocido y rico en galaxias. Para comprobar esto, la vecindad de PKS 1343−601 fue observada en la banda $I$ con la cámara *Wide Field Imager* (WFI) y el telescopio de 2.2-m de MPG-ESO del Observatorio de La Silla, Chile.

# Capítulo 3

# Las Observaciones y su Reducción

## 3.1 Introducción

En este capítulo se describen las observaciones y la reducción de los datos, los cuales consisten de imágenes de un área de aproximadamente 2°x 2° centrada en PKS 1343−601 ( $\ell = 309.^{\circ}7$, $b = 1.^{\circ}8$). Las imágenes fueron tomadas con la cámara *Wide Field Imager* en el telescopio de 2.2-m de MPG-ESO en La Silla, Chile. Un total de 16 campos fueron cubiertos con el WFI tomando 128 imágenes en la banda *I*. Estas imágenes fueron reducidas usando NOAO PC-IRAF[1] y la herramienta para desplegar imágenes DS9. También se utilizó el *Guide Star Catalog (GSC 1.2)* y el *Digital Sky Survey (ESO-DSS2i)* para la calibración de pixeles en coordenadas ecuatoriales.

## 3.2 Observatorio, Instrumentos y Observaciones

Las observaciones para esta tesis fueron hechas con la cámara WFI en el telescopio 2.2-m de Max Planck Gesellschaft (MPG) en el Observatorio de La Silla del ESO[2]. El observatorio de La Silla se encuentra en la parte sur del desierto de Atacama en Chile y su ubicación geográfica es $70^{\circ}44'4.''543$ al Oeste, $29^{\circ}15'15.''433$ al Sur y una altura de 2,335 metros. Las observaciones fueron hechas durante las noches de Mayo 19-21 de 1999 por el Dr. Patrick Alan Woudt.

La cámara WFI tiene un campo de observación de casi 0.8 grados, y el detector del WFI consiste de un arreglo de 4 x 2 CCD que cubren un área del cielo de $34'$ x $33'$.

[1]Image Reduction and Analysis Facility (IRAF)

[2]European Southern Observatory (ESO, por sus siglas en inglés).

Con esta cámara se tomaron 16 campos que cubren un área de 2°x 2° centrada en PKS 1343−601. La Fig. 3.1 muestra la distribución de los 16 campos y el arreglo de los 8 detectores CCD se muestra en la Fig. 3.2. Cada CCD consiste de 2k x 4k pixeles. Las observaciones se adquirieron utilizando el filtro n816 ($\lambda_c = 815.9$ nm).

## 3.3 El Proceso de Reducción de las Observaciones

### 3.3.1 Las Observaciones y su Reducción

Los datos para esta tesis consisten de la siguientes imágenes: Seis campos planos (*skyflats*) y 16 exposiciones como se muestran en la Fig. 3.1. El campo central (número uno) que incluye a PKS 1343−601 consiste de cinco superposiciones. La Fig. 3.3 muestra los tiempos de exposición y los *offsets* para el campo central. De esta manera, el campo central tiene mayor profundidad para detectar una mayor concentración de galaxias hacia PKS1343−601, si es que marca el centro de un cúmulo rico de galaxias. Cada campo de observación consiste de 8 imágenes, por lo tanto se obtuvieron un total de 48 campos planos y 160 imágenes.

### 3.3.2 Reducción de los Campos Planos

Los "campos planos" son usados para normalizar las imágenes tomadas con detectores CCD. Cada pixel de un CCD tiene diferente respuesta cuántica a la luz; 48 campos planos fueron reducidos y combinados para obtener un grupo final de 8 campos planos, uno para cada CDD del WFI. La reducción de los campos planos fue la siguiente: primeramente se determinó la sección no expuesta del CCD, la Fig. 3.4 muestra un campo plano y una amplificación de una esquina que muestra la sección no expuesta. Para cada CCD se seleccionó una sección no expuesta para determinar un promedio del número de cuentas por pixel que se acumulan en él durante el tiempo sin estar expuesto, lo cual se conoce como *overscan*. Para los CCDs 1, 2, 3 y 4, se tomó la sección [2121:2140, 31:3500], vea Fig. 3.2. La sección [2:22, 629:4098] se usó para los CCDs 5, 6 y 7, mientras que la sección [2121:2140, 629:4098] fue usada para el CCD 8; estas secciones fueron determinadas con la ayuda de *implot* de IRAF y sus comandos. Se utilizó también *colbias* de IRAF para calcular y sustraer el *overscan* y después cortar las secciones no expuestas de cada CCD. Los campos planos fueron combinados con *flatcombine* de IRAF, obteniendo así un campo plano más uniforme. Finalmente fueron normalizados con *imarith* e *imstatistics* de IRAF obteniendo así

8 campos planos normalizados. Estos campos planos fueron usados para aplanar (*flatfielding*) las imágenes.

### 3.3.3 Proceso de Reducción de Imágenes

Con la cámara WFI se tomaron 16 campos que dan un total de 160 imágenes, de las cuales 32 imágenes se obtuvieron con las cinco exposiciones del campo central (campo uno, vea Fig. 3.1). El resto de las 128 imágenes corresponden a los otros 15 campos (campo 2 al 16), 8 para cada uno de ellos. A todas las imágenes se les substrajo el "bias" y se les cortaron las áreas no expuestas con *colbias* de IRAF usando las secciones determianadas para los campos planos. El siguiente paso fue normalizarlas usando los 8 campos planos. Para el campo central (campo uno), se combinaron las 32 imágenes de cinco exposiciones para quedar solo 8. Para combinar estas imágenes se utilizó *imalign* de IRAF para calcular los *offsets* y finalmente *imcombine* de IRAF para combinarlas. El siguiente paso fue calibrar pixeles en coordenadas ecuatoriales.

## 3.4 La Búsqueda de Galaxias

Una vez terminado el proceso de reducción de imágenes, se empezó una búsqueda a ojo de galaxias. Dado que se observó a través del disco Galáctico, la búsqueda de galaxias a ojo es la más efectiva puesto que las imágenes están saturadas de estrellas. La Fig. 3.7 muestra una imagen la cual contiene cientos o miles de estrellas. Para la búsqueda de galaxias se utilizó SAOImage DS9 para desplegar las imágenes e *imexamine* de IRAF para inspeccionar los posibles candidatos a galaxias. SAOImage DS9 nos permite agrandar y variar el constraste de imágenes, mientras que con *imexamine* se puede inspeccionar la distribución de luz de objectos. La mayoría de las galaxias aparecen pequeñas y débiles (borrosas) en comparación a las estrellas más brillantes, de aquí que resulta útil agrandar las imágenes para su detección. En la Fig. 3.5 se muestra la misma imagen dos veces con diferente contraste. En la imagen de la derecha aparece una mancha angosta y alargada, mientras que en la imagen de la izquierda no se observa. La imagen de la derecha muestra objetos de menor brillo superficial permitiendo así observar la presencia de una mancha angosta y alargada con un poco más de brillo superficial que sus alrededores, posiblemente es una galaxia espiral vista de canto.

## 3.5 Calibración de Pixeles en Coordenadas Ecuatoriales

Las imágenes en las cuales se detectaron candidatos a galaxias se calibraron en coordenadas ecuatoriales. Para la calibración de sus posiciones en pixeles a posiciones en RA y Dec, primero se determinaron los centros para cada una de las 8 imágenes de cada campo del WFI. Segundo, con los centros de cada una de las 128 imágenes, se tomaron imágenes de aproximadamente del mismo tamaño del *Digitized Sky Survey 2-Infrared* (ESO DSS2i), las cuales están calibradas en coordenadas ecuatoriales y fueron utilizadas para encontrar estrellas en las imágenes del WFI que tienen posiciones en el *Guide Star Catalog* versión 1.2 (GSC 1.2). Las posiciones del GSC 1.2 se usaron para la calibración de pixeles en RA y Dec por tener menos incertidumbre. Con la ayuda de imágenes del ESO DSS2i se escogieron entre 6 y 10 estrellas para cada imagen del WFI que tienen posiciones en el GSC 1.2; las estrellas se seleccionaron de tal manera que estuvieran distribuidas lo más posible en toda la imagen y sin compañeras muy cercanas que interfirieran en la determinación de sus centro en pixeles con *imexamine* de IRAF. Para cada imagen se determinaron las posiciones en pixeles y coordenadas ecuatoriales (tomadas del GSC 1.2) de 6 a 10 estrellas. Estas posiciones (en pixeles y Ra-Dec) las utiliza *ccmap* de IRAF para hacer la transformación de coordenadas en pixeles a RA-Dec para cada imagen del WFI.

Este fue el proceso a seguir en la reducción imágenes en las cuales se detectaron candidatos a galaxias. Las imágenes, posiciones, diámetros, y posible morfología de los candidatos a galaxias encontrados se presentan en el siguiente capítulo.

# Capítulo 4

# Galaxias Encontradas en la Vecindad de PKS 1343−601

## 4.1 Introducción

En este capítulo se presentan y describen los candidatos a galaxias encontrados a ojo en las imágenes del WFI reducidas en el capítulo anterior. Se detectaron un total de 49, más 6 posibles candidatos a galaxias. Se presentan para estos objetos sus posiciones en coordenadas galácticas y ecuatoriales; además, se sugiere un tipo morfológico, un diámetro aparente, asi como una breve descripción de estos objetos. Por último, se menciona la detección de algunos de ellos en otras longitudes de onda.

## 4.2 Candidatos a Galaxias Detectados

Los candidatos detectados a galaxias aparecen borrosos, de bajo brillo superficial y pequeños, con la excepción de algunos de ellos, como por ejemplo la radio galaxia PKS 1343−601. En las búsquedas a ojo se detectaron 49 candidatos a galaxias y su posición, diámetro aparente, así como su posible morfología (ver la Tabla 4.1). Las columnas (2), (3), (4) y (5) de esta tabla contienen posiciones en coordenadas ecuatoriales (J2000) y Galácticas respectivamente. El diámetro aparente se da en la columna (6), mientras que la séptima da el valor de la extinción en la banda-$I$ ($A_I$) para la posición de cada galaxia de acuerdo con los mapas de extinción de polvo de DIRBE. La columna (8) sugiere una posible morfología para estos objetos. Por último, en la columna (9) se da una breve descripción de ellos.

### 4.2.1 Errores en Posición

Las posiciones de estos objetos fueron medidas dos veces para hacer un análisis estadístico de los errores (*random errors*) en la medición de las posiciones. El análisis estadístico da errorrs aleatorios de 0.″47 en RA y 0.″18 en Dec, lo cual da una consistencia interna en la medición de posiciones. La gran mayoría de estas galaxias no han sido previamente detectadas. Para las que se han detectado en otras longitudes de onda, sus posiciones tienen grandes incertidumbres; por lo tanto, no fue posible hacer una comparación de posiciones con datos externos para determinar errores sistemáticos.

### 4.2.2 Determinación de Diámetros

La mayoría de los candidatos a galaxias tienen diámetros de unos cuantos segundos de arco, con la excepción de algunos de ellos. Por ejemplo, las Galaxias 22 y 29 de la Tabla 4.1 parecen ser grandes espirales con diámetros aparentes de 15″ y 20″, respectivamente. Los objetos presentados en la Tabla 4.1 aparecen pequeños y de bajo brillo superficial debido a la extinción que tienen. Los diámetros dados en la Tabla 4.1 corresponden al 10% del pico de la curva de brillo superficial.

### 4.2.3 Clasificación Morfológica

La determinación del tipo morfológico es afectada fuertemente por la extinción. Sólo en algunos casos es más claro su tipo morfológico: Espiral o Elíptico. En la mayoría de ellos no es clara su morfología porque es muy probable que sólo se observen los bulbos o núcleos de las galaxias debido a la extinción tan alta. Por lo tanto, la columna 8 de la Tabla 4.1 solamente sugiere un tipo morfológico para la mayoría de ellos.

### 4.2.4 Imágenes de los Candidatos a Galaxias

La Figura 4.1 presenta las imágenes de los 49 candidatos a galaxias. El tamaño de estas imágenes es aproximadamente de 36 x 36 segundos de arco. Las imágenes 28 y 34 son ejemplos de espirales vistas de canto, severamente afectadas por la extinción. De los 49 objetos en Tabla 4.1, 24 de ellos son propuestos como espirales. Las imágenes 30 y 33 son ejemplos de galaxias elípticas con alta extinción. Para los otros 25 objetos restantes de la Tabla 4.1 se propone una morfología elíptica.

## 4.3 Posibles Candidatos a Galaxias

Seis objetos con bajo brillo superficial que no son estrellas fueron detectados, y su naturaleza no se puede determinar en base de estas imágenes. Por lo tanto, no es claro si son objetos extragalácticos. Observaciones más profundas en el cercano infrarrojo son necesarias para revelar su origen. Datos e imágenes de estos seis objetos se muestran en la Tabla 4.3 y Fig. 4.2. La Tabla 4.3 tiene las mismas columnas que la Tabla 4.1. Los datos presentados en esta tabla se obtuvieron de manera semajente a los de la Tabla 4.1.

### 4.3.1 Imágenes de los Posibles Candidatos a Galaxias

Las imágenes de estos seis posibles candidatos a galaxias se presentan en la Fig. 4.2 de esta tesis. Cinco de estos objetos tienen diámetros de unos cuantos segundos de arco, excepto el número 2 que parece ser mucho más extenso pero con muy bajo brillo superficial. Estas imágenes también tienen una dimensión de aproximadamente 36 x 36 segundos de arco. Observaciones profundas en el cercano infrarrojo son necesarias para determinar si son de origen extragaláctico.

## 4.4 Identificación con Objetos Conocidos

Con las posiciones de estos 55 objetos detectados a candidatos de Galaxias, se buscaron contrapartes en otras longitudes de onda. Para esta búsqueda, se utilizaron las siguientes bases de datos: La base de datos *CATS* (http://cats.sao.ru, Verkhodanov et al. 1997) y *NASA/IPAC Extragalactic Database* (*NED*, http://nedwww.ipac.caltech.edu). Solamente 14 galaxias de las listadas en las Tablas 4.1 y 4.3 han sido detectadas en otras longitudes de onda: cercano infrarrojo (DENIS[1]), lejano infrarrojo (IRAS), radio y rayos X. Varias de estas tienen posible contraparte en las observaciones del satélite IRAS. La búsqueda de posibles contrapartes en IRAS fue realizada tomando en cuenta lo siguiente:

**a** Las incertidumbres elípticas de posición en IRAS y la distancia de separación entre el candidato a galaxia y la posición del objeto detectado por IRAS.

**b** El término de "color" definido con 3 de las 4 bandas de IRAS (12 $\mu$m, 25 $\mu$m, 60 $\mu$m y 100 $\mu$m) $col_1 = f_{12} \cdot f_{25}/(f_{60})^2$ (Yamada et al. 1993), donde $col_1 < 1$ indica que el objeto detectado por IRAS puede ser una galaxia

[1]Búsqueda profunda en el cercano infrarrojo del cielo del sur (DENIS, por sus siglas en inglés)

**c** Posibles coincidencias con objetos detectados en el cercano infrarrojo, radio y/o rayos-X.

En la sección 4.4 se presentan las 14 galaxias que tienen detecciones en otras longitudes de onda. Siete de estos 14 candidatos a galaxias tienen posible detección con IRAS. Cinco tienen identificación con objetos detectados por DENIS, la número 20 por Rousseau et al. (2000) y las galaxias 15, 33, 34 y 40 por Anja Schröder (comunicación privada). Dos (33 y 37) tienen detección en rayos X y cuatro en radio. Las galaxias 3, 15, 20 y 49 tienen posible detección en muestreos profundos de HI. Una combinación de imágenes profundas en las bandas $I$, $J$ y $K$ del campo central (campo uno, ver Fig. 3.1), detectó las galaxias 29, 30, 33, 32, 34, 37 y 40 (Nagayama y Sato, comunicación privada). Estos resultados han sido proporcionados antes de su publicación por Takahiro Nagayama y Shuji Sato de la Universidad de Nagoya. Nagayama y Sato han detectado cinco galaxias más en el campo uno que no son visibles en las imágenes de la presente tesis porque tienen muy bajo brillo superficial debido a la alta extinción.

# Capítulo 5

# Análisis de la Distribución de las Galaxias Detectadas

## 5.1 Introducción

La distribución de los candidatos a galaxias presentados en el capítulo 4 es analizada en último capítulo. También se presenta una simulación del cúmulo de Coma puesto a la distancia y con los mismo niveles de extinción observados en PKS 1343−601. Finalmente se compara la distribución de Coma sujeta a los mismos niveles de extinción de PKS 1343−601 y la distribición de los candidatos a galaxias detectados.

## 5.2 Distribución de los Candidatos a Galaxias

La distribución en coordenadas Galácticas de los candidatos a galaxia encontrados en la vecindad de la radio galaxia PKS 1343−601 se muestra en la Fig. 5.1. Esta distribución contiene todos los objetos listados en las Tablas 4.1 y 4.3 del capítulo 4. En esta figura, los círculos representan galaxias que supongo son de morfología espiral, mientras que los círculos cruzados corresponden a galaxias con morfología elíptica. Los círculos vacíos corresponden a los 6 objetos para los cuales no se tienen suficiente información para clasificarlos como candidatos a galaxias. Quiero hacer notar que los candidatos a galaxias tienen una extinción alta en la banda $I$, por lo tanto sólo se sugiere una clasificación morfológica. Los contornos representan los siguientes niveles de extinción, determinados con los mapas de extinción de DIRBE (Schlegel et al. 1998): $A_I = 2^{\rm m}(amarillo)$, $3^{\rm m}$, $4^{\rm m}$, $5^{\rm m}$, $6^{\rm m}$, $7.5^{\rm m}$ y $10^{\rm m}$ (linea negra cortada), de arriba hacia abajo respectivamente. El contorno (cuadro negro) de la

vecindad observada alrededor de PKS 1343−601 se muestra también. La posición de PKS 1343−601 en esta distribución está marcada por el punto (rojo) más grande. El gran círculo (verde) corresponde al radio de Abell ($R_A$[1]) de 2°.2.

Se nota en esta distribución que hay más galaxias espirales en lugares con niveles menores de extinción, mientras que a niveles más altos de extinción se detectan mayormente elípticas. Las galaxias elípticas contienen mayormente en sus centros estrellas viejas (rojas) por lo cual son visibles a niveles más altos de extinción.

La distribución de galaxias está modulada por el gradiente de extinción en esta región; por lo tanto, no se observa una concentración de galaxias uniforme alrededor de PKS 1343−601, lo cual era esperado para un cúmulo muy obscurecido.

## 5.3 Una Comparación con el Cúmulo de Coma

Para saber si la distribución de galaxias de la Fig. 5.1 es lo que se esperaría para un cúmulo rico de galaxias muy obscurecido, se hizo una simulación con el cúmulo de Coma. En esta simulación se coloca a Coma a la distancia de PKS 1343−601 y con los mismo niveles de extinción. El cúmulo de Coma es rico en galaxias. Para la simulación se utililzó el catálogo de galaxias de Coma de Godwin et al. (1983). Este catálogo contiene 6,724 galaxias en un campo de 2.63 grados cuadrados con un límite de magnitud de $b_{26.5} = 21$. Este católogo no incluye los tipos morfológicos, por lo tanto, se consideraron dos casos en la simulación: que todas fueran elípticas, o todas fueran espirales; se describe el caso para elípticas y sólo se presenta el resultado para espirales al final.

Si Coma se situa en la posición de PKS 1343−601 y sin extinción, sólo 1979 galaxias de Coma que caen dentro del campo observado en la vecindad de PKS 1343−601. La Fig. 5.2 presenta la distribución en coordenadas galácticas de estas 1979 galaxias. En esta distribución se presentan galaxias con magnitudes $I \leq 17\overset{m}{.}5$. Las galaxias de Coma con magnitudes $I > 17\overset{m}{.}5$ no se incluyen por que por que el límite de magnitude en estas observaciones es de $I \simeq 17\overset{m}{.}5$. La Fig. 5.2 muestra una concentración muy clara de galaxias hacia el centro del cúmulo. La Fig. 5.3 muestra la distribución de galaxias de Coma presentada en la Fig. 5.2 bajo los niveles de extinción en la vecindad de PKS 1343−601. Una vez que la extinción se ha incluido en la simulación solamente quedan 54 galaxias, las demás están ocultadas por la extinción. La distribución de galaxias está correlacionada con el gradiente de extinción al igual que en la Fig. 5.1.

[1] $R_A = 1.7'/z$, donde $z = v_{obs}/c$

La distribución de galaxias de Coma, en que se supone únicamente morfología elíptica, se mostrada en la Fig. 5 3 y es muy parecida a la distribución presentada en la Fig. 5.1. En esta distribución se observa que las elípticas prevalecen a niveles altos de extinción como se observa en la Fig. 5.1, mientras que las espirales se presentan mayormente a nivels mas bajos. La distribución de las galaxias de Coma suponiendo sólo morfología espiral se presentan en la Fig. 5.4 y es consistente también con la presentada en la Fig. 5.1. Muy pocas o ninguna espiral permanece con niveles altos de extinción. La simulación de Coma a la distancia de PKS 1343−601 y con los mismos niveles de extinción muestra que la distribución de galaxias presentada en la Fig. 5.1 es consistente con la presencia de un cúmulo rico de galaxias muy obscurecido.

# Capítulo 6

# Conclusiones y Plan a Futuro

El objetivo de esta tesis fue la búsqueda de galaxias alrededor de la radio galaxia PKS 1343−601 para determinar si este objeto marca el centro de otro cúmulo rico de galaxias en la región central del Gran Atractor. Esta búsqueda constistió en inspeccionar visualmente 128 imágenes en la band-$I$ tomadas con el telescopio de 2.2-m y la cámara WFI en el Observatorio de La Silla. En esta búsqueda fue posible detectar galaxias hasta el límite de magnitud $I_{std} \simeq 17\overset{m}{.}5$. En estas imágenes, 55 candidatos a galaxias fueron detectados hasta niveles de extinción $A_I = 5\overset{m}{.}5$ de acuerdo con los mapas de extinción de polvo de DIRBE. La distribución de estas galaxias fue comparada con la distribución del cúmulo de Coma puesto a la distancia y bajo las mismas condiciones en las que se observó PKS 1343−601. Al situar a Coma en estas condiciones, sólo 54 galaxias serían visibles de sus 6,724 galaxias. La distribución en coordenadas Galácticas de estas 55 galaxias de Coma es semejante a la distribución de las 55 galaxias encontradas. En los dos casos se observa que la distribución de galaxias está modulada por el gradiente de extinción en está región. Estos resultados son evidencia que la radio galaxia PKS 1343−601 marca el centro de un cúmulo rico de galaxias.

Estos resultados son una motivación para continuar con la búsqueda de nuevos miembros de este cúmulo que no fueron detectados en esta primera búsqueda. Un mapeo de este cúmulo en el cercano infra-rrojo in las bandas $J$, $H$ y $K$ está en progreso. Los resultados preliminares del mapeo del centro de este cúmulo confirman mis detecciones de galaxias en el campo central y detecta 5 nuevos miembros. Estas imágenes nuevas en el infra-rrojo cercano prometen revelar nuevas galaxias de este cúmulo obscurecido.

# An Obscured Cluster of Galaxies in the Great Attractor Region


Thesis Presented for the Degree of
MASTER OF SCIENCES (ASTRONOMY)
at the Institute of Astronomy
**Universidad Nacional Autónoma de México**

**Manuel Ochoa Silva**

November 2002

*To my parents*

# Acknowledgements

First of all, I want to thank my parents for their support that has been so important and meaningful for my career; thank you so much mom and dad!

It is my pleasure to thank my thesis directors Dr. Heinz J. Andernach and Dr. Renée C. Kraan-Korteweg for their advice, motivation, guidance and support during this thesis. The results presented in this thesis have been possible thanks to their valuable contributions. Without their collaboration this thesis would not have appeared as it is presented. My gratitude to my friend Dr. Andernach for his friendship.

I would like also to thank and acknowledge the following persons:

Dr. Patrick A. Woudt for the I-band images and his help in the data reduction.

Dr. Roger Coziol for computational help, counsel and support to finish my thesis.

Dr. Aanja Schröder for making her DENIS data available to me prior to publication.

I made use of the following two databases: CATS (Verkhodanov et al. 1997) of the Special Astrophysical Observatory, Russia, and the NASA/IPAC Extragalactic Database (NED) which is operated by the Jet Propulsion Laboratory, California Institute of Technology, under contract with the National Aeronautics and Space Administration.

Finally, I specially want to thank and acknowledge the "*posgrado*" of the *Instituto de Astronomía* and our *máxima casa de estudios* (UNAM) for their support and my educaction.

# Contents

# Abstract

The Great Attractor (GA) is a dynamically important mass overdensity, first noticed through a large-scale systematic flow of galaxies in the local Universe. Theoretical reconstructions of the mass density field from peculiar velocities predict the peak of the GA overdensity to lie behind the southern Milky Way at $(\ell, b, v) \sim (320°, 0°,$ 4,000 km $s^{-1})$ (Kolatt et al. 1995). The nature and extent of the GA has been subject of much debate during the past decade, partly due to the fact that it is heavily obscured by the southern Milky Way. The largest concentration of mass as yet detected within the GA region is the Norma cluster, also known as ACO 3627, which accounts for about 10% of the predicted mass of the GA. Is there another Norma-type cluster behind the Milky Way in the GA central region? No further clusters have been identified in the GA overdensity and large part of it may still be hidden by the Milky Way.

Many rich galaxy clusters (including the Norma cluster) are strong X-ray sources and show radio emission of its central galaxy, like the radio galaxy PKS 1610−608 in Norma. The fact that the second brightest extragalactic radio source in the southern sky ($f_{20cm}$ = 79 Jy, McAdam 1991, and references therein), PKS 1343−601 at $(\ell, b, v, A_I) \sim (309.^{\circ}7, 1.^{\circ}8,$ 3,872 km $s^{-1}$, $4.5^{m})$ (West & Tarengi 1989, Woudt 1998, Kraan-Korteweg & Woudt 1999) lies within the general region of the GA, suggests that it may be the central galaxy of another rich cluster at the core of the GA.

In this thesis, I analyze deep I-band images centered on PKS 1343−601. A field of about $2° \times 2°$ around PKS 1343−601 was imaged in the $I$-band with 15 different single exposures of 600 seconds, 5 exposures of 300 seconds (central field) and a seeing of about $0.5''$. A meticulous search of galaxies by eye of all fields revealed 49 galaxy candidates. These galaxies were detected up to extinction levels of $A_I = 5.^{m}5$. The distribution of these galaxies is modulated by the extinction gradient in this region. Therefore, an actual concentration of galaxies towards PKS 1343−601 was not observed. However, I show in a simulation that the distribution of the Coma cluster galaxies at the position and extinction levels of PKS 1343−601 within the

observed field of view looks very similar to the distribution of the galaxies found in the vicinity of PKS 1343−601. Thus, the observed distribution of galaxies around PKS 1343−601 is consistent with the presence of a rich, Coma-like, cluster of galaxies.

# Chapter 1

# Introduction

## 1.1 Preamble

Galaxies are distributed in space forming large-scale structures (LSS) of filaments, great walls, voids, and clusters. These gigantic formations of galaxies can be traced almost everywhere in the sky, except in a speficic area where the dust of our Galaxy thickens, producing a band devoid of galaxies that closely matches the Galactic disk. The Milky Way Galaxy acts as a natural barrier in such a way that it obscures as much as 25% of the optical extragalactic sky creating a gap in the distribution of galaxies. Such incompleteness in the maps of the galaxy distribution limits the studies of large-scale structure formation and dynamics of the nearby Universe. In terms of redshift, the nearby Universe is taken out to 10, 000 $\mathrm{km\,s^{-1}}$, 150 Mpc (Fairall 1998). A volume-limited sample of galaxies out to 30, 000 $\mathrm{km\,s^{-1}}$ is known as the local Universe, but incompleteness starts as low as 1600 $\mathrm{km\,s^{-1}}$ (not 16, 000 $\mathrm{km\,s^{-1}}$ !) (Fairall - private comunication). The dust and stars from the Galactic disk obscure extragalactic light, making galaxies appear smaller and fainter the closer they lie to the Galactic Plane (GP). Extinction increases towards the GP rendering diameter- and magnitude-limited samples of galaxies incomplete, thus creating a "Zone of Avoidance" (ZOA) in the "whole" sky maps of galaxy distributions.

The incompleteness of optical galaxy catalogues increases towards the Zone of Avoidance. Our understanding of several key issues of large-scale structure is limited by the incompleteness of galaxies in the ZOA. The mass distribution within a redshift distance of 6000 $\mathrm{km\ s^{-1}}$ behind the ZOA is dynamically relevant due to its contribution to gravitational motions of the Local Group (LG) for example. Interpolations based on POTENT (Dekel 1994; Kolatt, Dekel & Lahav 1995), see Chapter 2, show

that the direction of the peculiar velocity vector of the LG changes as much as 35° if the known mass within $b \sim \pm 20°$ is accounted for (Kolatt et al. 1995).

The study of peculiar velocities of galaxies suggest the existence of a large concentration of mass known as the Great Attractor (GA) behind the southern Milky Way. Such an overdensity is of great dynamical importance in the nearby Universe. The GA seems to be responsible in part for the large-scale streaming motion in the local Universe, including the LG. The mass of large-scale structures hidden behind the ZOA strongly affects the estimation of cosmological parameters such as the density and biasing parameters, $\Omega_\circ$[1] and $b$[2] The mass density peak of the GA region is predicted to be at $\ell = 320°$, $b = 0°$, and at a radial velocity of $cz = 4,500$ km $s^{-1}$ (Burstein et al. 1990, Kolatt et al. 1995). The existence of the GA has been of much controversy during the past decade because of the failure of detecting a large concentration of galaxies in this region. If light traces mass, a large concentration of galaxies should be observed in the GA region. However, such a concentration of galaxies has not been observed so far due to the fact that a major part of the GA lies behind the southern Milky Way.

Deep optical searches in the southern Milky Way have revealed that ACO 3627 is the most conspicuous concentration of galaxies in the central region of the GA. ACO 3627 at $\ell = 325.^\circ3$, $b = -7.^\circ2$ and $v = 4,848\,\mathrm{km\,s^{-1}}$ is a nearby, rich cluster of galaxies at the center of the GA (Woudt 1998). The existence of another more obscured, rich cluster of galaxies in the GA region hidden by the Milky Way is suspected. The strong southern radio source PKS 1343−601 at $\ell = 309.^\circ7$ and $b = 1.^\circ8$ could mark the center of another rich cluster of galaxies in the GA region. Hence, the scientific motivation of this project is to investigate whether or not this suspected rich cluster of galaxies really exists.

## 1.2 Large Scale Structure and the ZOA: a historical perspective

The existence of the ZOA was first noticed by Proctor (1878) as the "Zone of Few Nebulae". He observed an empty band in the distribution of nebulae based on the data from the "General Catalogue of Nebulae" of Sir John Herschel (1864). John

[1]The density parameter (at present time) : $\Omega_\circ = \rho_\circ/\rho_c = \frac{8\pi G}{3H_\circ^2}\rho_\circ$ (Ohanian & Ruffini 1994).

[2]The galaxy-galaxy correlation function is a biased indicator of the mass correlation function, in an approximately linear relation: $\xi_{gg} = b^2\xi_{mass}$, $b$ is the biasing parameter which needs to be determined by comparing the theory with observations (Padmanabhan 1993 & Peacock 1999).

Herschel added 500 nebulae to his father's list for the north. In order to complete an all-sky survey, he observed at the Cape of Good Hope and discovered 1,700 nebulae in the southern hemisphere. He published his "General Catalogue" in 1864 which is a compilation of all 4,630 nebulae known at the epoch.

While compiling his "General Catalogue", John Herschel noticed a prominent concentration of nebulae in Virgo and that the majority of nebulae appeared as being separated from the Milky Way. He also recognized different types of nebulae. The nebulae found far from the plane of the Milky Way appeared different from those detected at low Galactic latitudes which were later identified as "planetary" nebulae.

Sir John Herschel was the first to recognize the Local Supercluster (LSC). He described it as a roughly spherical system centered on Virgo. He noticed that our stellar system, the Galaxy, is located far from this dense central region and is one of its outlying members. He observed that the distribution of galaxies was far from being uniform. Branches and protuberances come out from the denser central part of the LSC. In one of these branches and far from the center, our Galaxy is located. This description of the LSC is in good agreement with today's observations. His findings were deduced from the simple counting of nebulae in the sky.

The first plots of the distribution of nebulae were made by Proctor. They were based on Herschel's "General Catalogue" and were published in his book *The Universe of Stars* (Proctor 1878). Figure 1.1 shows one of the plots included in Proctor's book, where he describes in detail the major groups of nebulae observed. Although some of his interpretations were incorrect, he recognized some of the major large-scale structures known today. He also recognized the region avoided by the nebulae as the plane of the Milky Way. At that time the reason for this avoidance, the existence of dust in the Galactic Plane and its obscuring effects, was not known.

The true nature of the nebulae was subject of much debate until the idea of "island universes" proposed by Immanuel Kant proved correct with the observations of Edwin Hubble in the 1920's. Using the most powerful telescope at that time, the 100-inch Hocker reflector at Mount Wilson in California, he identified Cepheid variables, standard candles, in the spiral nebulae of Andromeda. The so derived distance to Andromeda proved unambiguously its extragalactic nature. Soon, the extragalactic nature of other nebulae, especially those with known spiral structure, could be confirmed.

Hubble's discovery of the extragalactic nature of the nebulae was published in *The Realm of the Nebulae* (Hubble 1936). It opened the study of large-scale structures.

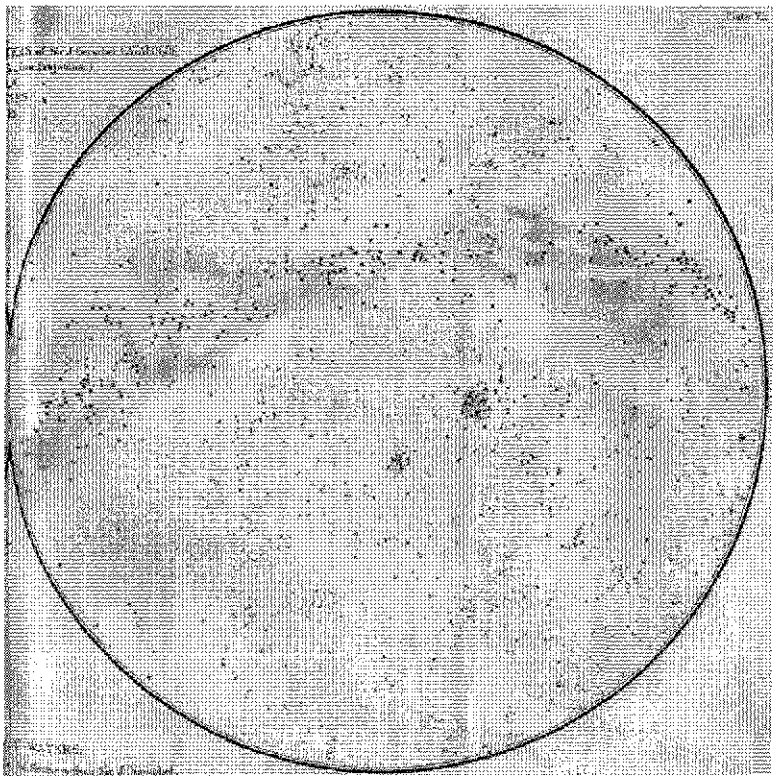

Figure 1.1: A plot of the nebulae from Herschel's *General Catalogue* drawn by Richard Proctor and Sidney Waters (From R.A. Proctor, *The Universe of Stars*).

In his book he presented a survey of 44,000 galaxies. The number of visible galaxies decreases rapidly close to the GP. This clearly revealed a "Zone of Avoidance" that was then interpreted to be the consequence of the obscuration produced by the disk of the Milky Way. Also, the existence of groups and clusters of galaxies became more evident from this survey.

Only about 20 rich clusters of galaxies were known before the National Geographic Palomar Observatory Sky Survey (POSS) of the 1950's. The latter revealed the existence of thousands of rich clusters of galaxies. The Palomar Observatory Sky Survey was done with a 48-inch Schmidt telescope that produced wide-angle photographs that cover the entire sky visible from Palomar. George Abell studied all the photographic plates for his doctoral thesis. In 1958, he published a catalogue containing 2,712 rich clusters of galaxies found on the photographic plates from the National Geographic Society-Palomar Observatory Sky Survey (Abell 1958). Large-scale structures and the Zone of Avoidance became even more evident from the galaxy surveys that followed the POSS.

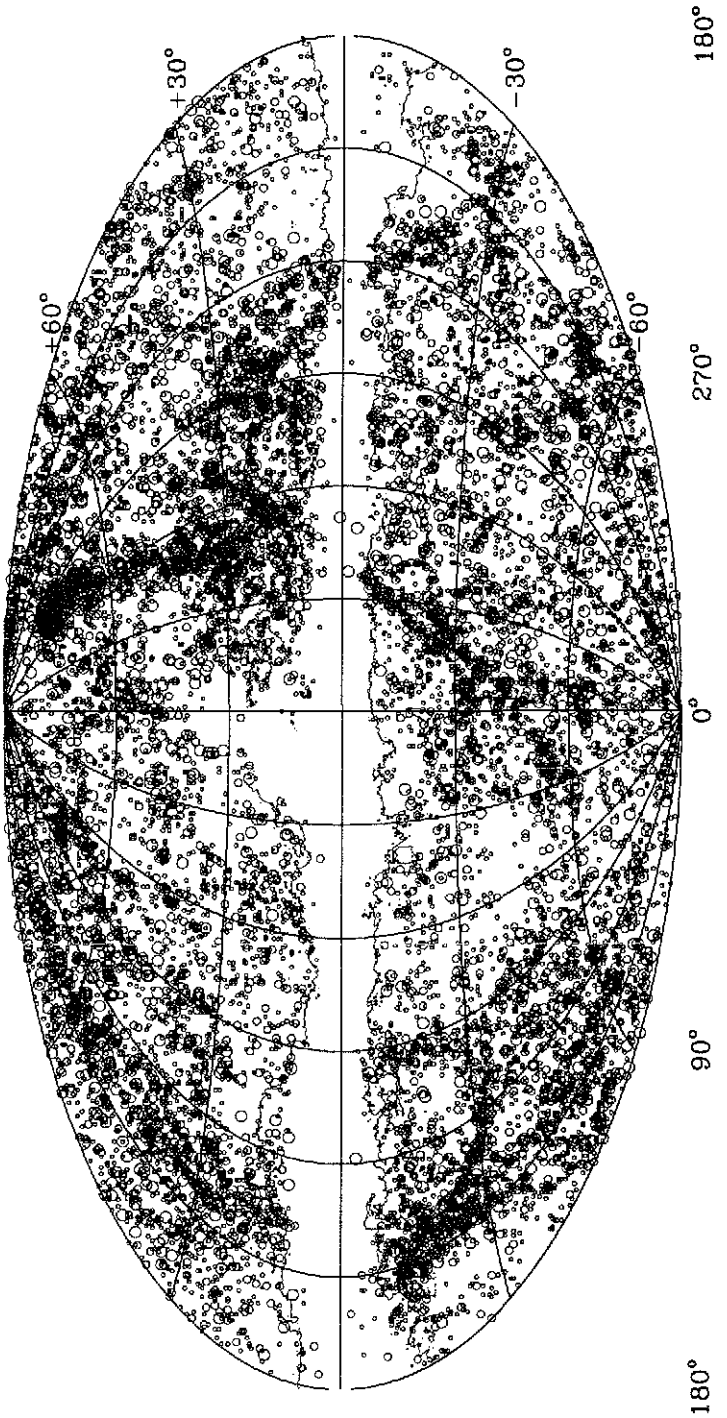




Figure 1.2: Aitoff equal-area projection in Galactic coordinates showing all known galaxies with $D \geq 1'.3$ and the extinction contour in the $B$-band of $A_B = 1^m.0$ as determined by the DIRBE dust extinction maps (figure from Kraan-Korteweg 2000b).

## 1.3 The Distribution of Galaxies in All-Sky Maps

A "whole" sky catalogue of galaxies can be achieved by merging three catalogues of galaxies: the Uppsala General Catalogue (UGC) for the north that covers $\delta \geq -2.^{\circ}5$ (Nilson 1973), the ESO Uppsala Catalogue for the south $\delta \leq -17^{\circ}$ (Lauberts 1982), and the Morphological Catalogue of Galaxies (MCG) for the region of $-17.^{\circ}5 < \delta < -2.^{\circ}5$ (Vorontsov-Velyaminov & Archipova 1963-74). The data from these three catalogues is homogenized by applying the galaxies diameters adjustments proposed by Lahav: $D = 1.15D_{UGC}$, $D = 0.96D_{ESO}$, and $D = 1.29D_{MCG}$ (Lahav 1987). This whole-sky catalogue is complete for galaxies with diameters greater than $D = 1.'3$ (Hudson & Lynden-Bell 1991).

The resulting distribution of the galaxies from the merging of the above three catalogues is displayed in Fig 1.2 in an equal-area Aitoff projection (from Kraan-Korteweg 2000b). Galaxies are displayed in Galactic coordinates with the Galactic center, $\ell = 0^{\circ}$ and $b = 0^{\circ}$, at its origin. The galaxies in Fig 1.2 are diameter-coded. Small circles correspond to galaxies with diameters $1.'3 \leq D < 2'$. Galaxies with diameters $2' \leq D < 3'$ are represented by medium-sized circles and large circles mark the positions of galaxies with diameters $D \geq 3'$.

The clumpy distribution of galaxies is suggestive of large-scale structures in the nearby Universe. In Fig 1.2, we can identify the Local Supercluster as a great circle (the Supergalactic Plane) with the Virgo cluster at its center at $(\ell, b) \sim (284^{\circ}, 74^{\circ})$ and the Centaurus Wall which is seen as a concentrated band of galaxies that crosses the southern Milky Way at the predicted position of the GA at $\ell = 320^{\circ}$ and $b = 0^{\circ}$ (Kolatt et al. 1995). The Centaurus Wall is a continuous large-scale structure that includes the Indus, Pavo, Telescopium, Centaurus and Hydra clusters. The Centaurus region hosts the GA which is located where the Virgo southern extension merges with the Centaurus Wall. The GA region is of great dynamical importance because of the streaming motion of galaxies in the local Universe, including the Local Group, directed towards it. The Pavo $(332^{\circ}, -24^{\circ})$, Centaurus $(302^{\circ}, 22^{\circ})$, and Hydra $(270^{\circ}, 27^{\circ})$ clusters are seen as part of the Centaurus Wall in Fig. 1.2. The Perseus-Pisces chain curving into the ZOA between $\ell = 95^{\circ}$ and $\ell = 165^{\circ}$ is another large-scale structure recognized in Fig 1.2. The Antlia $(273^{\circ}, 19^{\circ})$, Indus and Fornax clusters are also visible. The dipole of the Cosmic Microwave Background direction is found at $\ell = 276^{\circ}$ and $b = 30^{\circ}$ and is due to the motion of the LG towards this direction at a speed of 627 km s$^{-1}$ (Kogut et al. 1993). In this plot the most obvious feature is a broad band of about $20^{\circ}$ width which is almost empty of galaxies, the Zone of

Avoidance.

The distribution of galaxies behind the Milky Way has to be unveiled in order to determine the origin of the peculiar velocity of the LG with respect to the CMB and other velocity flow fields in the local universe such as the streaming motion towards the GA. The determination of the apex of the LG motion can be improved with a reduction of the width of the ZOA (Kraan-Korteweg & Lahav 2000). Theoretical reconstructions of the density field (Kolatt et al. 1995), based on the mass distribution out to $\sim 6{,}000\,\mathrm{km\,s^{-1}}$, have shown that the mass distribution within $\pm$ 20° of the ZOA strongly affects the direction of the gravitational acceleration of the LG. The direction of the acceleration vector of the LG changes as much as $\approx 35°$ when the mass distribution within $\pm$ 20° ZOA is included (Kolatt et al. 1995).

In the last decade, systematic optical, near-infrared, far-infrared, systematic blind HI and X-ray galaxy surveys were initiated to reduce the width of the ZOA. Although hampered by extinction, optical surveys are more effective than HI and far infrared searches to unveil clusters rich in E and S0 galaxies. Early type galaxies normally trace the mass density peaks in the Universe. Deep optical searches revealed that ACO 3627 (the Norma Cluster) is a rich cluster of galaxies hidden by the southern Milky Way (Woudt 1998). ACO 3627, a nearby and very massive cluster of galaxies at $\ell = 325\overset{\circ}{.}3$ and $b = -7\overset{\circ}{.}2$ with a redshift of $v = 4,844$ km s$^{-1}$ (Kraan-Korteweg et al. 1996; Woudt et al. 2000a & 2000b), is the most prominent known concentration of galaxies at the core of the GA region.

There is a large probability for the existence of another rich cluster of galaxies in the central region of the GA overdensity where the obscuration of background objects is higher. Galaxies are optically almost invisible at these extinction levels. The strong southern radio source PKS 1343−601 at $\ell = 309\overset{\circ}{.}7$ and $b = 1\overset{\circ}{.}8$ with a $v = 3,800$ km s$^{-1}$ lies in the central region of the GA hidden behind an extinction layer in the optical of $A_B = 12^{\mathrm{m}}$. The central galaxy in rich clusters is often a strong radio emitter. PKS 1343−601 could mark the bottom of the potential well of another rich cluster of galaxies at the core of the GA region supported by extended X-ray emission.

The scientific motivation for this thesis is to unveil the members of such a rich cluster of galaxy if it exists. Hence, the surroundings of this strong southern radio source were imaged in the I-band with WFI and the 2.2-m MPG-ESO telescope (see section 3.2). Sixteen WFI fields containing 128 images of the surrounding region of PKS 1343−601 were obtained. This project consists in the reduction of these data to verify whether this suspected rich cluster exists.

## 1.4 Outline of this Thesis

This thesis is presented in 6 chapters. A historical perspective and an introduction to the known large-scale structures in the nearby Universe was given in this Chapter 1. The second chapter covers in detail the deep optical searches of galaxies in the Zone of Avoidance. The reduction process of 16 I-band WFI fields (128 images) is described in Chapter 3. The results from meticulous searches by eye for galaxy candidates on 128 I-band images are presented Chapter 4, while Chapter 5 is dedicated to the analysis of the distribution of the unveiled galaxies. Finally, the conclution of this research and the future plans are presented in Chapter 6.

# Chapter 2

# Deep Optical Searches and Clustering of Galaxies Behind the ZOA

## 2.1 Introduction

Stars and dust in the plane of the Milky Way obscure about 25% of the optical and 10% of the IRAS extragalactic sky creating a "Zone of Avoidance" (ZOA) in the distribution of optical and infrared visible galaxies. As early as in 1878, the existence of the ZOA was pointed out by Proctor as the "Zone of the few Nebulae" (Proctor 1878) in the distribution of nebulae made with the "General Catalogue of Nebulae" data of Sir John Herschel, 1864. Harlow Shapley proposed to define the ZOA as the region delimited by "the isopleth of five galaxies per square degree from the Lick and Harvard surveys" (Shapley 1961), while a mean rate of 54 gal./sq.deg. was found in unobscured regions of the sky (Shane & Wirtanen 1967).

Astronomers interested in extragalactic studies tend to avoid the ZOA due to the inherent difficulties of finding galaxies and analyzing the few obscured galaxies already known there. However, revealing the large-scale structures hidden by the Milky Way is important for our understanding of the dynamics of the local Universe and for the determination of certain cosmological parameters, such as for example the origin of the peculiar velocity of the Local Group, the dipole[1] in the Cosmic Microwave Background (CMB) radiation and the value of the cosmological density parameter

[1]The dipole anisotropy in the CMB is due to the peculiar motion of the LG relative to the CMB, $v_p = 627$ km s$^{-1}$ towards $\ell = 270°$ and $b = 30°$ (kogut et al. 1993).

$\Omega_\circ$ on large scales.

Therefore, the ZOA has been subjected to multi-wavelength systematic explorations by various groups of astronomers and include most wavelengths of the electromagnetic spectrum: X-rays, optical, near (NIR) and far infrared (IRAS) and HI wavelengths. This chapter focuses on current results from optical surveys that have been carried out to unveil the large-scale structures that lie behind the Milky Way.

## 2.2 Deep Optical Searches of Galaxies Behind the ZOA

Systematic deep optical searches to uncover partially obscured galaxies in the Zone of Avoidance have been performed by various groups of astronomers using the available sky surveys such as the Palomar Observatory Sky Surveys (POSS I and POSS II) in the north and the ESO-SRC (UK Science Research Council) Southern Sky Atlas. Thousands of faint and partially obscured galaxies with diameters D$\geq$ 0.'1, not previously catalogued, have been found by eye in the above searches. The best available technique is visual examination as the fields of the ZOA are crowded by stars in the disk of the Galaxy which complicates the detection of faint and small galaxies. Because of this difficulty the detection of galaxies by eye for Galactic latitudes $|b| \leq 15°$ is more efficient than galaxy extraction by automated measuring machines such as COSMOS[2] (Drinkwater et al. 1995), APM[3] (Lewis et al. 1996) or the application of Artificial Neural Networks (ANN). In a pilot project, ANN uncover galaxies with diameters D$\geq$ 25″ at low Galatic latitudes (Naim 1995), $b \sim 5°$, but with a relatively low detection rate of approximately 30–40% of known galaxies found by eye. Therefore, the detection of galaxies by eye remains as the most reliable technique to identify faint and small galaxies in crowded star fields, even though it is very time-consuming.

In order to unveil new galaxies and clustering behind the ZOA, it is crucial to have a detailed understanding of the foreground extinction due to the Galactic plane. Moreover, it is indispensable to have both a high-resolution, well-calibrated map of the foreground extinction and understand clearly how Galactic extinction affects the

[2]COSMOS (COordinates, Sizes, Magnitudes, Orientations, and Shapes) is a plate scanning machine at the Royal Observatory Edinburgh, www.aao.gov.au/local/www/surveys/cosmos, (Andenarch 1999).

[3]The *Automated Plate Measuring Machine* (APM) is located at the Institute of Astronomy, Cambridge UK, www.ast.cam ac uk/~apmcat, (Andenarch 1999).

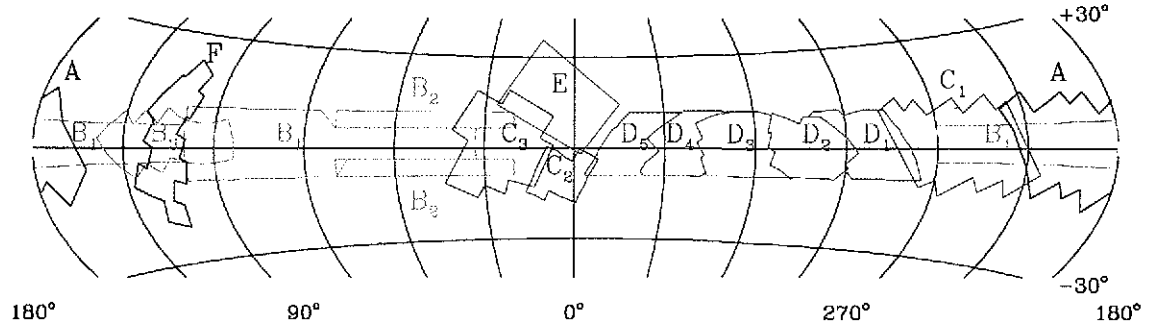


Figure 2.1: The different deep optical searches to uncover partially obscured galaxies in the ZOA. The distribution is centered on $\ell = 0°$ and $b = 0°$. The labels in the figure identify the different searches. See Kraan-Korteweg (2000b) for details on each search.



observed galaxy parameters in order to make corrections for absorption effects. The extinction maps by Burstein & Heiles (1982) have been the standard, but they do not include the ZOA ($|b| < 10°$). The Schlegel et al. (1998) full-sky 100 $\mu$m maps from a reprocessed composite of the *COBE*/DIRBE[4] and *IRAS*/ISSA[5] maps (DIRBE maps) improve the estimated value of the foreground extinction. These full-sky dust maps from the DIRBE experiment measure directly the dust column density and have a better angular resolution of 6.'1, in comparison to $\sim 20-30'$ for the H I maps, and twice as reliable than the Burstein-Heiles maps.

Deep optical searches of galaxies in the ZOA have so far uncovered about 50,000 previously unknown galaxies. Figure 2.1 shows the different galaxy surveys carried out in the ZOA. For details and results on each one of these surveys and the respective references see Kraan-Korteweg (2000b). These systematic deep optical searches cover the entire ZOA defined as the area of the sky delimited by the foreground extinction contour of $A_B = 1.^{m}0$ according to the DIRBE dust maps (Schlegel et al. 1998). This can be substantiated by comparing Fig. 2.1 with Fig. 1.2 in Chapter one.

As an example of the results from recent deep optical galaxy searches, the distri-

[4]The DIRBE experiment (Diffuse Infrared Background Experiment) on board the *COBE* satellite imaged the full sky in 10 broad photometric bands, from 1 to 240$\mu$m, with a 0.°7 beam (Schlegel et al. 1998).

[5]The Infrared Astronomy Satellite (IRAS) mission made the first full-sky maps of the diffuse background radiation in 4 broadband infrared channels, centered at 12, 25, 60, and 100 $\mu$mi with a bean of $\sim 5'$ (Joint *IRAS* Science Working Group 1998).

bution of galaxies found in the searches in the $D_1$-$D_5$ region are presented in Fig. 2.2. Small dots represent newly discovered galaxies while large dots corresponds to previously known galaxies with $D \geq 1'.3$ (Lauberts 1982). The three contour levels in this figure represent the extinction levels of $A_B = 1^m.0$ (cyan), $3^m.0$ (magenta) and $5^m.0$ (black) according to the DIRBE dust maps (Schlegel et al. 1998). From this distribution it is obvious that galaxies can readily be detected up to an extinction level of three magnitudes. Few galaxies are still identifiable at the extinction levels $3^m.0 < A_B \leq 5^m.0$. At extinction levels above five magnitudes, only a handful of galaxies are still recognized.

The deep optical surveys in the ZOA for the Hydra-Antlia ($D_2$), Crux ($D_3$), and Great Attractor ($D_4$) regions are complete to an apparent diameter of D= 14″ for extinction levels $A_B \leq 3^m.0$ (Woudt 1998, Kraan-Korteweg 2000a and Woudt & Kraan-Korteweg 2001).

Galaxies observed through obscuration layers of dust appear to be fainter and smaller as a function of extinction. For a spiral galaxy at a foreground extinction layer of $A_B = 1^m.0$ only about 80% of its unobscured diameter is visible. A spiral galaxy seen through an extinction layer of $A_B = 3^m.0$ will be reduced to a diameter that is 22% of its unobscured apparent size.

The reduction of galaxy diameters by absorption was investigated by Cameron (1990). He artificially absorbed a sample of spiral and elliptical galaxies with known surface photometry in order to establish the relationship between absorption and diameter reduction. Such a relationship is distinct for spirals when compared to ellipticals. As absorption increases, late-type galaxy diameters are reduced at a faster rate than that of early-type galaxies. He obtained the following diameter reduction factor as a function of the extinction in the optical $B$-band, $A_B$:

$f(\mathrm{Diam}) = 10^{0.10 A_B^{1.7}}$ for spiral galaxies
$f(\mathrm{Diam}) = 10^{0.13 A_B^{1.3}}$ for ellipticals and S0 galaxies

where $f(\mathrm{Diam})$ is the ratio by which diameters are reduced as a function of absorption.

When applying these diameter corrections to obscured spiral and elliptical galaxies at the apparent completeness limit of $D = 14''$, their intrinsic optical diameters will be $D^\circ \sim 60''$ and $50''$ respectively for $A_B = 3^m.0$. An elliptical galaxy with $D^\circ \sim 60''$ will have an apparent diameter below the completeness limit for $A_B > 3^m.0$ and therefore remain undetected. Thus, deep optical surveys are complete for galaxies with intrinsic diameters $D^\circ \geq 1'.0$ to extinction levels of $A_B \leq 3^m.0$.

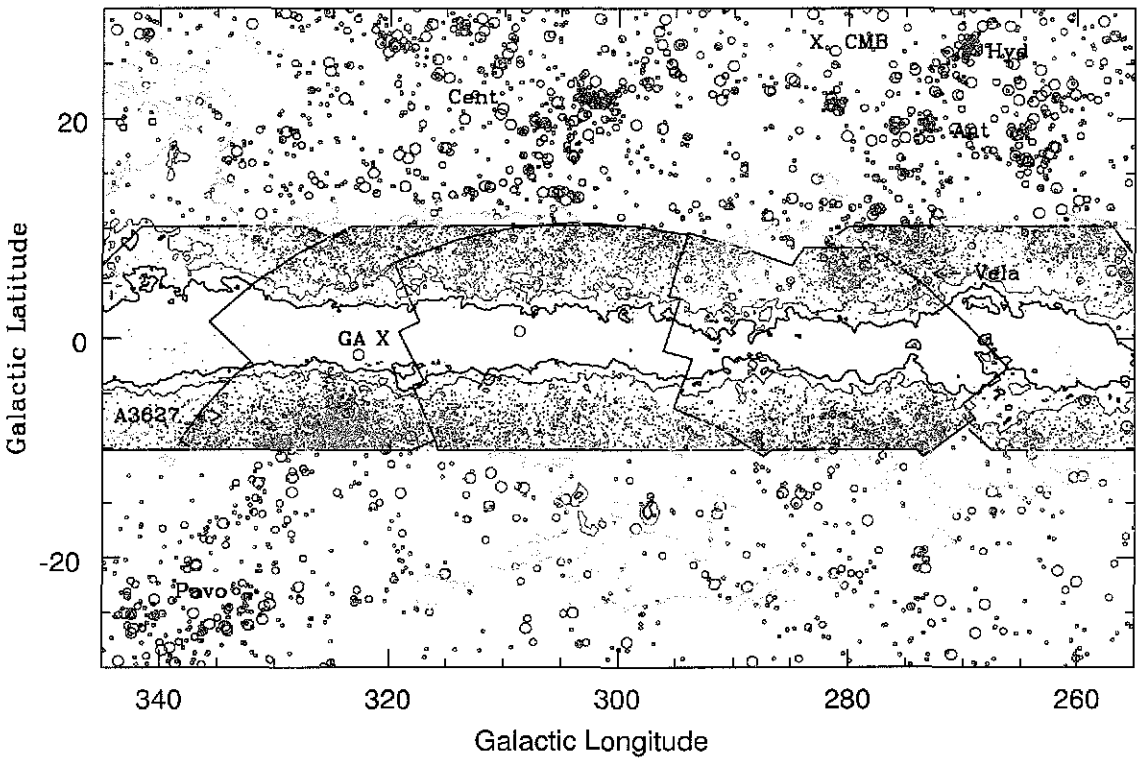


Figure 2.2: Distribution in Galactic coordinates of galaxies. The open circles are Lauberts galaxies with $D \geq 1'.3$, shown also in Fig 1.2. The small dots are the galaxies with $D \geq 12''$ detected by deep optical searches in the region $D_{1-5}$ (From R.C. Kraan-Korteweg 2000b).

The UGC, ESO-Uppsala, and MCG catalogues can now be complemented with the data obtained from deep optical searches in the ZOA to obtain a "whole" sky catalogue with a reduced ZOA. It is complete up to extinction-corrected diameters of $D^\circ = 1'.3$ for extinction levels $A_B \leq 3^m.0$. Figure 2.3 shows the Aitoff projection of the improved whole-sky distribution of galaxies with a narrowed ZOA (Kraan-Korteweg 2000b). Here, all ESO, UGC and MCG galaxies with extinction-corrected diameters $D^\circ \geq 1^m.3$ are plotted as well as the galaxies from the different ZOA optical searches with $D^\circ \geq 1'.3$ and $A_B \leq 3^m.0$ for which diameters and positions are available. The contour line in Fig 2.3 is the extinction contour level of $A_B = 3^m.0$ given by the DIRBE dust maps (Schlegel et al. 1998). Regions in the ZOA for which galaxy diameters and positions are not availabe are marked. Comparing Fig. 2.3 to Fig. 1.2, one sees that deep optical surveys reduce the ZOA considerably. The large-scale

structures that seem to continue across the ZOA are more pronounced, such as for example: the concentration of galaxies in the Great Attractor (GA) region centered at $(\ell, b) \sim (320°, 0°)$ and the Perseus-Pisces chain crossing the Galactic plane at $\ell = 165°$. Supplemented whole-sky maps with a reduced ZOA improve our understanding of the streaming motions in the local Universe, the total gravitational attraction on the Local Group, and the influence of the GA on the velocity flow fields of its surroundings.

## 2.3 Galaxy Clustering within the Great Attractor Region

The interpretation of the nature and the extent of the mass density enhancement dubbed the Great Attractor (GA) by Alan Dressler has been quite controversial due to its location behind the Galactic Plane (GP). A group of astronomers, later known as the "Seven Samurai" (7S), uncovered an enormous overdensity of mass in the local Universe (Lynden-Bell et al. 1988) from the Faber-Jackson[6] relationship for about 400 elliptical galaxies distributed all over the sky. They concluded from this study that the peculiar motion of the Local Group was shared by galaxies over a much larger volume of space. They proposed that this cosmic flow was induced by an enormous concentration of mass in the direction of $(\ell, b) \sim (307°, 9°)$ at a distance of 4,500 km $s^{-1}$ (Lynden-Bell et al. 1988, Burstein et al. 1990). They proposed the GA model with the following characteristics to explain the observed bulk flow (Dressler 1991):

1. The existence of a large overdensity of mass
2. Its center in redshift space lies at approximately 4,000 km $s^{-1}$
3. Peculiar velocities should decline when approaching the GA and reverse at the far side of the GA.

The above three predictions have been partially confirmed (Dressler & Faber 1990a,b; Dressler 1991). Hence, if light traces mass, a large concentration of galaxies should be observed in the GA direction, but that was not seen. The existence of a GA therefore remains controversial.

The confirmation of the GA has important cosmological implications since it challenges the "cold-dark-matter" (CDM) model. Such a concentration of mass would be exceedingly rare if not absent in a CDM universe. The concentration of mass in the GA region is predicted to be $\sim 5.4 \times 10^{16}$ solar masses (Lynden-Bell et al. 1988).

[6]The correlation between the luminosity of an elliptical galaxy and the velocity dispersion of the stars in its central region.

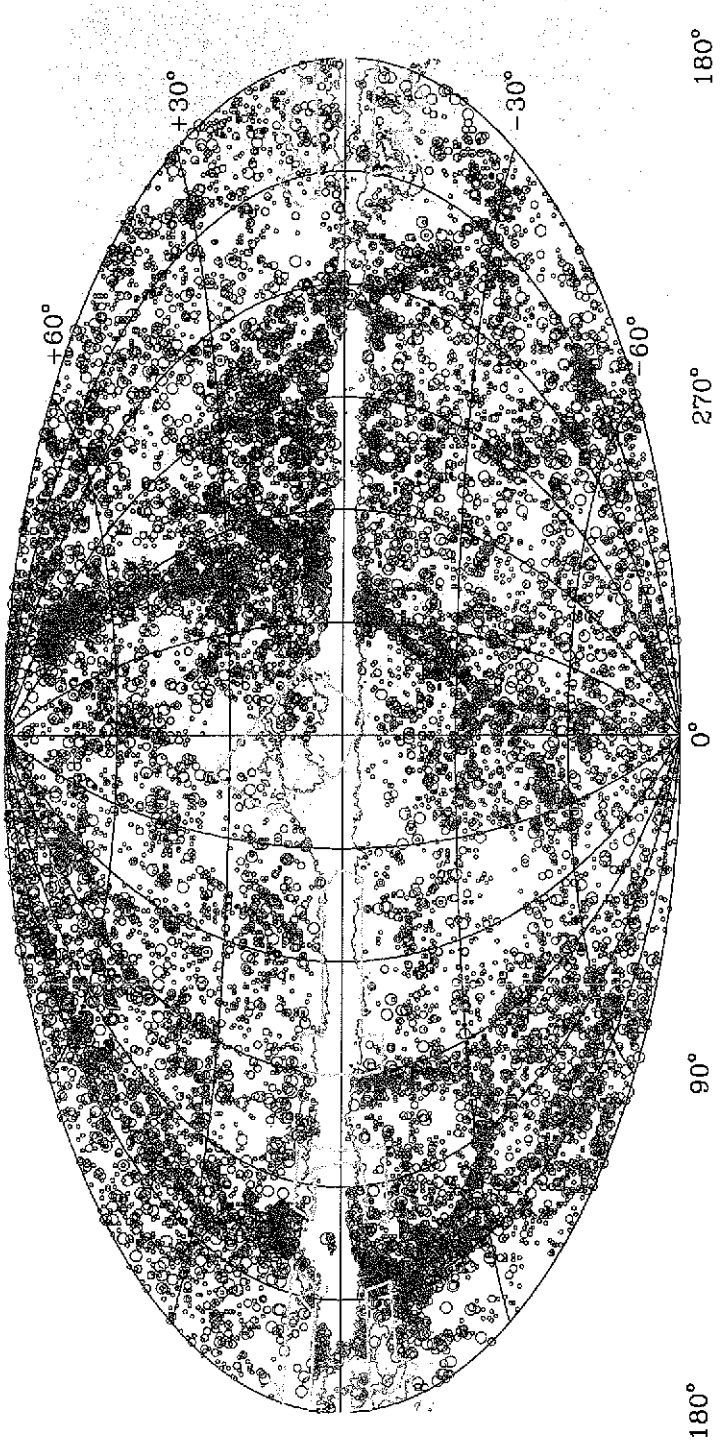


Figure 2.3: Aitoff equal-area distribution in Galactic coordinates of the ESO, UGC, and MGC galaxies with extinction-corrected diameters $D^{\circ} \geq 1'.3$. This plot includes also galaxies, with $D^{\circ} \geq 1'.3$ for extinction levels $A_B \leq 3^{m}.0$, from systematic deep optical surveys in the ZOA. (From Kraan-Korteweg 2000b).

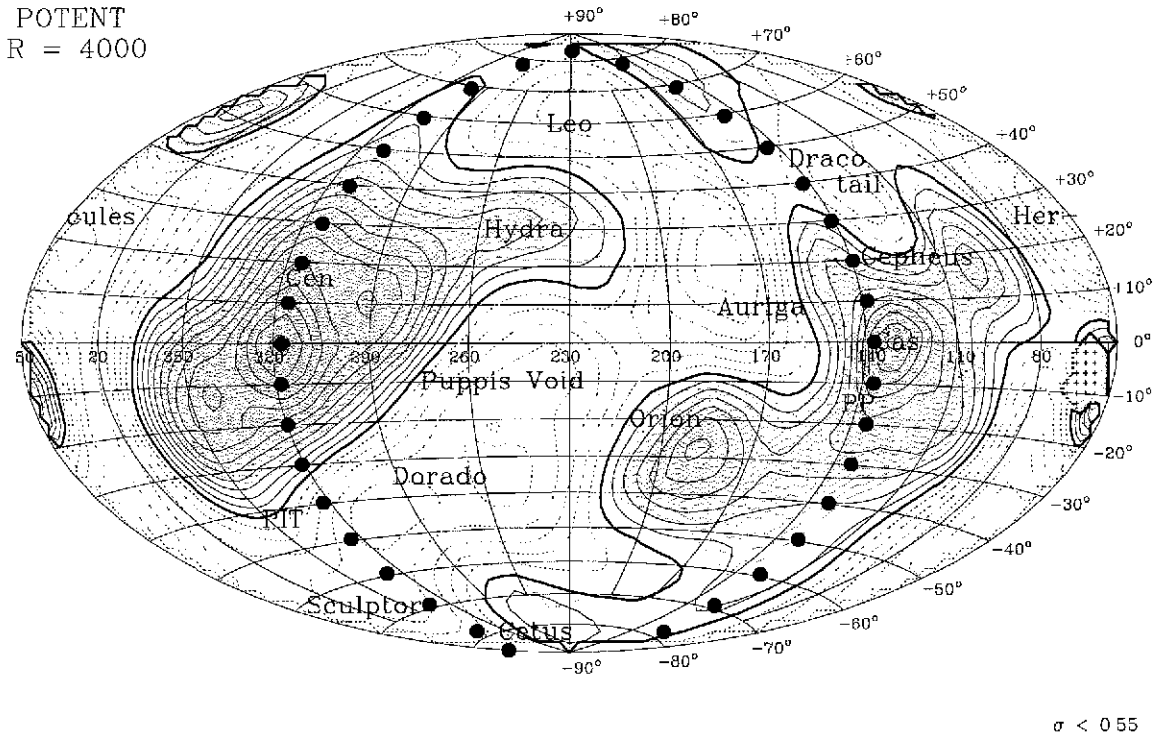




Figure 2.4: All-sky density fluctuation contours at 4,000 km $s^{-1}$, in Galactic coordinates, recovered by POTENT from observed peculiar velocities centered at $\ell = 230°$ and $b = 0°$. Note the GA region, seen as a broad overdense region that runs from Hydra and Centaurus to PIT. This overdensity has its maximum behind the ZOA. The bold dots mark the Supergalctic plane (From Kolatt et al. 1995).

As a complementary statistical approach to unveil large-scale structures behind the ZOA, mathematical methods are used to reconstruct the galaxy distribution obscured by the Milky Way. The POTENT analysis can reconstruct the potential field from available peculiar velocities of galaxies (Bertschinger & Dekel 1989). Observed peculiar velocities of galaxies in quasilinear gravitational instability are used by POTENT to reconstruct for instance the smoothed mass density field. Kolatt et al. (1995) used peculiar velocities from both sides of the ZOA as probes to trace the distribution of mass behind the ZOA.

Their mass-density fluctuation field at a redshift of 4000 km $s^{-1}$ is displayed in Fig 2.4. It predicts the peak of the GA overdensity at $(\ell, b)) \sim (320°, 0°)$. Here, the GA overdensity extends from Hydra and Centaurus to the Pavo-Indus-Telescopium

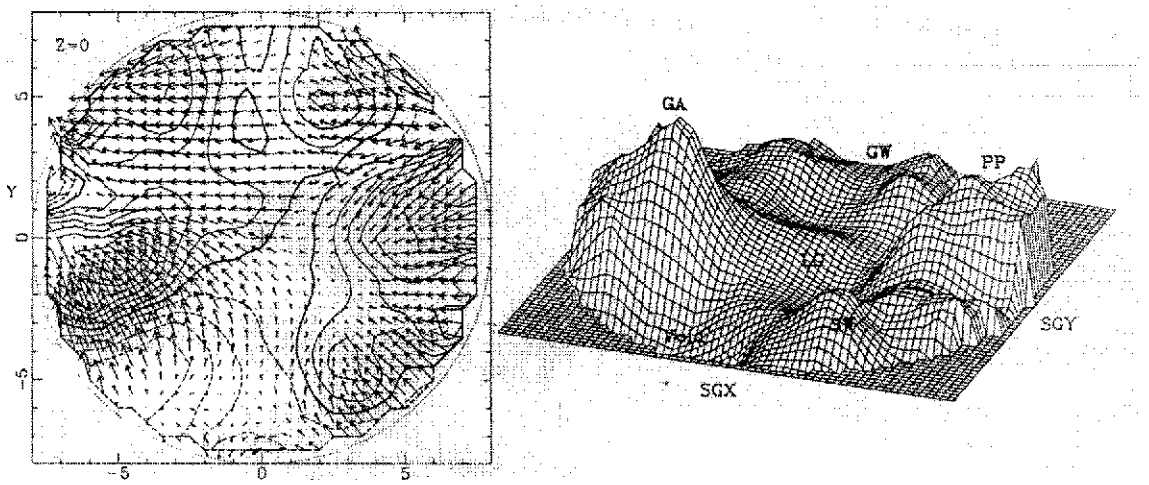


Figure 2.5: Velocity and mass-density fluctuations in the super galactic plane as recovered by POTENT (left panel). A surface plot of the mass-density fluctuation field is shown in the left panel. (From Dekel 1994, 1995)

(PIT) region. This overdensity is seen as the most pronounced feature in Fig. 2.4. The smoothed potential fields are an important tool to predict the existence of massive superclusters, although they are not able resolve individual clusters within these superclusters.

Figure 2.5 shows the 3D velocity field and mass-density fluctuation field as recovered by POTENT using the Mark III[7] velocities of approximately 3000 galaxies and a $12h^{-1}$Mpc smoothing (Dekel 1994, 1995). The arrows in the left panel are projections onto the Supergalactic Plane of the peculiar velocity vectors in the CMB frame. The right panel shows mass-density contours deduced from the flow pattern in the left panel if these are due to mass and gravity. In both plots, the position of the LG is located at the center. The main large-scale structures in the local Universe are easily visible in these plots. In both panels, the GA is visible at the left side. The Perseus-Pisces (PP) supercluster is visible on the right, the Great Wall (GW) of Coma is at the top. The PP peak dominates the right side extending to Aquarius, Cetus and the Southern Wall near to the south Galactic pole. A void of galaxies, an underdense region, is found between the overdense regions of GA and PP. This void

[7]The Mark III Catalog of Galaxy Peculiar Velocities comprises five different types of data files and has been used as input for POTENT reconstruction of velocity and density fields , as well as other velocity analyses (Willick et al. 1995, 1996 & 1997)

coincides with the observed galaxy void of Sculptor.

## 2.4 ACO 3627: The Norma Cluster

ACO 3627 is a cluster of galaxies found near the center of the Great Attractor region. From deep optical galaxy searches and redshifts, Kraan-Korteweg et al. (1996) and Woudt (1998) concluded that ACO 3627 is the most massive cluster within the GA region known to date. ACO 3627 is located near to the predicted peak of the GA overdensity. This cluster was listed by Abell et al. (1989) in the all-sky catalogue "A Catalog of Rich Clusters of Galaxies" as cluster 3627. This all-sky catalog of clusters contains 4073 rich clusters of galaxies. Each cluster has at least 30 members within the magnitude range between the third brightest cluster member $m_3$ and $m_3 + 2$. Abell et al. (1989) defined rich clusters as those clusters with more than 50 members within the Abell radius $R_A = 1.7'/z$, where $z = v_{obs}/c$.

ACO 3627 has been named the Norma Cluster because of its prominence and location in the Norma constellation. The Norma cluster lies at $(\ell, b) = (325°.3, -7°.2)$, only 9° from the predicted center of the GA. Because it is obscured by the Milky Way, its prominence was never noted and it attracted little attention. The Norma cluster has an observed recession velocity of 4,882 km $s^{-1}$ (Kraan-Korteweg et al. 1996) which puts it also in redshift space at the heart of the GA. It has a large galaxy velocity dispersion of 897 km $s^{-1}$ implying that it is very massive. Kraan-Korteweg et al. (1996) determined a virial mass of 5.1 x $10^{15} h_{50}^{-1} M_\odot$ for this cluster. This mass alone accounts only about 10% for the GA mass which is on the order of $\sim 10^{16}$ solar masses. However, this massive cluster is one of the most likely clusters that appears the bottom of the GA's gravitational potential well.

ACO 3627 is the only rich cluster listed in the all-sky catalogue of Abell et al. (1989) behind the Milky Way. The predominance of early-type galaxies ($\sim$ 50%) at its core confirms its richness. Rich clusters are in general strong X-ray emitters. Analysis of ROSAT observations with the Position Sensitive Proportional Counter (PSPC) determined that the Norma cluster is the sixth brightest cluster in the ROSAT all-sky survey next to Virgo, Perseus, Coma, Ophiuchus and Centaurus clusters with a luminosity of 2.2 x $10^{44}$ erg $s^{-1}$ in the ROSAT energy band of 0.1-2.4 keV. While all the other X-ray bright clusters were well known, the Norma cluster was missed in previous X-ray surveys because of confusion with the Galactic X-ray bright binary 1H 1556-605. The ROSAT PSPC observations confirmed in fact that Norma is as massive as Coma (Böhringer et al. 1996). Similar to Coma, two dominant cD galaxies lie at

the core of ACO 3627. Simulations show that if Coma were located at the position of ACO 3627, it would look nearly identical to what it is seen for ACO 3627.

## 2.5 An Uncharted Nearby Cluster of Galaxies

Since the predicted mass of the GA region is about $10^{16}$ solar masses (Lynden & Bell et al. 1988), the Norma cluster with a mass of $10^{15}$ solar masses accounts only for 10% of the GA's mass. Velocity flows and mass-density fluctuations maps such as those shown in Fig. 2.4 and Fig. 2.5 indicate that the GA is a large extended concentration of mass. Only one rich cluster (ACO 3627) has been detected in that region. Hence, there may be more clusters hidden by the Milky Way which may be part of the large and extended mass concentration of the GA region.

The existence of another uncharted cluster of galaxies, similiar to Norma cluster, in the central region of the GA would have serious implications on our current understanding of the dynamical processes in the local Universe, within redshift distances of about 6,000 km $s^{-1}$.

There are strong indications that the second brightest extragalactic radio source in the southern sky PKS 1343−601, $f_{20cm} = 79$ Jy (McAdam 1991 and references therein), could mark the bottom of the potential well of another massive cluster in the GA overdensity. This radio galaxy at $(\ell, b, v) \sim (309.^{\circ}7, 1.^{\circ}8, 3,872$ km $s^{-1})$ lies behind the Milky Way. It is optically heavily obscured by 12 magnitudes of extinction in the $B$-band.

The optical counterpart of PKS 1343−601 resulted to be a heavily reddened E0 galaxy (West & Tarenghi 1989). With a recession velocity of $cz = 3{,}872$ km $s^{-1}$ this object seems to be a giant elliptical galaxy. West & Tarenghi (1989) reported an observed diameter of 28″ for this galaxy. Once corrected for extinction according to Cameron (1990), the observed diameter corresponds to an extinction-corrected diameter of 232″ at a distance of 73 Mpc.

This radio galaxy also shows significant X-ray emission. A short exposure image of PKS 1343−601 from the Einstein X-ray satellite shows two strong point X-ray sources in its vicinity (McAdam 1991). Because of the high foreground extinction, the ROSAT satellite did not detect X-ray emission in this region. However, diffuse hard X-ray emission from its radio lobes was detected with the ASCA satellite (Tashiro et al. 1998).

With an optical obscuration of about 12 magnitudes, not even the brightest galaxies pertaining to a cluster at that position would be visible. Figure 2.6 shows for

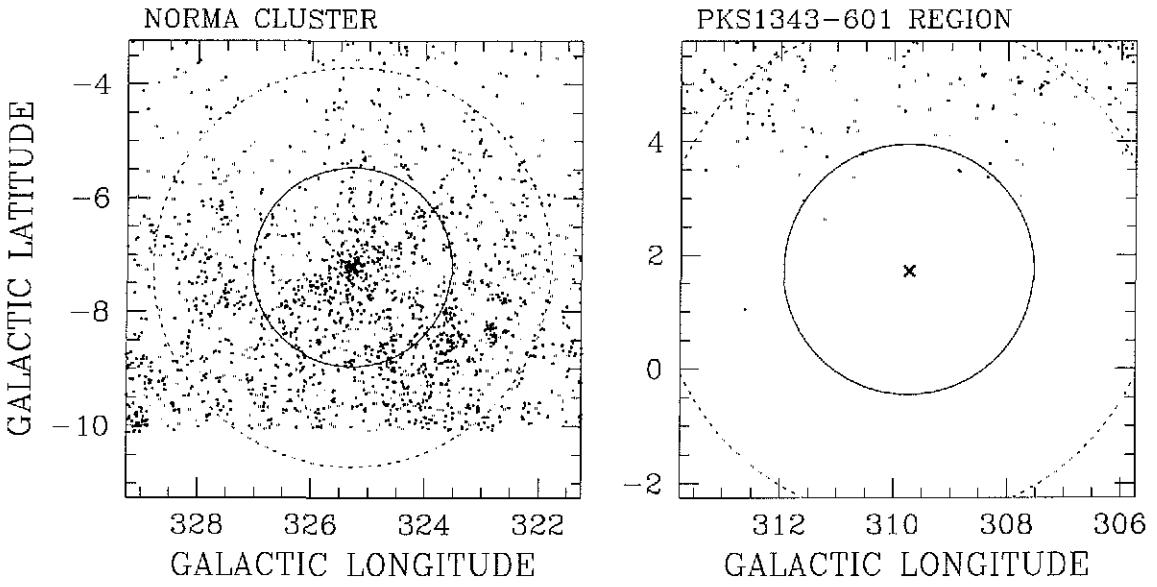




Figure 2.6: A comparison between the Norma cluster (left panel) with an extinction of $A_B \sim 1\overset{m}{.}5$ and the heavily obscured galaxies uncovered in the vicinity of PKS 1343−601 (right panel) with an extinction of $A_B \sim 12^m$.(From Kraan-Korteweg 2000b).

comparison the Norma cluster (left panel), known from deep optical ZOA searches (Woudt & Kraan-Korteweg 2001), artificially set at the distance and position of PKS 1343−601 (right panel). The inner circles in both distributions mark the respective Abell radius and the distribution of galaxies in the right panel is modulated by the extinction gradient. It is obvious that optical searches fail in uncovering galaxies at high levels of extinction. Observations in the near- and far-infrared where extinction effects are less severe are required to determine whether or not the giant elliptical radio galaxy PKS 1343−601 lies at the center of a massive cluster of galaxies.

To verify this, the region was imaged within its Abell radius in the $I$-band with the Wide Field Imager camera mounted on the MPG-ESO 2.2-m telescope at La Silla Observatory. Since extinction effects are less severe in the $I$-band ($A_I = 4\overset{m}{.}5$), observations in the $I$-band could unveil early-type galaxies members of this cluster if it is real. The observations and reductions are discused in the next chapter, before presenting the results in Chapter 4.

# Chapter 3

# Observations and Reductions

## 3.1 Introduction

This chapter describes the observations and the data reduction process. The observations were done within an area of 2° x 2° centered at the radio galaxy PKS 1343−601 ($\ell = 309\overset{\circ}{.}7$, $b = 1\overset{\circ}{.}8$) and were taken in the $I$-band with the Wide Field Imager (WFI) camera and the MPG-ESO 2.2-m telescope at La Silla Observatory, Chile. A total of 16 WFI fields were taken containing 128 $I$-band images. These images were reduced using the NOAO PC-IRAF[1] and the astronomical imaging and data visualization application SAOImage DS9. In Section 3.5, the Guide Star Catalogue (GSC 1.2) and the Digital Sky Survey (ESSO-DSSi) are used for the calibration of pixels in equatorial coordinates.

## 3.2 Observatory, Instruments and Observations

The observations for this thesis were provided by Dr. Patrick Alan Woudt of the Department of Astronomy of the University of Cape Town at the European Southern Observatory (ESO) La Silla, Chile, where he used the Wide Field Imager (WFI) mounted on the MPG/ESO 2.2-m telescope. The observations were made during three nights from May 19 to 21, 1999. The reduction and analysis of these observations are part of this thesis. The data consist of 16 fields that cover a field of 2° x 2° centered on a suspected rich cluster of galaxies marked by the strong radio galaxy PKS1343−601. Figure 3.1 shows the distribution of the 16 WFI fields taken in Galactic coordinates. The large circle in this figure corresponds to a circle with an Abell radius of $2\overset{\circ}{.}2$ and

[1]Image Reduction and Analysis Facility

Table 3.1: The observed fields are shown in this table with the filter used, the exposure time and the telescope pointing coordinates.

| WFI Field | Date of Observation | Filter 815.871 nm | Exp. Time (sec) | R.A. ($^h$ $^m$ $^s$) | Dec. ($^\circ$ $'$ $''$) | Equinox |
|---|---|---|---|---|---|---|
| Skyflat | 1999-05-20 | n816 | 1 | | | |
| Skyflat | 1999-05-20 | n816 | 4 | | | |
| Skyflat | 1999-05-20 | n816 | 5 | | | |
| Skyflat | 1999-05-20 | n816 | 7 | | | |
| Skyflat | 1999-05-20 | n816 | 9 | | | |
| Skyflat | 1999-05-20 | n816 | 14 | | | |
| PF01 | 1999-05-19 | n816 | 300 | 13 43 23.1 | −60 09 31 | B1950 |
| PF01 | 1999-05-19 | n816 | 300 | 13 43 31.1 | −60 08 31 | B1950 |
| PF01 | 1999-05-19 | n816 | 300 | 13 43 19.1 | −60 09 01 | B1950 |
| PF01 | 1999-05-19 | n816 | 300 | 13 43 27.1 | −60 10 01 | B1950 |
| PF01 | 1999-05-19 | n816 | 300 | 13 43 15.1 | −60 10 31 | B1950 |
| PF02 | 1999-05-19 | n816 | 600 | 13 47 23.1 | −59 39 31 | B1950 |
| PF03 | 1999-05-20 | n816 | 600 | 13 43 23.1 | −59 39 31 | B1950 |
| PF04 | 1999-05-20 | n816 | 600 | 13 39 23.1 | −59 39 31 | B1950 |
| PF05 | 1999-05-20 | n816 | 600 | 13 39 23.1 | −60 09 31 | B1950 |
| PF06 | 1999-05-20 | n816 | 600 | 13 39 23.1 | −60 39 31 | B1950 |
| PF07 | 1999-05-20 | n816 | 600 | 13 43 23.1 | −60 39 31 | B1950 |
| PF08 | 1999-05-20 | n816 | 600 | 13 47 23.1 | −60 39 31 | B1950 |
| PF09 | 1999-05-20 | n816 | 600 | 13 47 23.1 | −60 09 31 | B1950 |
| PF10 | 1999-05-21 | n816 | 600 | 13 49 23.1 | −59 09 31 | B1950 |
| PF11 | 1999-05-21 | n816 | 600 | 13 45 23.1 | −59 09 31 | B1950 |
| PF12 | 1999-05-21 | n816 | 600 | 13 41 23.1 | −50 09 31 | B1950 |
| PF13 | 1999-05-21 | n816 | 600 | 13 37 23.1 | −59 09 31 | B1950 |
| PF14 | 1999-05-20 | n816 | 600 | 13 35 23.1 | −59 39 31 | B1950 |
| PF15 | 1999-05-20 | n816 | 600 | 13 35 23.1 | −60 09 31 | B1950 |
| PF16 | 1999-05-20 | n816 | 600 | 13 35 23.1 | −60 39 31 | B1950 |

is centered at the position of PKS 1343−601. Field one is a superposition of five WFI exposures to obtain a better resolution at the center. Every WFI field consists of 8 images, the total amount of images treated in this thesis consists of 48 skyflats and 160 science images where the central field is the sum of five individual exposures.

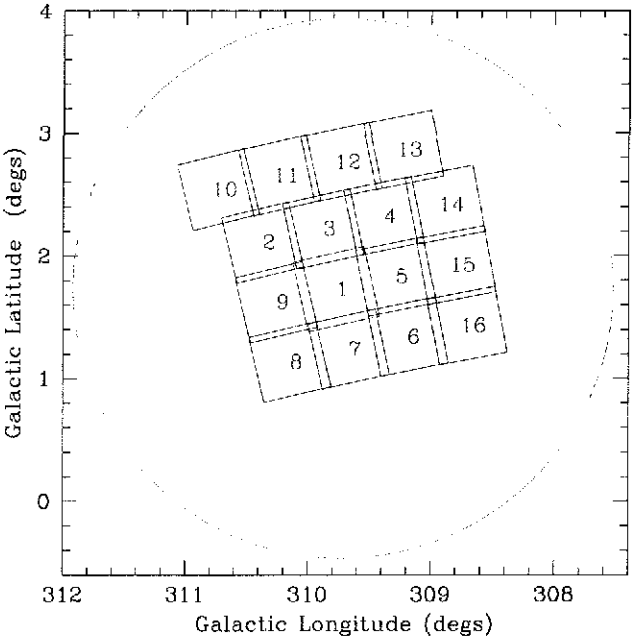




Figure 3.1: The 16 WFI fields imaged in the $I$-band around PKS 1343−601

### 3.2.1 The MPG-ESO Telescope at La Silla

The La Silla Observatory of ESO is located on the southern edge of the Atacama desert in Chile. Its geographical location is at 70°44′4.″543 W, 29°15′15.″433 S and an altitude of 2335 meters. The 2.2-m telescope is property of the Max Planck Gesellschaft (MPG) and has been on indefinite loan to ESO since 1984. Its mount is an equatorial-fork and it has a Ritchey-Chretien optical design. The WFI camera was the instrument used in this telescope for the observations.

### 3.2.2 The WFI

The Wide Field Imager (WFI) is a focal reducer-type camera. It is permanently mounted at the Cassegrain focus of the MPG-ESO 2.2-m telescope. Its field of view has a diameter of almost 0.8 degrees. Its detector has a coverage of 34′ x 33′. With these characteristics the WFI exceeds the field of view by at least a factor of two compared to other La Silla or VLT ESO instruments. The WFI consists of a mosaic of 4 x 2 CCD detectors, each 2142 × 4128 pixels. Therefore, one WFI fits file consists of 8 individual frames. The arrangement of the 8 chips is shown in Fig. 3.2. Each chip is about 2k x 4k in size. The gap between the chips is narrow and it yields a filling

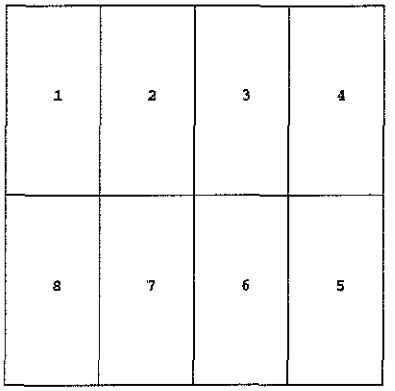


Figure 3.2: The CCD setup in the WFI detector at the MPG-ESO 2.2-m telescope.

factor of 95.9%. This instrument offers an excellent sensitivity from the atmospheric UV cut-off to the near IR. The WFI has a pixel scale of 0.238 arcsec/pixel. The observations for the present work were taken with the filter n816 which is centered at $\lambda_c = 815.9$ nanometers and a full-width at half-maximum of 20.928 nm. This is a narrower filter in comparison to the standard $I$-band filter.

## 3.3 The WFI Data Reduction Process

### 3.3.1 The Observational Data

The data consist of the following observations: six WFI skyflats and twenty WFI field exposures taken around the strong radio source PKS 1343−601. Table 3.1 shows the filter and the exposure times for each observation. To obtain a full spatial coverage for the central field (PF01), five exposures were taken with offsets shown in Fig. 3.3. Hence, the final central field PF01 is a superposition of five fields slightly offset for improved spatial coverage.

With the five exposures of field PF01, there are 20 exposures for a total of 16 different fields shown in Fig 3.1. One WFI FITS file consists of eight individual frames (images). The total data amount therefore to 48 skyflats and 160 science images and the reduced data consists of eight normalized flats and 128 reduced images.

The following notation was applied to the WFI data. Each WFI FITS-file (or field) consists of eight individual frames or images. The notation for flats is `nflat#` where `#` indicates the frame number, from 1 to 8. Reduced images were named `PFN_#`, where `P` refers to PKS1343-601, and `F` stands for field. Moreover, `N` is the field number from

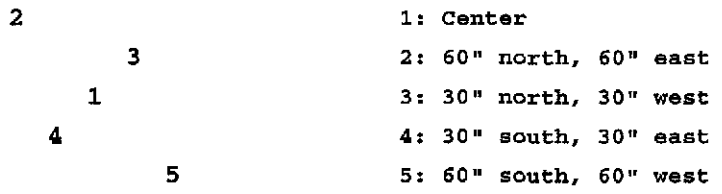


Figure 3.3: The offsets applied to the 5 exposures of the central field, PF01.

1 to 16 and # the frame number 1 to 8. For example, frame number 3 of field twelve is called image `PF12_3`. For images calibrated in equatorial coordinates, `RADec` precedes the previous notation. For example, the image in RA and Dec for frame 3 of field number twelve is `RADecPF12_3`. Since all images are FITS files, the image names are followed by the extension ".fits", for example `PF12_3.fits`.

### 3.3.2 Reduction Process for the Flat Fields

"Flat fields" are used for CCD normalization. In a CCD, each pixel has a different quantum response to light. Therefore, "flats" are used to normalize the pixels in a CCD to the mean of all the pixels. For the six skyflat exposures, 48 flat fields had to be reduced and combined. They were overscan subtracted and combined to one common skyflat. The first step in this procedure was the determination of the overscan-region in each frame. Figure 3.4 shows the WFI flat frame 3 as an example of a flat with its unexposed borders. The overscan subtraction for frame number three was given by a section on the right unexposed region as shown in Fig. 3.4. The image on the right hand side is an amplified section of the bottom right corner of the left image and shows part of the unexposed area of the CCD used to compute the overscan subtraction.

Each WFI flat field consists of 8 frames (images). The size of each frame is 2142 x 4128 pixels. The overscan regions were determined with IRAF's task *implot*. The *implot* commands *c*, *l*, *e*, and *r* were used to create column, line, expand, and reset plots respectively. With these *implot* commands and column commands

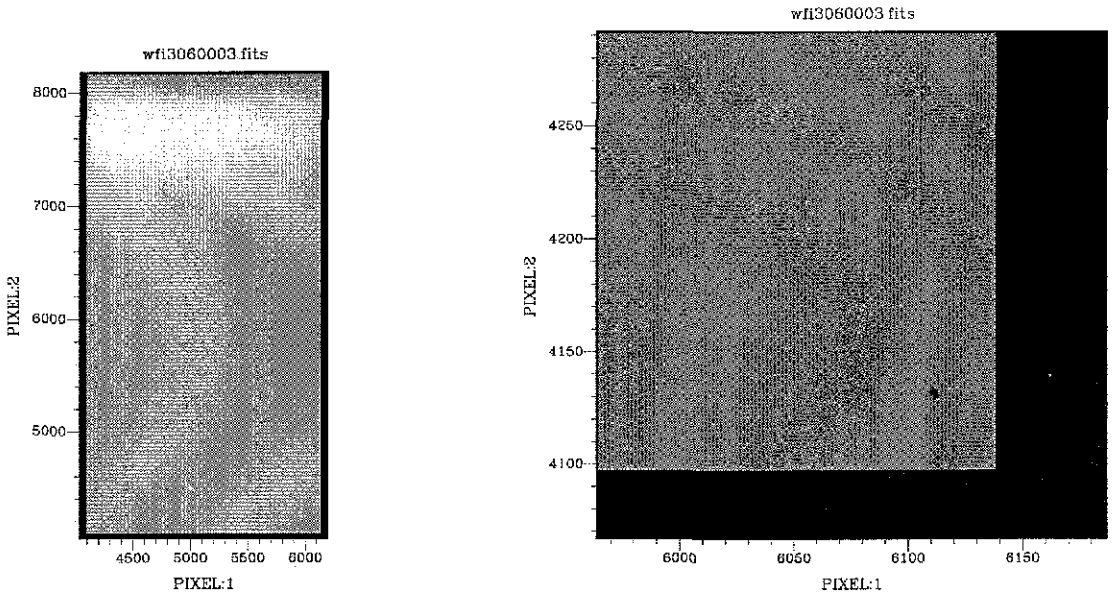


Figure 3.4: Frame number 3 of the WFI flat. The right image is an amplification of the bottom right corner of the left image (flat) to show a part of the section used to compute the overscan subtraction.

like: *c N M* and *l N M* the overscan regions for the eight flat frames were determined. N and M determine de range of columns or lines to be plotted. For frames 1, 2, 3, and 4, the overscan regions are the same: [2121:2140, 31:3500]. Frames 5, 6, and 7 have their overscan region in [2:22, 629:4098]. An overscan region of [2121:2140, 629:4098] was selected for frame 8 because it is upside down with respect to frame number 1.

In addition to the region used for the overscan susbtraction there were other sections on the CCD's that were not exposed, for example the bottom edge of the right hand side image shown in Fig. 3.4. These unexposed regions of the flats were trimmed including the unexposed areas from which the overscan subtraction was computed. The trimming of each frame was determined using the *implot* task. Similar to the overscan regions, frames have different trimming sections. For frames 1, 2, 3, and 4, the trimming sections are [51:2094, 31:4128]. A trimming of [49:2092, 1:4098] was applied to frames 5, 6, and 7, and a trimming of [51:2094, 1:4098] to frame number 8.

The frames were then overscan-subtracted and trimmed using the IRAF task *colbias*. After the overscan-subtraction and trimming, the final image sizes are 2044 x 4098 pixels. The six different skyflat exposures for each frame were combined into one using the IRAF task *flatcombine*. The task *imstatistics* was used to compute the

mean of each frame. The eight frames were normalized with *imarith*, dividing them by the mean value calculated with *imstatistics*. The resulting eight normalized flat frames were used to flatfield the Wide Field Imager data.

### 3.3.3 Reduction Process for the WFI Images

The WFI data consist of 16 fields with a total of 160 images including the images of five different exposures of the central field, PF01. All frames were bias-subtracted and trimmed with *colbias* using the same bias and trimming sections as for the flats. The images were then divided by the normalized flats with the IRAF task *imarith*. Besides the transformation from pixel to equatorial coordinates, this was the end of the reduction process except for the central field images, `PF01_1`, ... , `PF01_8`.

For the central field (PF01), five exposures were made with offsets as shown in Fig. 3.3. To be able to combine the five exposures for each of the eight frames, the offset of the five exposures relative to one of them had to be determined. The offsets were computed with the IRAF task *imexamine* as follows: four of the five exposures for one frame were displayed at the same time in the image display tool SAOImage DS9. DS9 can display a maximum of four images at one time and the fifth image was displayed as soon as one of the previous ones was not needed anymore. The idea was to find the offset of four of them with respect to the fifth one. A star that could be identified in all five was marked. Then, with *imexamine* the pixel coordinates of that star were determined in all five images. With the pixel coordinates for one star, the offsets of four images with respect to the fifth were determined. The IRAF task *imalign* was used to improve further the offset coordinates. The offsets were stored in a text file that was then used as input of *imalign* parameter `shifts`. Also, *imalign* requires a list of the pixel coordinates of 24 stars as the input for its parameter `coords`. The coordinates of these 24 stars were given to *imalign* to further improve the offsets calculated using only one star. The *imalign* ouput are the improved offset values. A text file containing the improved offsets was used as the input for the IRAF task *imcombine* parameter `offsets`. The five images for each frame of field one were finally combined using this IRAF task. Once all data images were trimmed, flatfielded and combined accordingly, one can proceed with the search for galaxies (see section 4).

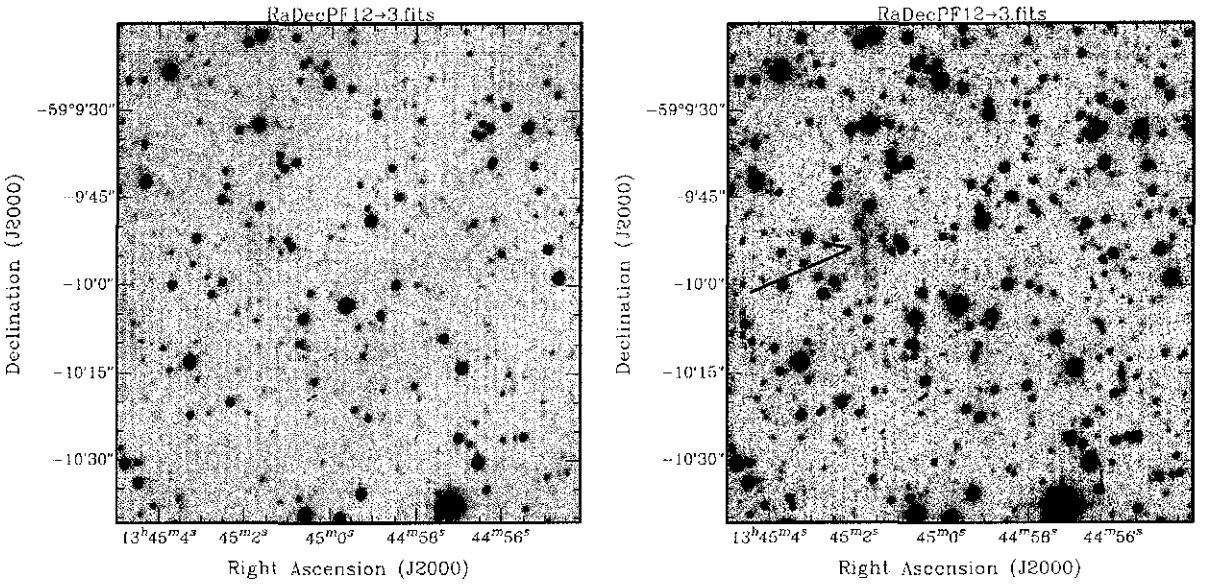


Figure 3.5: Both images are the same and are part of field 12 frame 3 image, RaDecPF12_3. The image on the left side is displayed with a higher cutoff intensity level than the one on the right side. A very flat galaxy, possibly an edge-on spiral, is observed in the image on the right.

## 3.4 The Search of Galaxies by Eye

With all the 128 images reduced, the search for galaxies by eye could begin. Most of the galaxies in the WFI images are fainter and smaller than stars, partly due to the extinction. Hundreds or thousands of stars are present in each of the images since we are looking along the Galactic plane. Therefore, searching galaxies by eye is more efficient and simple than using a mathematical extraction algorithm. As an example of the crowding Fig. 3.7 shows the image of PF12_3 in RA and Dec coordinates. Figure 3.7 clearly illustrates the very high number of stars present in all images.

Using IRAF and the image display tool SAOImage DS9, a meticulous search for galaxies was done by eye on each of the 128 reduced images. XImtool is another image display tool that can be used instead of DS9. I personally preferred the use of DS9 since XImtool runs only under 8 bits whereas I was using a PC running Red Hat Linux OS at 16 bits.

My search for galaxies was conducted as follows: One image at a time was displayed using DS9, zooming into the image and continously varying the contrast. In this way galaxies can be spotted through the difference in the way their size and

surface brightness change compared to stars. An example of this change in galaxy's appearance by varying the image contrast can be visualized in Fig. 3.5. A very low surface brightness galaxy, probably an edge-on spiral is recognizable in the right panel of Fig. 3.5, while it is not visible at all in the left panel. Notice that fainter objects are visible in the right panel compared to the left panel of Fig. 3.5. By changing the contrast of a displayed image, the cut-off intensity level of that image can be varied and fainter objects can be identified.

Once a galaxy candidate was found, IRAF task *imexamine* was used substantially to help with the classification of a candidate as a galaxy. *Imexamine* has some very helpful commands to ascertain the morphology of the objects as galaxies. These basically are the following commands: $s$ to make surface plots, $r$ to plot radial profiles and $e$ for contour plots of possible galaxy candidates.

## 3.5 Calibration of Pixels in Equatorial Coordinates

To determine the equatorial coordinates RA and Dec of the identified galaxies and galaxy candidates, it was necessary to transform the image coordinates given in pixels to RA and Dec coordinates. To accomplish this, one first had to determine the observed central position of every image. Then, with images calibrated in RA and Dec from the *European Southern Observatory* online *Digitized Sky Survey 2-Infrared* (DSS2i), star positions from the *Guide Star Catalog* version 1.2 (GSC 1.2) and the IRAF tasks *imexamine* and *ccmap*, the transformations from pixel to equatorial coordinates for all images could be accomplished. This procedure is explained in more detail in the following sections.

### 3.5.1 Determination of the Image Centers

The data consist of 16 WFI exposures. The detector of the WFI has a mosaic of 4x2 CCD detectors, each of which has 2142 columns and 4128 rows. For each of the 16 observed fields there are eight CCD images of 2142 columns by 4128 rows of pixels before reduction. Using the pointing coordinates of the telescope for the 16 fields as listed in Table 3.1 and the relative positions of the eight CCD detectors (WFI's field of view), the coordinates of the centers of all eight subimages of each of the WFI fields were determined. Figure 3.2 shows the eight CCD setup for each WFI field. Although the exact WFI field of view is 0.567° x 0.55°, I worked with a field of view of 0.54° x 0.54° for symmetry reasons and to simplify the calculations as only rough

Table 3.2: Estimated centers for the data images (Equinox B1950.0)

| Subfield | $\alpha$ (1950) | $\delta$ (1950) | Subfield | $\alpha$ (1950) | $\delta$ (1950) |
|---|---|---|---|---|---|
| PF01_1 | 13 45 24.39 | -60 01 25 | PF09_1 | 13 49 25 | -60 01 25 |
| PF01_2 | 13 44 19.54 | -60 01 25 | PF09_2 | 13 48 20 | -60 01 25 |
| PF01_3 | 13 43 14.7 | -60 01 25 | PF09_3 | 13 47 16 | -60 01 25 |
| ... | ... | ... | PF09_4 | 13 46 11 | -60 01 25 |
| | | | PF09_5 | 13 46 10 | -60 17 37 |
| | | | ... | ... | ... |

estimates of the image centers are required.

Using the pointing coordinates of the telescope, the size of the observed field and the knowledge that there are 8 chips with narrow gaps between them, the subimage centers could be calculated. In Table 3.2, the centers for the first three subimages of the central field (PF01) and for the first five subimages of field PF09 are shown as an example. When comparing the DSS-2i with the data images, I found an offset in the pointing of the telescope. This offset occurs in both RA and Dec directions. The shift in RA is positive and varies from field to field. It is around 25 arcsec $\pm$ few arcsec. The offset in Dec is about the same as in RA. Instead of calculating it, I selected DDS-2i images big enough so that they always covered the whole area of the data images. The DSS-2i images did not need to match the data images exactly as they were only needed to identify the stars that were used for the coordinate transformations.

### 3.5.2 The ESO Online Digitized Sky Survey (ESO-DSS2i)

The Science Archive Facility of ESO and the Space Telescope - European Coordinating Facility (ST-ECF) provides access to the Digitized Sky Surveys phase 2 (DSS-2) produced by the Space Telescope Science Institute (STScI) through its Catalogs and Surveys Branch (CASB). The DSS-2 is the digitized version of the photographic sky surveys plates from the Palomar and UK Schmidt telescopes. The sky coverage for each of these plates is 6.5 x 6.5 degrees. Since my data images are in the I band, DDS-2 images were downloaded from the infrared on-line version (DSS-2i) that had 27% of the sky available in 2001, including the area of the sky where the observations of PKS 1343−601 were taken. The estimated central positions in RA and Dec of the data images as well as their size in arcminutes (8.′1 x 16.′2) were used to obtain

images from the DSS-2i that correspond to the part of the sky covered by the data images. Since the data consist of 16 fields that gives a total of 128 images, the same number of DSS-2i images were downloaded. ESO DSS2i can be consulted on the web at http://archive.eso org/dss/dss.

### 3.5.3 The Guide Star Catalog

The *Guide Star Catalog* (GSC) is made available by the CASB of the STScI. The GSC is also based on the sky survey plates from Palomar and UK Schmidt telescopes. The first generation GSC (GSC I) was constructed by CASB to support the pointing and target acquisition for the Hubble Space Telescope. The first generation version 1.2 of the GSC was used in this thesis to obtain accurate star positions. The STScI in collaboration with the *Astronomisches Rechen-Institut* produced a new astrometric recalibration of GSC I. This new astrometric reduction, GSC 1.2, of the GSC plate material has eliminated the major systematic errors that were found in the previous version (GSC 1.1). The GSC I is an all-sky optical catalog that has the positions and magnitudes of approximately 19 million stars and other objects in the magnitude range from $6^m$ to $15^m$. The GSC is available on the web at http://www-gsss.stsci.edu/gsc/GSChome.htm.

### 3.5.4 SAOImage DS9

DS9 is the astronomical imaging and data visualization tool that was used to display and analyze DSS-2i and data images. DS9 is produced by the research and development group of the High Energy Astrophysics Division (HEAD) of the Smithsonian Astrophysical Observatory (SAO). It provides support for FITS images and easy communication with IRAF. Among the many features that DS9 offers are: multiple frame buffers, region manipulation, blinking, tiling, geometric markers, colormap manipulation, rotation, scaling (scale algorithms), zooming, pan, and several coordinate systems. DS9 is a stand-alone application and free distributed software. For more information about DS9 or to download it, consult its homepage: http://hea-www.harvard.edu/RD/index.html.

### 3.5.5 IRAF Tasks: *imexam* and *ccmap*

Both IRAF tasks *imexam* and *ccmap* were used in the transformation of positions from pixel coordinates to right ascension and declination coordinates. IRAF's task

*imexam* is useful to examine images through various types of plots and text outputs. This task has several features of IRAF image display and graphics facilities. The *ccmap* task makes use of a list of matched pixel and equatorial coordinates to compute the transformation of coordinates for an image. The IRAF tasks have two types of parameters: required and hidden parameters. The parameters determine how the task operations will be done.

### 3.5.6 The Transformation of Pixels to Equatorial Coordinates

The transformations from pixel to RA and Dec coordinates were done for all the images in which galaxies were found. The first step was to get DSS-2i images and GSC 1.2 star positions for the area of the sky covered by all 128 data images. Knowing the data image centers and their size, 128 DSS-2i images and lists of star positions were obtained for the same area of the sky. Since the DSS-2i images are calibrated in equatorial coordinates, they were used to identify the stars in data images that have positions in the GSC 1.2.

The number of stars contained in the 128 GSC 1.2 lists for the data images ranges from 80 to 150 stars. A sample of the first 50 stars in the GSC 1.2 star position list for the data image PF12_3 is shown in Table 3.3. Generally between 5 to 10 stars were selected from the GSC 1.2 star list to obtain a low *rms* (about 0.1") for RA and Dec transformations. The GSC 1.2 star position list has to be prepared for the star selection process. The selection criteria was the following: Star positions with errors larger than 0.4 were deleted from the list. The remaining stars were sorted by magnitude in order to select stars with magnitudes in the range $12.5 \leq \mathrm{m} < 15.0$. Stars with magnitudes $m \leq 12.5$ are too bright and stars with $m \geq 15.0$ are too faint to obtain good measurements of their centers in pixel coordinates. The list was also sorted in decreasing Dec to delete from list those stars which were not in the data image. This procedure led to a final list of stars which were possible candidates to be used for the coordinate transformations. As an example, the selection of stars from Table 3.3 is shown in Table 3.4.

To identify the selected stars with equatorial positions on the data images, a data image with its corresponding DSS-2i image was displayed in DS9 in tile mode. From the sorted star position list, a star was selected. Then, using its coordinates as given in the GSC, the star was searched on the DSS-2i image which is calibrated in equatorial coordinates. Once the star was found in the DSS-2i image, the DSS-2i was used as

Guide Star Catalogue (copyright,AURA 1989-1998)

Position (J2000) : 13 44 38.95 -59 16 27.9  Box (arcmin): 18.00 x 18.00
No.Entries : 148  No.Selected : 148

| Guide | Star ID | H | M | S | D | M | S | err | Mag | err | Bp | Cl | Plt | n | IIPDGBFN | [illegible] |
|---|---|---|---|---|---|---|---|---|---|---|---|---|---|---|---|---|
| 8675 | 2334 | 13 | 44 | 49.89 | -59 | 08 | 10.1 | 0.3 | 12.80 | 0.40 | 0 | 02 | 007L | 2 | FFTFFFTF | 1976.256 |
| 8675 | 2334 | 13 | 44 | 49.90 | -59 | 08 | 9.8 | 0.3 | 12.55 | 0.40 | 0 | 02 | 02EW | 2 | FFTFFFTF | 1975.497 |
| 8675 | 1270 | 13 | 45 | 0.33 | -59 | 08 | 38.0 | 0.4 | 13.75 | 0.40 | 0 | 30 | 02EW | 1 | FFTFFFFF | 1975.497 |
| 8675 | 2505 | 13 | 43 | 39.95 | -59 | 09 | 7.4 | 0.3 | 13.27 | 0.40 | 0 | 02 | 02EW | 1 | FFTFFFFF | 1975.497 |
| 8675 | 1776 | 13 | 45 | 13.66 | -59 | 09 | 46.3 | 0.4 | 10.09 | 0.40 | 0 | 02 | 007L | 2 | FFTFFFTF | 1976.256 |
| 8675 | 1776 | 13 | 45 | 13.70 | -59 | 09 | 46.0 | 0.4 | 10.46 | 0.40 | 0 | 02 | 02EW | 2 | FFTFFFTF | 1975.497 |
| 8675 | 1200 | 13 | 43 | 44.93 | -59 | 10 | 5.4 | 0.3 | 14.05 | 0.40 | 0 | 30 | 02EW | 1 | FFTFFFFF | 1975.497 |
| 8675 | 1920 | 13 | 43 | 43.91 | -59 | 10 | 10.3 | 0.8 | 13.25 | 0.40 | 0 | 22 | 007L | 2 | FFTFFFTF | 1976.256 |
| 8675 | 1920 | 13 | 43 | 44.03 | -59 | 10 | 11.8 | 2.1 | 13.13 | 0.40 | 0 | 22 | 02EW | 2 | FFTFFFTF | 1975.497 |
| 8675 | 1504 | 13 | 45 | 22.28 | -59 | 10 | 1.5 | 0.3 | 13.17 | 0.40 | 0 | 02 | 007L | 2 | FFTFFFTF | 1976.256 |
| 8675 | 1504 | 13 | 45 | 22.30 | -59 | 10 | 1.2 | 0.3 | 12.92 | 0.40 | 0 | 02 | 02EW | 2 | FFTFFFTF | 1975.497 |
| 8675 | 1132 | 13 | 44 | 0.17 | -59 | 10 | 12.7 | 1.2 | 13.42 | 0.40 | 0 | 30 | 02EW | 1 | FFTFFFFF | 1975.497 |
| 8675 | 1546 | 13 | 43 | 44.36 | -59 | 10 | 18.8 | 0.3 | 11.38 | 0.40 | 0 | 22 | 007L | 2 | FFTFFFTF | 1976.256 |
| 8675 | 1546 | 13 | 43 | 44.32 | -59 | 10 | 18.3 | 0.3 | 11.50 | 0.40 | 0 | 22 | 02EW | 2 | FFTFFFTF | 1975.497 |
| 8675 | 2400 | 13 | 45 | 35.11 | -59 | 10 | 4.5 | 0.3 | 13.34 | 0.40 | 0 | 01 | 007L | 2 | FFTFFFTF | 1976.256 |
| 8675 | 2400 | 13 | 45 | 35.12 | -59 | 10 | 4.1 | 0.3 | 12.92 | 0.40 | 0 | 30 | 02EW | 2 | FFTFFFTF | 1975.497 |
| 8675 | 1474 | 13 | 45 | 6.63 | -59 | 10 | 10.9 | 0.4 | 13.13 | 0.40 | 0 | 01 | 007L | 2 | FFTFFFTF | 1976.256 |
| 8675 | 1474 | 13 | 45 | 6.58 | -59 | 10 | 11.1 | 0.3 | 12.84 | 0.40 | 0 | 30 | 02EW | 2 | FFTFFFTF | 1975.497 |
| 8675 | 1050 | 13 | 45 | 15.63 | -59 | 10 | 13.0 | 0.4 | 11.67 | 0.40 | 0 | 03 | 007L | 2 | FFTFFFTF | 1976.256 |
| 8675 | 1050 | 13 | 45 | 15.65 | -59 | 10 | 12.8 | 0.4 | 11.80 | 0.40 | 0 | 02 | 02EW | 2 | FFTFFFTF | 1975.497 |
| 8675 | 1634 | 13 | 44 | 38.99 | -59 | 10 | 37.0 | 1.2 | 13.46 | 0.40 | 0 | 02 | 02EW | 1 | FFTFFFFF | 1975.497 |
| 8675 | 2036 | 13 | 44 | 8.08 | -59 | 11 | 50.7 | 0.3 | 13.42 | 0.40 | 0 | 02 | 02EW | 1 | FFTFFFFF | 1975.497 |
| 8675 | 2491 | 13 | 45 | 37.33 | -59 | 11 | 50.2 | 0.4 | 13.50 | 0.40 | 0 | 02 | 007L | 2 | FFTFFFTF | 1976.256 |
| 8675 | 2491 | 13 | 45 | 37.35 | -59 | 11 | 50.2 | 0.4 | 13.03 | 0.40 | 0 | 30 | 02EW | 2 | FFTFFFTF | 1975.497 |
| 8675 | 1102 | 13 | 44 | 29.08 | -59 | 12 | 24.0 | 0.3 | 13.55 | 0.40 | 0 | 30 | 007L | 2 | FFTFFFTF | 1976.256 |
| 8675 | 1102 | 13 | 44 | 29.13 | -59 | 12 | 23.3 | 0.3 | 13.38 | 0.40 | 0 | 30 | 02EW | 2 | FFTFFFTF | 1975.497 |
| 8675 | 1216 | 13 | 43 | 58.17 | -59 | 12 | 32.2 | 0.6 | 14.57 | 0.40 | 0 | 30 | 02EW | 1 | FFTFFFFF | 1975.497 |
| 8675 | 1616 | 13 | 44 | 29.18 | -59 | 12 | 36.9 | 0.3 | 12.21 | 0.40 | 0 | 00 | 007L | 2 | FFTFFFTF | 1976.256 |
| 8675 | 1616 | 13 | 44 | 29.18 | -59 | 12 | 36.1 | 0.3 | 11.71 | 0.40 | 0 | 00 | 02EW | 2 | FFTFFFTF | 1975.497 |
| 8675 | 1532 | 13 | 43 | 57.99 | -59 | 12 | 50.6 | 0.3 | 15.08 | 0.40 | 0 | 30 | 02EW | 1 | FFTFFFFF | 1975.497 |
| 8675 | 1138 | 13 | 43 | 56.76 | -59 | 12 | 59.3 | 1.2 | 14.80 | 0.40 | 0 | 30 | 007L | 2 | FFTFFFTF | 1976.256 |
| 8675 | 1138 | 13 | 43 | 57.13 | -59 | 12 | 58.6 | 0.3 | 14.13 | 0.40 | 0 | 30 | 02EW | 2 | FFTFFFTF | 1975.497 |
| 8675 | 1446 | 13 | 43 | 39.14 | -59 | 13 | 27.1 | 1.2 | 13.52 | 0.40 | 0 | 02 | 02EW | 1 | FFTFFFFF | 1975.497 |
| 8675 | 2490 | 13 | 45 | 2.59 | -59 | 13 | 21.4 | 0.3 | 13.54 | 0.40 | 0 | 30 | 007L | 2 | FFTFFFTF | 1976.256 |
| 8675 | 2490 | 13 | 45 | 2.57 | -59 | 13 | 20.6 | 0.3 | 13.21 | 0.40 | 0 | 30 | 02EW | 2 | FFTFFFTF | 1975.497 |
| 8675 | 182 | 13 | 44 | 57.89 | -59 | 13 | 22.7 | 0.4 | 11.88 | 0.40 | 0 | 02 | 007L | 2 | FFTFFFTF | 1976.256 |
| 8675 | 182 | 13 | 44 | 57.88 | -59 | 13 | 21.9 | 0.3 | 11.96 | 0.40 | 0 | 02 | 02EW | 2 | FFTFFFTF | 1975.497 |
| 8675 | 1948 | 13 | 45 | 14.08 | -59 | 13 | 37.1 | 0.3 | 14.17 | 0.40 | 0 | 30 | 02EW | 1 | FFTFFFFF | 1975.497 |
| 8675 | 1162 | 13 | 45 | 20.92 | -59 | 13 | 37.8 | 1.2 | 13.77 | 0.40 | 0 | 30 | 02EW | 1 | FFTFFFFF | 1975.497 |
| 8675 | 1452 | 13 | 45 | 21.55 | -59 | 13 | 50.4 | 0.3 | 13.52 | 0.40 | 0 | 30 | 02EW | 1 | FFTFFFFF | 1975.497 |
| 8675 | 2439 | 13 | 43 | 46.05 | -59 | 14 | 4.7 | 0.3 | 14.92 | 0.40 | 0 | 30 | 02EW | 1 | FFTFFFFF | 1975.497 |
| 8675 | 988 | 13 | 45 | 22.53 | -59 | 13 | 52.3 | 0.3 | 14.84 | 0.40 | 0 | 30 | 02EW | 1 | FFTFFFFF | 1975.497 |
| 8675 | 94 | 13 | 43 | 47.92 | -59 | 14 | 5.0 | 1.2 | 14.25 | 0.40 | 0 | 30 | 02EW | 1 | FFTFFFFF | 1975.497 |
| 8675 | 3300 | 13 | 43 | 57.27 | -59 | 14 | 9.9 | 0.2 | 6.56 | 0.10 | 4 | 03 | 56 | 1 | TFTFFFFT | 2000.000 |
| 8675 | 3301 | 13 | 44 | 1.80 | -59 | 14 | 10.8 | 0.2 | 7.77 | 0.10 | 4 | 03 | 56 | 1 | TFTFFFFT | 2000.000 |
| 8675 | 757 | 13 | 44 | 7.40 | -59 | 14 | 12.4 | 1.2 | 14.63 | 0.40 | 0 | 30 | 02EW | 1 | FFTFFFFF | 1975.497 |
| 8675 | 2130 | 13 | 44 | 8.69 | -59 | 14 | 13.8 | 0.4 | 14.17 | 0.40 | 0 | 30 | 02EW | 1 | FFTFFFFF | 1975.497 |
| 8675 | 3198 | 13 | 43 | 47.30 | -59 | 14 | 17.2 | 1.2 | 13.28 | 0.40 | 0 | 00 | 007L | 1 | FFTFFFFF | 1976.256 |
| 8675 | 1808 | 13 | 44 | 9.70 | -59 | 14 | 14.4 | 0.8 | 15.06 | 0.40 | 0 | 30 | 02EW | 1 | FFTFFFFF | 1975.497 |
| 8675 | 2330 | 13 | 44 | 11.75 | -59 | 14 | 15.0 | 0.4 | 15.17 | 0.40 | 0 | 30 | 02EW | 1 | FFTFFFFF | 1975.497 |
| 8675 | 1314 | 13 | 44 | 13.95 | -59 | 14 | 16.1 | 0.3 | 15.13 | 0.40 | 0 | 30 | 02EW | 1 | FFTFFFFF | 1975.497 |

Table 3.3: The first 50 of 140 stars of the GSC 1.2 star positions list for data image PF12_3.

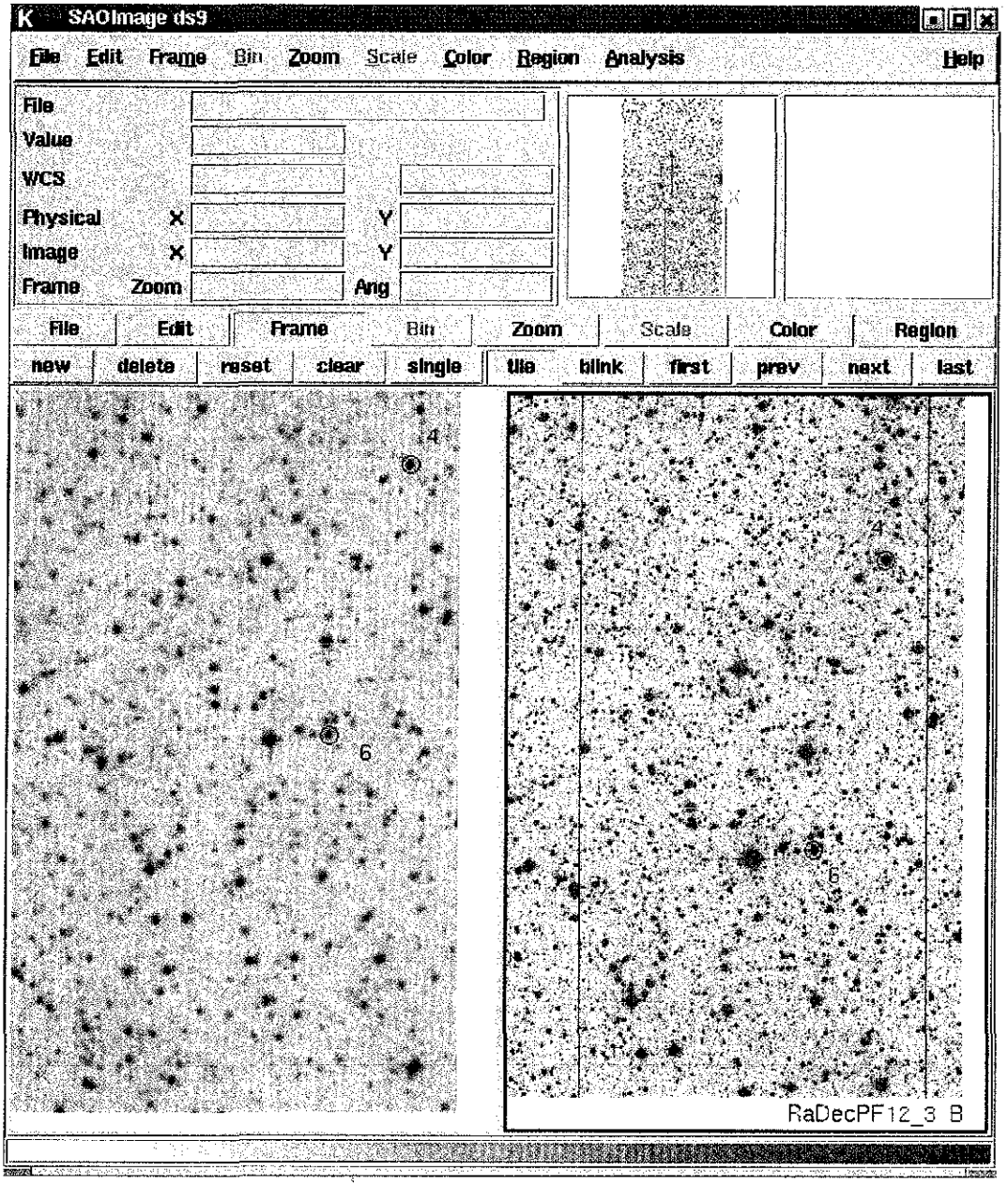


Figure 3.6: Two stars that have equatorial positions in the GSC 1.2 are marked in data image PF12_3 (right panel) after they where identified using its respective DSS-2i image (left panel) calibrated in equatorial coordinates.

Guide Star Catalogue (copyright,AURA 1989-1998)

Position (J2000) : 13 44 38.95 -59 16 27.9  Box (arcmin): 18.00 x 18.00
No.Entries : 148  No.Selected : 148

s#: selected star  s: n□ used  N: bad selection

| | Guide Star ID | H | M | S | D | M | S | err | Mag | err | Bp | Cl | Plt | n | IIPDGBFN | |
|---|---|---|---|---|---|---|---|---|---|---|---|---|---|---|---|---|
| s1 | 8675 | 2334 | 13 | 44 | 49.90 | -59 | 08 | 9.8 | 0.3 | 12.55 | 0.40 | 0 | 02 | 02EW | 2 | FFTFFFTF | 1975.497 |
| | 8675 | 2334 | 13 | 44 | 49.89 | -59 | 08 | 10.1 | 0.3 | 12.80 | 0.40 | 0 | 02 | 007L | 2 | FFTFFFTF | 1976.256 |
| | 8675 | 1474 | 13 | 45 | 6.58 | -59 | 10 | 11.1 | 0.3 | 12.84 | 0.40 | 0 | 30 | 02EW | 2 | FFTFFFTF | 1975.497 |
| s2 | 8675 | 2036 | 13 | 44 | 8.08 | -59 | 11 | 50.7 | 0.3 | 13.42 | 0.40 | 0 | 02 | 02EW | 1 | FFTFFFFF | 1975.497 |
| | 8675 | 1102 | 13 | 44 | 29.13 | -59 | 12 | 23.3 | 0.3 | 13.38 | 0.40 | 0 | 30 | 02EW | 2 | FFTFFFTF | 1975.497 |
| | 8675 | 1102 | 13 | 44 | 29.08 | -59 | 12 | 24.0 | 0.3 | 13.55 | 0.40 | 0 | 30 | 007L | 2 | FFTFFFTF | 1976.256 |
| s3 | 8675 | 2490 | 13 | 45 | 2.57 | -59 | 13 | 20.6 | 0.3 | 13.21 | 0.40 | 0 | 30 | 02EW | 2 | FFTFFFTF | 1975.497 |
| | 8675 | 2490 | 13 | 45 | 2.59 | -59 | 13 | 21.4 | 0.3 | 13.54 | 0.40 | 0 | 30 | 007L | 2 | FFTFFFTF | 1976.256 |
| | 8675 | 2014 | 13 | 44 | 29.89 | -59 | 14 | 40.2 | 0.3 | 13.17 | 0.40 | 0 | 30 | 02EW | 1 | FFTFFFFF | 1975.497 |
| s | 8675 | 916 | 13 | 44 | 8.10 | -59 | 14 | 47.7 | 0.3 | 13.78 | 0.40 | 0 | 30 | 02EW | 2 | FFTFFFTF | 1975.497 |
| | 8675 | 1918 | 13 | 44 | 9.21 | -59 | 14 | 47.7 | 0.3 | 12.51 | 0.40 | 0 | 00 | 02EW | 2 | FFTFFFTF | 1975.497 |
| | 8675 | 1918 | 13 | 44 | 9.26 | -59 | 14 | 48.3 | 0.3 | 13.54 | 0.40 | 0 | 00 | 007L | 2 | FFTFFFTF | 1976.256 |
| | 8675 | 916 | 13 | 44 | 8.05 | -59 | 14 | 48.4 | 0.3 | 14.88 | 0.40 | 0 | 30 | 007L | 2 | FFTFFFTF | 1976.256 |
| | 8675 | 2321 | 13 | 44 | 9.72 | -59 | 16 | 33.6 | 0.3 | 14.88 | 0.40 | 0 | 30 | 02EW | 1 | FFTFFFFF | 1975.497 |
| N | 8675 | 2585 | 13 | 44 | 24.98 | -59 | 17 | 45.4 | 0.3 | 13.71 | 0.40 | 0 | 30 | 02EW | 1 | FFTFFFFF | 1975.497 |
| s4 | 8675 | 2533 | 13 | 44 | 7.50 | -59 | 18 | 14.0 | 0.3 | 13.46 | 0.40 | 0 | 02 | 02EW | 1 | FFTFFFFF | 1975.497 |
| | 8675 | 1214 | 13 | 44 | 11.45 | -59 | 19 | 19.1 | 0.3 | 13.29 | 0.40 | 0 | 30 | 02EW | 1 | FFTFFFFF | 1975.497 |
| | 8675 | 2044 | 13 | 44 | 3.69 | -59 | 19 | 51.7 | 0.2 | 13.17 | 0.40 | 0 | 30 | 02EW | 2 | FFTFFFTF | 1975.497 |
| | 8675 | 2044 | 13 | 44 | 3.68 | -59 | 19 | 51.9 | 0.3 | 13.29 | 0.40 | 0 | 30 | 007L | 2 | FFTFFFTF | 1976.256 |
| s5 | 8675 | 1466 | 13 | 45 | 0.23 | -59 | 19 | 53.6 | 0.3 | 13.50 | 0.40 | 0 | 30 | 02EW | 1 | FFTFFFFF | 1975.497 |
| s6 | 8675 | 790 | 13 | 44 | 12.87 | -59 | 21 | 11.6 | 0.3 | 13.59 | 0.40 | 0 | 00 | 02EW | 1 | FFTFFFFF | 1975.497 |
| s7 | 8675 | 1392 | 13 | 44 | 46.57 | -59 | 21 | 27.1 | 0.3 | 12.96 | 0.40 | 0 | 02 | 02EW | 2 | FFTFFFTF | 1975.497 |
| | 8675 | 1392 | 13 | 44 | 46.53 | -59 | 21 | 27.4 | 0.3 | 13.25 | 0.40 | 0 | 01 | 007L | 2 | FFTFFFTF | 1976.256 |
| | 8675 | 2313 | 13 | 44 | 28.35 | -59 | 22 | 24.6 | 0.3 | 13.50 | 0.40 | 0 | 30 | 02EW | 1 | FFTFFFFF | 1975.497 |
| | 8675 | 1430 | 13 | 44 | 12.70 | -59 | 22 | 43.1 | 0.3 | 13.42 | 0.40 | 0 | 02 | 02EW | 1 | FFTFFFFF | 1975.497 |
| | 8675 | 2562 | 13 | 44 | 4.32 | -59 | 24 | 43.9 | 0.3 | 12.50 | 0.40 | 0 | 02 | 02EW | 2 | FFTFFFTF | 1975.497 |
| | 8675 | 2550 | 13 | 45 | 49.43 | -59 | 24 | 50.8 | 0.3 | 12.76 | 0.37 | 0 | 30 | 02EW | 2 | FFTFFFTF | 1975.497 |
| | 8675 | 2550 | 13 | 45 | 49.45 | -59 | 24 | 51.3 | 0.3 | 13.21 | 0.40 | 0 | 30 | 007L | 2 | FFTFFFTF | 1976.256 |
| | 8675 | 2090 | 13 | 45 | 34.30 | -59 | 25 | 18.3 | 0.3 | 13.17 | 0.37 | 0 | 30 | 02EW | 1 | FFTFFFFF | 1975.497 |



Table 3.4: Final star position list for image PF12_3 after applying the selection criteria. Seven stars were selected for the transformation of coordinates. These are the entries marked as s1 through s7 in column 1.

a finding chart to search for the star on the data image. If the star was found on the DSS-2i image but not on the data image, it was discarded. Then, another star was selected from the GSC list and searched in the DSS-2i image. If it was found in both DSS-2i and in the data images, it was retained. This procedure was repeated for up to 7 or 9 stars. Two selected stars in the data image PF12_3 are shown in Fig. 3.6. The image on the left side is the DSS-2i image and the data image is on the right side. Both show stars 4 and 6 out of 7 stars selected for the transformation of coordiniates.

In order to achieve a uniform transformation over the entire image, the selected stars should be distributed uniformly over the entire image. While this was the ideal

```
# [1] RaDecPF12_3.fits -
#   COL     LINE     RMAG     FLUX      SKY    N  RMOM ELLIP    PA     PEAK GFWHM
 487.92 3932.55     8.96 2610672.0   497.54   50  4.40 0.158  84.4 64875.81 11.02
1838.94 2999.73    10.09 918104.6    224.28   49  3.57 0.070  73.0 59304.53  3.70
  75.29 2624.42    10.00 998611.5    231.93   51  3.65 0.047  65.4 61517.42  3.79
1849.09 1387.32     9.92 1072015.1   253.64   51  3.64 0.083  66.6 67650.66  3.71
 152.66  971.41    10.42 680579.4    211.73   52  3.67 0.058  64.9 41448.09  3.82
1672.64  641.11    10.41 683518.0    219.86   51  3.66 0.040  68.6 41592.21  3.84
 588.46  581.01     9.36 1798993.0   336.43   49  3.85 0.028  52.0 69477.68  5.97
```

Table 3.5: IRAF's *imexam* ouput that contains pixel coordinates of seven selected stars. Pixel coordinates are given in columns 1 and 2.

procedure, the distribution of the usable stars did not always allow this. Another matter that must be taken into consideration is that a selected star should be isolated. This could be verified with IRAF task *imexamine*. If the selected star did not have nearby companions, then its pixel coordintes were measured. *Imexamime* commands *s*, and *e* give surface and contour plots which were used for inspection and could prove that a selected star does not have stars of similar or brighter magnitude nearby that will affect the computing of its positions by gaussian fitting.



```
 487.92 3932.55 13:44:49.90 -59:08:09.8
1838.94 2999.73 13:44:08.08 -59:11:50.7
  75.29 2624.42 13:45:02.57 -59:13:20.6
1849.09 1387.32 13:44:07.50 -59:18:14.0
 152.66  971.41 13:45:00.23 -59:19:53.6
1672.64  641.11 13:44:12.87 -59:21:11.6
 588.46  581.01 13:44:46.57 -59:21:27.1
```

Table 3.6: Input file for the IRAF task *ccmap* containing pixel and equatorial coordinates.

With typically 7 to 10 stars selected, DS9 was switched to single mode to have only the data image displayed. The crosshair was selected under edit to mark each zoomed star. Then, the IRAF text output command "," was used to measure the center of the star in pixel coordinates. After the centers of all selected stars were measured, a text file output is obtained. An example is shown in Table 3.5. Columns 1 and 2 give pixel coordinates of the selected stars. *Imexamine* has a hidden parameter named `logfile`. The filename assigned to the `logfile` parameter is the text file in which *imexamine* text output is recorded. Table 3.5 is an example. With these pixel coordinates for the selected stars and their respective equatorial coordinates from the

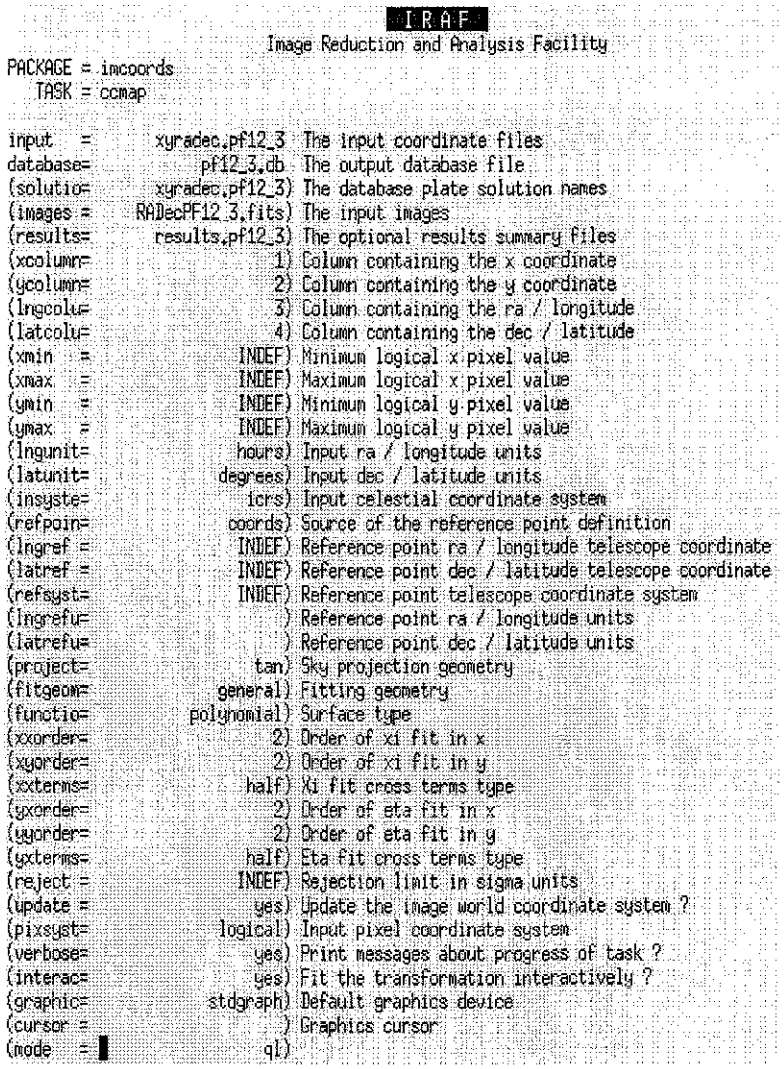

```
                                IRAF
                    Image Reduction and Analysis Facility
PACKAGE = imcoords
   TASK = ccmap

input   =      xyradec.pf12_3  The input coordinate files
database=         pf12_3.db  The output database file
(solutio=     xyradec.pf12_3) The database plate solution names
(images =    RADecPF12_3.fits) The input images
(results=     results.pf12_3) The optional results summary files
(xcolumn=                  1) Column containing the x coordinate
(ycolumn=                  2) Column containing the y coordinate
(lngcolu=                  3) Column containing the ra / longitude
(latcolu=                  4) Column containing the dec / latitude
(xmin   =             INDEF) Minimum logical x pixel value
(xmax   =             INDEF) Maximum logical x pixel value
(ymin   =             INDEF) Minimum logical y pixel value
(ymax   =             INDEF) Maximum logical y pixel value
(lngunit=             hours) Input ra / longitude units
(latunit=           degrees) Input dec / latitude units
(insyste=              icrs) Input celestial coordinate system
(refpoin=           coords) Source of the reference point definition
(lngref =             INDEF) Reference point ra / longitude telescope coordinate
(latref =             INDEF) Reference point dec / latitude telescope coordinate
(refsyst=             INDEF) Reference point telescope coordinate system
(lngrefu=                  ) Reference point ra / longitude units
(latrefu=                  ) Reference point dec / latitude units
(project=                tan) Sky projection geometry
(fitgeom=            general) Fitting geometry
(functio=         polynomial) Surface type
(xxorder=                  2) Order of xi fit in x
(xyorder=                  2) Order of xi fit in y
(xxterms=               half) Xi fit cross terms type
(yxorder=                  2) Order of eta fit in x
(yyorder=                  2) Order of eta fit in y
(yxterms=               half) Eta fit cross terms type
(reject =             INDEF) Rejection limit in sigma units
(update =               yes) Update the image world coordinate system ?
(pixsyst=           logical) Input pixel coordinate system
(verbose=               yes) Print messages about progress of task ?
(interac=               yes) Fit the transformation interactively ?
(graphic=          stdgraph) Default graphics device
(cursor =                  ) Graphics cursor
(mode   =                ql)
```



Table 3.7: IRAF task *ccmap* required and hidden parameters and their inputs for data image PF12_3.

GSC 1.2 a combined file with both pixel and equatorial coordinates is prepared. An example is given in Table 3.6. Text files as the one shown in Table 3.6 were part of the input files needed by the IRAF task *ccmap* to compute the equation of transformation of pixel to equatorial coordinates.

The task *ccmap* requires several input files to compute the transformation of coordinates. In Table 3.7, an example of the required and hidden parameters for this task with its respective values are shown. The `input` parameter takes the text file containing the matched pixel and equatorial coordinates. For image PF12_3 that

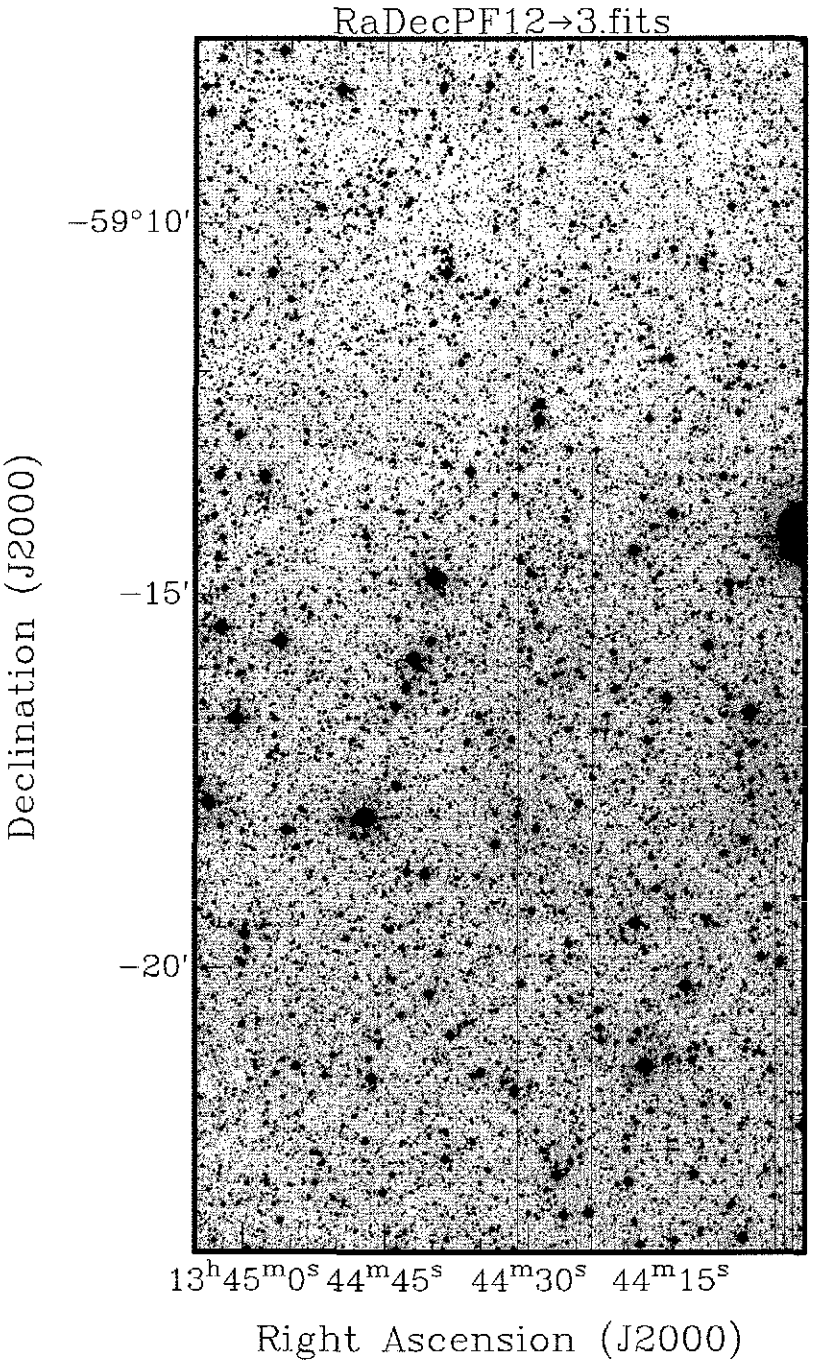


Figure 3.7: The $I$-band image of field number 12 and frame number 8. Its exposure time is 600 seconds.

file was named `xyradec.pf12_3`, where `xyradec` stand for pixel and equatorial coordinates respectively and `pf12_3` refers to the image of field number 12 and frame number 3. The other required parameter `database` needs as input the name of a text file in which the computed plate solutions of the transformation are stored. That textfile was named `db.pf12_3`, `db` for database and `pf12_3` for image PF12_3. For the parameters `images` and `results`, the inputs are the image `RADecPF12_3` and a text file which records a summary of the results of the transformation. The calibrated image PF12_3 was renamed RADecPF12_3. After *ccmap* is executed, the image header is modified so that pixel coordinates may be transformed to equatorial coordinates. There are more parameters for the *ccmap* task and my inputs for them are shown in Table 3.7.

This was the procedure followed to reduce all the images in which galaxies were found. The properties such as positions, diameters, possible morphological type as well as the images of the uncovered galaxies are presented in the next chapter.

# Chapter 4

# Galaxies Unveiled around the Radio Galaxy PKS 1343−601

## 4.1 Introduction

In this chapter I present the galaxy candidates found in searches by eye on the 128 WFI $I$-band images reduced in the previous chapter. I discovered 49 likely galaxies and 6 uncertain galaxy candidates. Positions in equatorial and Galactic coordinates as well as apparent diameters were determined for these galaxy candidates. A morphological type and a brief description of each candidate is given. $I$-band images of all galaxy candidates and uncertain candidates are shown. Cross-identifications with possible counterparts known from other wavebands (near and far-infrared, radio, and X-rays) are made.

## 4.2 Detected Galaxy Candidates

Galaxy candidates are generally objects that have a fuzzy appearance with, at these extinction levels, low surface brightness that do not resemble stars and have non-Gaussian radial profiles. In 128 deep $I$-band images that were searched for galaxies around PKS 1343-601, 49 candidates for galaxies were detected. These 49 candidates are listed with their properties in Table 4.1 which includes their position in equatorial and Galactic coordinates, apparent diameter and likely morphology.

Column one of Table 4.1 contains the running number of each galaxy candidate which are ordered in Right Ascension (J2000). Column one also includes the name of the $I$-band image in which they were found. The image nomenclature was ex-

Table 4.1: Positions, apparent diameters, morphological type and extinction $A_I$ of the 49 galaxy candidates around the radio galaxy PKS 1343−601.

| MO Ident. (1) | R.A ($^h$ $^m$ $^s$) (2) | Dec ($^\circ$ $'$ $''$) (3) | $\ell$ ($^\circ$) (4) | $b$ ($^\circ$) (5) | $D$ ($''$) (6) | $A_I$ ($^m$) (7) | Morph Type (8) | Description (9) |
|---|---|---|---|---|---|---|---|---|
| 1, pf15_5-2 | 13 36 45.0 | −60 31 48 | 308 48 | 1.85 | 2.6 | 2.9 | S | Very faint and small edge-on spiral |
| 2, pf15_5 | 13 37 26.9 | −60 25 46 | 308 58 | 1.94 | 2.8 | 3.5 | S? | Very low surface brightness and small |
| 3, pf14_5 | 13 37 29.1 | −60 04 27 | 308 65 | 2.29 | 2.4 | 2.9 | E | Very small with a nearby faint star |
| 4, pf14_3 | 13 38 04.3 | −59 41 18 | 308 79 | 2.65 | 2.9 | 3.4 | S | Low surface brightness edge-on spiral |
| 5, pf14_6 | 13 38 51.0 | −60 03 05 | 308 82 | 2.28 | 2.4 | 3.4 | E | Very small and perhaps E0 |
| 6, pf13_4-3 | 13 39 21.5 | −59 14 40 | 309 03 | 3.06 | 3.1 | 2.1 | S | *Faint, very small spiral which maybe* interacting with galaxy candidate 7 |
| 7, pf13_4 | 13 39 21.6 | −59 14 42 | 309 03 | 3.06 | 3.1 | 2.1 | E | Blended with a star and perhaps interacting with galaxy candidate 6 |
| 8, pf14_2 | 13 39 26.3 | −59 47 58 | 308 94 | 2.51 | 2.9 | 3.2 | E | Small and faint, possibly an E2 |
| 9, pf13_4-2 | 13 39 50.1 | −59 13 11 | 309.10 | 3.07 | 2.6 | 2.1 | S | Faint bulge with with low surface brightness halo (perhaps the disk) |
| 10, pf13_3 | 13 40 56.6 | −59 12 37 | 309.24 | 3.05 | 2.9 | 2.2 | E | Small and faint, possibly an E2 |
| 11, pf13_3-2 | 13 40 57.0 | −59 11 22 | 309.25 | 3.07 | 3.1 | 2.0 | S | Large and very faint halo (disk) around a bright spot. Maybe interacting with a possible nearby galaxy |
| 12, pf14_1 | 13 41 03.1 | −59 39 44 | 309.17 | 2.61 | 3.4 | 3.2 | S | Very low surface brightness and small edge-on |
| 13, pf13_2 | 13 41 14 3 | −59 21 52 | 309.25 | 2.90 | 2.4 | 2.5 | E | Small and faint, only its central part is observed, possibly E3 |
| 14, pf13_7 | 13 41 58 9 | −59 24 28 | 309.33 | 2.83 | 3.1 | 2.7 | E | Appears small, possibly E0 |
| 15, pf06_6 | 13 42 09 6 | −61 08 19 | 309.02 | 1.13 | 2.4 | 5.2 | E | Very faint, fuzzy object |
| 16, pf13_8-2 | 13 42 42 8 | −59 28 41 | 309.41 | 2.75 | 2.1 | 3.0 | S | Faint bulge with very dim halo (disk) |
| 17, pf13_8 | 13 42 44 4 | −59 28 54 | 309.41 | 2.74 | 3.6 | 3 0 | E | Small and faint, possibly E1 |
| 18, pf12_5 | 13 43 52 6 | −59 24 57 | 309.57 | 2.78 | 2.6 | 2.6 | E | Small and faint, maybe E2 |
| 19, pf12_6 | 13 44 03 5 | −59 29 22 | 309.57 | 2.70 | 2.5 | 3.0 | E | Small and faint, partially covered by a faint star |
| 20, pf05_2 | 13 44 03 6 | −60 19 35 | 309.41 | 1.88 | 3.6 | 4 6 | E1 | With small,faint nearby star |
| 21, pf12_3-4 | 13 44 23 0 | −59 13 17 | 309.67 | 2.96 | 3.6 | 2 3 | E | Possibly an E2 |
| 22, pf12_3-5 | 13 44 25 6 | −59 11 54 | 309.68 | 2.98 | 15.0 | 2.3 | S | Large and faint spiral with 2 stars near its bulge |
| 23, pf04_1 | 13 44 29 5 | −59 49 46 | 309.56 | 2.36 | 6.7 | 3 5 | S | Small, edge-on, very faint disk and partially hidden by a star |
| 24, pf12_3-3 | 13 44 37 5 | −59 09 51 | 309.71 | 3.01 | 3.0 | 2.3 | S | Very small and faint, maybe face-on |
| 25, pf12_3-2 | 13 44 41 4 | −59 10 22 | 309.72 | 3.00 | 2 6 | 2.3 | E | Small and faint, possibly an E3 |
| 26, pf12_3-6 | 13 44 46 7 | −59 11 52 | 309.72 | 2.97 | 2.9 | 2.3 | E | Only bulge is visible, maybe an E3 |
| 27, pf12_3-7 | 13 44 51 9 | −59 20 53 | 309.70 | 2.82 | 2.6 | 2.6 | S | Small bulge with fuzzy, faint halo |
| 28, pf12_3 | 13 45 01 8 | −59 09 51 | 309.76 | 3.00 | 19.6 | 2.2 | S | Large late-type edge-on spiral; bulge is not well defined |
| 29, pf01_5 | 13 45 25 3 | −60 29 15 | 309.54 | 1.69 | 2.4 | 5.1 | E | Low surface brightness center with faint halo |
| 30, pf01_4 | 13 45 50.6 | −60 09 06 | 309.66 | 2.01 | 4.3 | 3.6 | E1 | Large and blended with a bright star |

Table 4.1: continued.

| MO Ident (1) | R.A. ($^h\,^m\,^s$) (2) | Dec ($^\circ\,'\,''$) (3) | $\ell$ ($^\circ$) (4) | $b$ ($^\circ$) (5) | $D$ ($''$) (6) | $A_I$ ($^m$) (7) | Morph. Type (8) | Description (9) |
|---|---|---|---|---|---|---|---|---|
| 31, pf03_6 | 13 46 12.5 | −59 57 23 | 309 74 | 2.19 | 2 9 | 3.6 | S | Bright bulge with faint disk, only half of the disk is visible |
| 32, pf01_3-2 | 13 46 20.3 | −60 22 44 | 309.67 | 1.77 | 1.8 | 5.3 | S | Very small, low surface brightness |
| 33, pf01_3 | 13 46 49.1 | −60 24 29 | 309.72 | 1.73 | 3.8 | 5.5 | E0 | The giant radio galaxy PKS 1343−601 |
| 34, pf01_7 | 13 47 18.5 | −60 34 13 | 309.75 | 1 56 | 2.9? | 5.5 | S | Large edge-on spiral (from Nagayama & Sato) |
| 35, pf11_4 | 13 47 24 1 | −59 10 55 | 310.06 | 2 91 | 3.1 | 2.4 | S | Small, very low $SB$ and blended with a faint star |
| 36, pf11_4-2 | 13 47 25 5 | −59 12 28 | 310.05 | 2 89 | 5.8 | 2 4 | ? | Small bright bulge with a very large extended halo, possibly a spiral |
| 37, pf01_7-2 | 13 47 36 0 | −60 37 03 | 309.77 | 1.51 | 2 0 | 5 5 | E | Perhaps the bright bulge of an E0 |
| 38, pf03_7 | 13 47 53.1 | −59 55 32 | 309 96 | 2.17 | 1 7 | 3 7 | S | Small bulge with a faint halo (disk) |
| 39, pf03_7-2 | 13 48 04.2 | −59 58 13 | 309 97 | 2.13 | 1 2 | 3.8 | S? | Very low surface brightness and tiny |
| 40, pf01_1 | 13 48 27.5 | −60 11 47 | 309 97 | 1.89 | 3.1 | 4.6 | E | Small and faint, possibly E0 |
| 41, pf08_4 | 13 49 56.3 | −60 40 44 | 310.04 | 1.38 | 3.6 | 4.9 | E | Very low surface brightness and fuzzy |
| 42, pf02_6 | 13 50 24.7 | −60 05 39 | 310.23 | 1.94 | 3.8 | 4.4 | E0 | Blended with a bright star |
| 43, pf11_1 | 13 50 29.4 | −59 07 54 | 310.45 | 2.87 | 2.6 | 1.7 | S | Faint, small bulge with faint halo |
| 44, pf09_3 | 13 50 41 8 | −60 19 06 | 310 21 | 1 71 | 3.8 | 4.5 | E | Possibly an E3 |
| 45, pf11_1-2 | 13 50 46 9 | −59 23 09 | 310.43 | 2 62 | 4.1 | 2.8 | E1 | Bright bulge and faint halo |
| 46, pf09_6 | 13 51 08 3 | −60 39 22 | 310.19 | 1 37 | 3.6 | 4.7 | E | Small and very low $SB$ close to a bright star |
| 47, pf10_6 | 13 52 05.1 | −59 30 59 | 310.56 | 2.45 | 3.4 | 3 0 | S | Bright bulge with faint disk |
| 48, pf10_3 | 13 52 15.4 | −59 17 02 | 310 64 | 2.68 | 2 9 | 2 0 | S? | Small and very faint |
| 49, pf10_1 | 13 55 14.2 | −59 11 05 | 311 03 | 2.68 | 2 4 | 2 0 | S | Faint and small bulge with y very low $SB$ disk |

plained in Chapter 3. Columns 2 and 3 present the galaxy Right Ascension (RA) and Declination (Dec) for the equinox J2000. Galaxy positions in Galactic coordinates ($\ell$, $b$) are recorded in columns 4 and 5 respectively. The sixth column in Table 4.1 contains the measured apparent diameter of galaxies in arcseconds. Column 7 gives the extinction in the $I$-band ($A_I$) at each galaxy position according to the DIRBE dust maps (Schlegel et al. 1998). This is an approximation since the calibration of

the DIRBE extinction values are not well established for low latitudes. The possible morphological type is given for each galaxy in column 8. Finally, the last column gives a brief description of each galaxy candidate.

### 4.2.1 Accuracy of the Positional Measurements

Galaxy positions in RA and Dec were measured directly from the in equatorial coordinates calibrated images using the following procedure: Data images were displayed with the astronomical image display tool "SAOImage ds9". Galaxy candidates were enlarged (zooming in) to show identifiable details. The centers of each galaxy candidate was considered to coincide with the highest surface brightness area (avoiding superimposed stars). The center of each galaxy candidate was read out from DS9 by setting the cursor in "crosshair" mode on its pixel of highest surface brightness. Galaxy positions were measured twice this way in order to determine their random uncertainties. The statistical analysis of two positional measurements for each of the 49 galaxy candidates give a mean offset of 0.″0636 and 0.″0742 in RA and Dec respectively. A dispersion of 0.″4708 in RA and 0.″1756 in Dec was determined. The statistical analysis of these 49 galaxy positions give a random error of 0.″47 in RA and 0.″18 in Dec showing the internal consistency in the positional measurements.

Three of the 49 galaxies listed in Table 4.1 were identified on their common overlapping areas in a second different image. Therefore, they have two measurements of their positions that come from different images. These are galaxies 30, 33 and 34. Table 4.2.1 lists the individual determined positions. To confirm the internal consistency of the positional measurements, the mean and the standard deviation of the offsets of these three galaxies were determined. The offsets in RA and Dec are 0.″8 and 0.″0.01 with a corresponding dispersion of 0.″68 and 0.″23.

As most of these galaxies were unknown before, it is not possible to compare the accuracy of these positions with other external data. Anja Schröder's search in a pilot project using the NIR, DENIS[1] images ($I$, $J$ and $K$-band) in this area has 5 galaxies in common with the galaxies detected here. These are galaxies 15, 20, 33, 34 and 40 of Table 4.1. However, there still are some problems with the astrometry of DENIS images. Current galaxy positions obtained from DENIS images have a systematic deviation of few arcseconds. Some galaxies have also counterparts in radio (see section 4.4). But galaxy positions derived from radio observations are even less accurate than those from DENIS images. Therefore, at the moment there are no

[1]DEep Near Infrared Survey of the southern sky

Table 4.2: Equatorial positions (J2000) of three galaxies with independent determinations.

| Galaxy Candidate | R.A. (h m s) | Dec. (° ′ ″) | R.A. (h m s) | Dec. (° ′ ″) |
|---|---|---|---|---|
| 30 | 13:45:50.568 | -60:09:05.60 | 13:45:50.614 | -60:09:05.61 |
| 33 | 13 46 49.078 | -60 24 29.42 | 13:46:49.081 | -60:24:29.22 |
| 34 | 13 47 18.518 | -60 34 12.99 | 13:47:18.555 | -60:34:13.24 |

substantial external data available to compare the accuracy of the positions reported in Table 4.1.

### 4.2.2 Diameter Determination

Most of the galaxy candidates listed in Table 4.1 have apparent diameters of a few arcseconds with the exception of two large ones. Galaxies 22 and 29, which seem to be large spirals, have apparent diameters of 15″ and 20″ respectively. One should recall however, that most of the galaxy candidates listed in Table 4.1 are not intrinsically small and/or faint, they only appear faint and small because they lie behind an extinction layer of several magnitudes in the $I$-band. Therefore, we mainly see the most luminous part of galaxies, i.e. their bulges. The diameters reported in column 6 of Table 4.1 generally correspond to the central region of galaxies where their surface brightness is higher. The listed major diameters correspond to the size of the brightness countour of 10% of the peak brightness. The brightness radial profile was obtained with IRAF *imexamine*. In most cases it was possible to plot the radial profile of the emitted light of these galaxies. The radial profile plots were used to determine the galaxy diameters, except for a few galaxies with very low surface brightness. A visual estimation of the major diameter was done for those low surface brightness galaxies.

### 4.2.3 Morphological Classification

The determination of the morphological type is also severely affected by the foreground extinction mainly caused by our Galaxy. Similar to the diameter determinations, the morphological classification given in column 8 of Table 4.1 is a rough estimation. Only in some cases the spiral or elliptical nature of these galaxies was

clear but not always. The distinction between the bulge of a spiral galaxy and an early-type galaxy remains ambiguous in many cases since they are highly obscured. Elliptical galaxies show a more compact light distribution in the radial profile plots than spiral galaxies which display more extended light profiles. The light profile was thus useful in the assessment of morphology for those galaxies whose morphology was uncertain from visual inspection.

### 4.2.4 Images and a Brief Description of the Galaxy Candidates

The images of the 49 proposed galaxy candidates are presented in Figure 4.1. The size of each image is about $36''\times36''$ and the location of these galaxies in the images is indicated by an arrow. Most galaxy candidates are small and have low surface brightness.

Twenty four of the 49 galaxy candidates listed in Table 4.1 are classified as spiral. Images 1 and 4 are examples of small and faint spirals. The object in image 4 seems to be an edge-on spiral. Image 22 shows a very low surface brightness object that could be a spiral with some foreground stars. A large edge-on spiral of low surface brightness with an apparent diameter of about $20''$ is displayed in image 28. A small and faint edge-on spiral is shown in image 34. This appears as a large edge-on spiral in an combination of $I$, $J$ and $K$-band images (from Nagayama & Sato before been published).

Twenty-five galaxy candidates have an elliptical morphology. Some of them appear as large and bright objects while others are faint and smaller even though they may not be intrinsically faint and/or small. The object shown in image 33 is the giant elliptical radio galaxy PKS 1343-601. Image 30 contains another example of a large elliptical galaxy. Most of the 25 galaxy candidates with proposed elliptical morphology are fainter and smaller. Image 5 shows a small, faint elliptical candidate. Other examples of smaller ellipticals are images 17 and 18.

In some of these images, straight vertical lines are bad pixel columns.

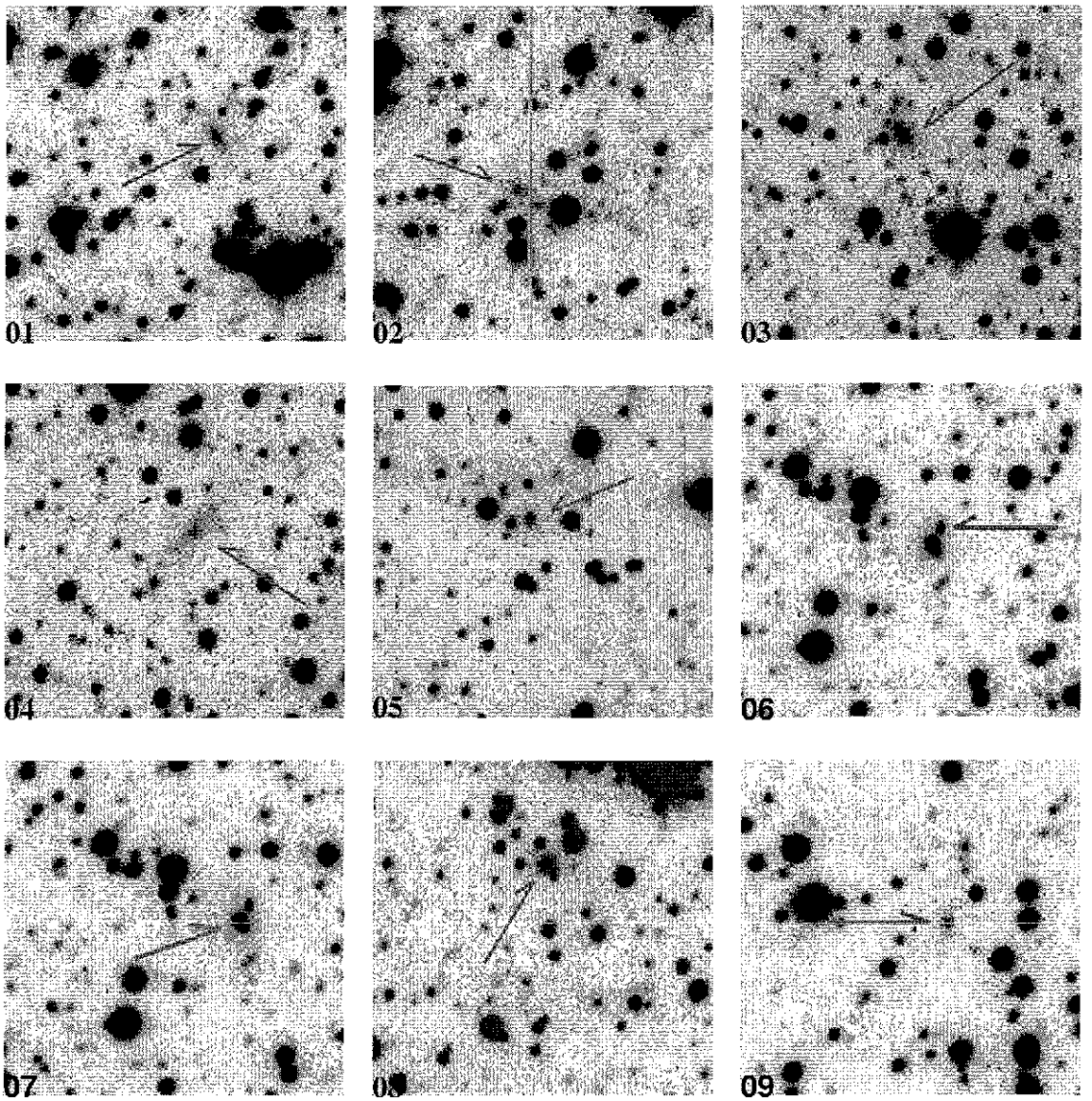


Figure 4.1: *I*-band images of the 49 galaxy candidates found in the vicinity of the radio galaxy PKS 1343-601. Every image is about 36 x 36 arcsec. RA is the horizontal and Dec is the vertical axis. North is up and east is left.

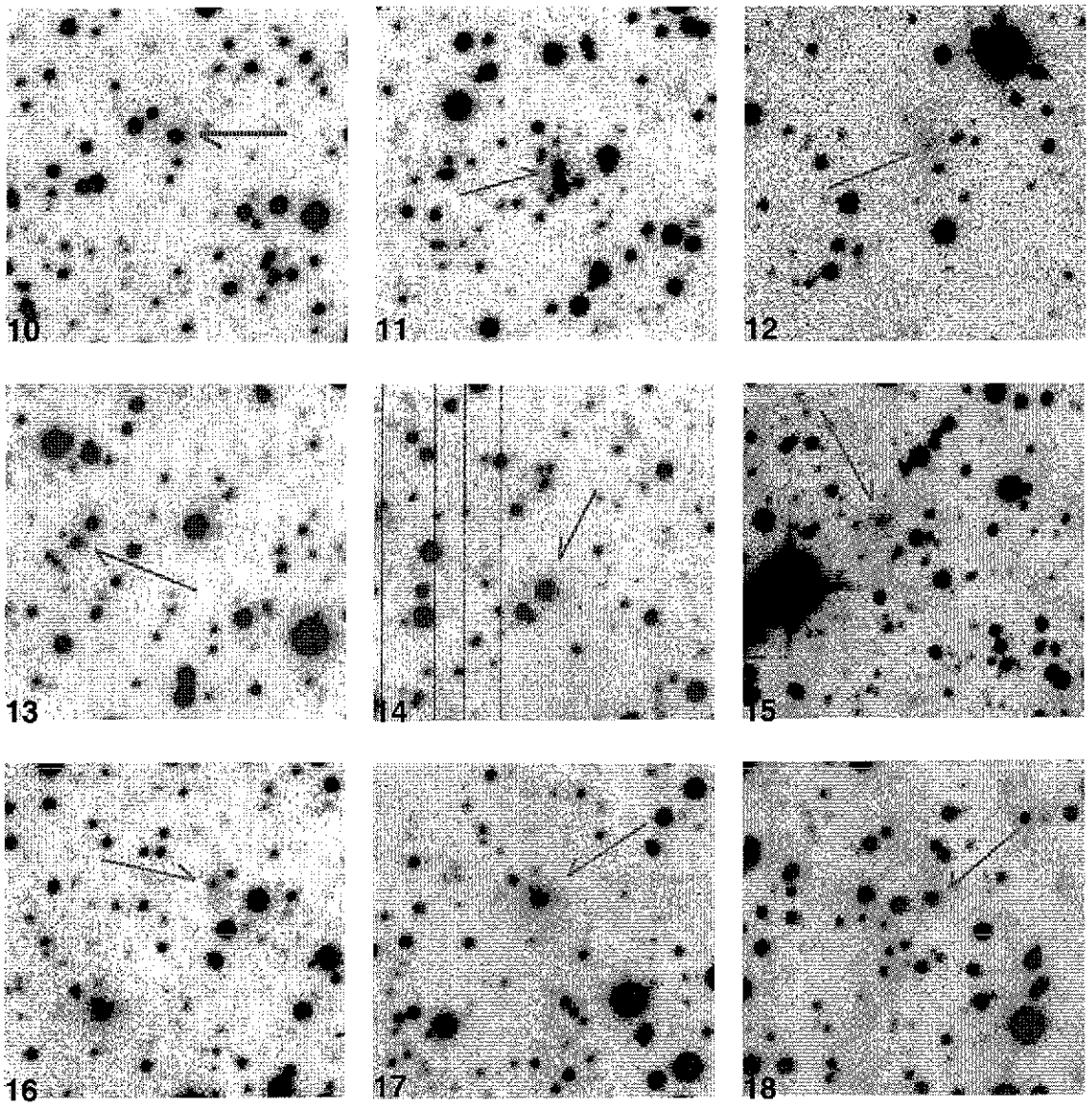


Figure 4.1: continued.

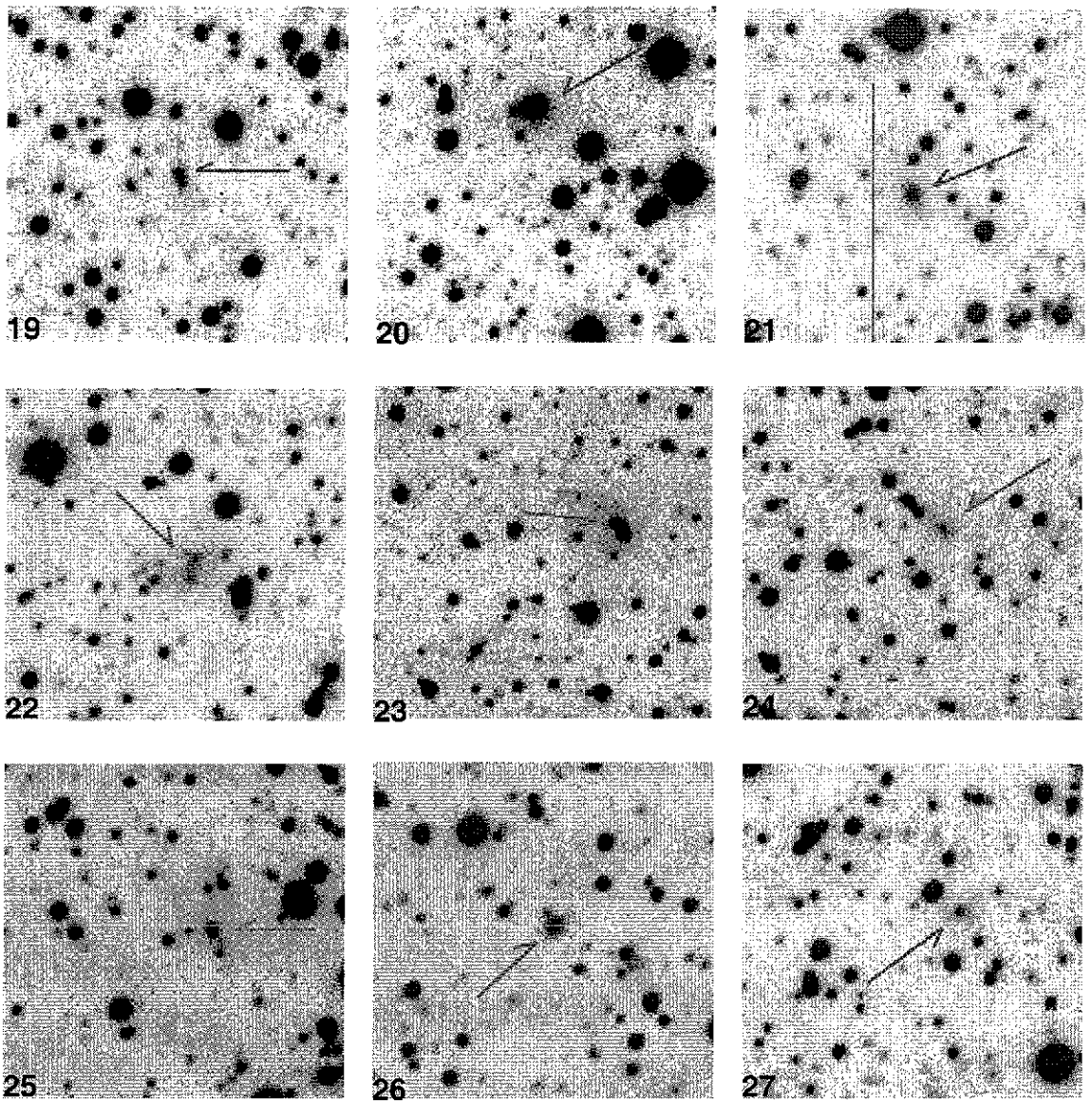


Figure 4.1: continued.

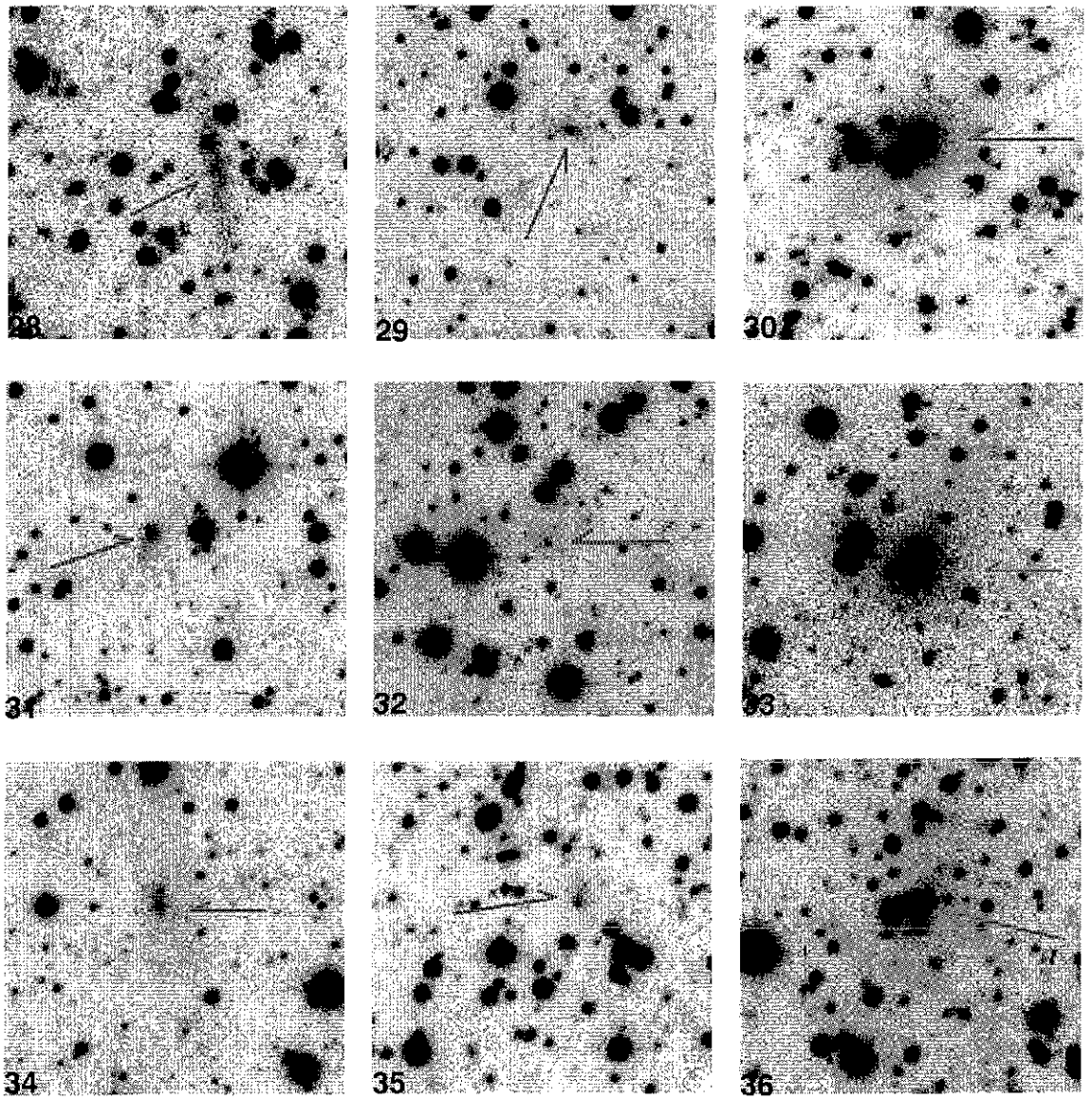


Figure 4.1: continued.

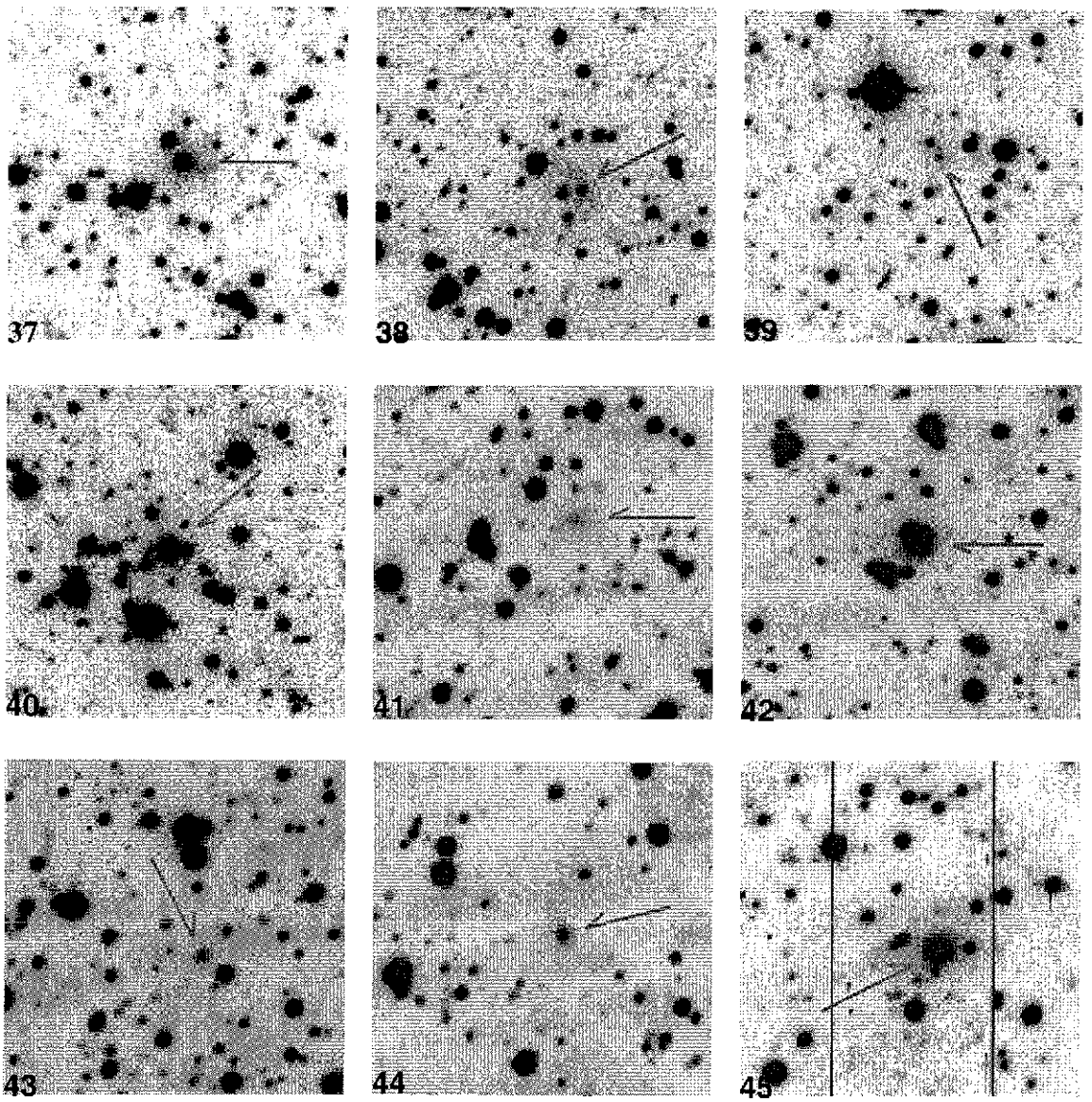


Figure 4.1: continued.

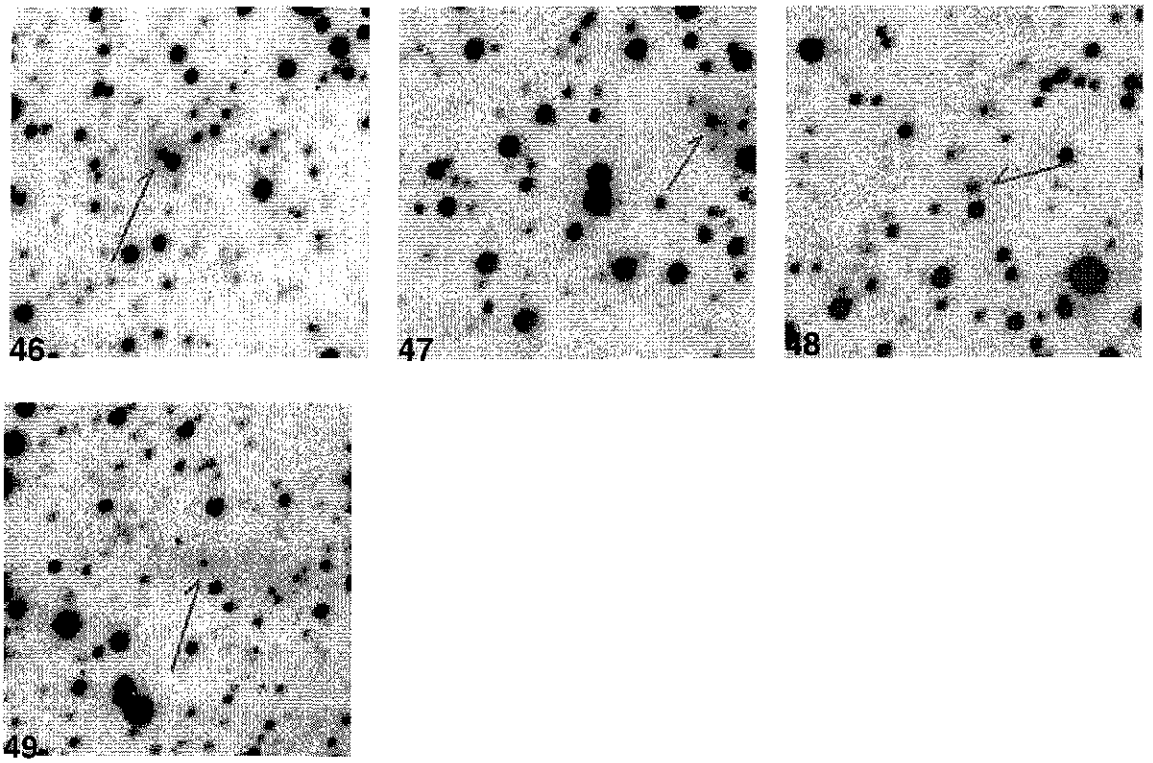


Figure 4.1: continued.

## 4.3 Uncertain Galaxy Candidates

Six low surface brightness objects have been detected which are not stars, but its extragalactic nature is not clear. These objects are included here as uncertain galaxy candidates and their properties are listed in Table 4.3 with the same entries as Table 4.1. The galaxies are ordered in increasing Right Ascension (J2000).

The galaxy positions shown in Table 4.3 have the same statistical uncertainties as the positions in Table 4.1 which are described in section 2 of this chapter (see section 4.2.1). The images of the six uncertain galaxy candidates are displayed in Figure 4.2.

### 4.3.1 Description of the Uncertain Galaxy Candidates Images

Five of the uncertain galaxy candidates appear small and with very low surface brightness except the one shown in image 2 where a fuzzy region of low surface brightness

Table 4.3: The six uncertain galaxy candidates

| Label | RA | Dec | $\ell$ | $b$ | $D$ | $A_I$ | Morph | Description |
|---|---|---|---|---|---|---|---|---|
| | ($^h$ $^m$ $^s$) | ($^\circ$ $'$ $''$) | ($^\circ$) | ($^\circ$) | ($''$) | ($^m$) | Type | |
| (1) | (2) | (3) | (4) | (5) | (6) | (7) | (8) | (9) |
| 1, pf16_4 | 13 37 22.8 | −60 40 08 | 308.53 | 1.70 | 2.9 | 3.1 | ? | Small, very low $SB$, and has non-stellar light profile |
| 2, pf14_5 | 13 37 49 0 | −60 01 36 | 308 67 | 2.32 | ? | 3 2 | ? | Fuzziness blended with a bright bright star |
| 3, pf12_3 | 13 44 41 3 | −59 10 17 | 309 72 | 3.00 | 2 0 | 2 3 | ? | Maybe a bright star partially covering a faint galaxy |
| 4, pf11_4 | 13 47 14.4 | −59 16 53 | 310 01 | 2.82 | 2.1 | 2 9 | S | Very small, faint fuzzy patch |
| 5, pf11_1 | 13 50 24.7 | −59 17 25 | 310 41 | 2.72 | 1 8 | 2 5 | E ? | Small and faint spot close to a very bright star |
| 6, pf10_1-2 | 13 54 44.4 | −59 12 21 | 310.97 | 2.68 | 1.7 | 2.0 | S? | Bright small spot with faint circular halo. Perhaps a planetary nebula |

of about 10″ diameter is seen (see Fig. 4.2). The origin of this fuzzy patch is uncertain due to a bright nearby star. It maybe a nearby dwarf spheroidal. Further observations are needed in order to reveal the nature of this object.

In image 1 of Fig. 4.2, a fuzzy and faint object is indicated with the arrow. It is included in the list of uncertain galaxy candidates because it has a non-stellar radial light profile. However, it could be a blend of two small, faint stars. A tiny and fuzzy object that seems to be behind a star is indicated by the arrow in image 3. The arrow points at a star that is partially covering a small, faint object which could be a highly obscured galaxy. Image 4 displays a fuzzy patch indicated by an arrow which has low surface brightness and non-stellar radial light profile. Another small, faint and fuzzy object is seen near to a bright star in image 5. From visual inspections and its light radial profile, it seems to be a galaxy candidate but this is not clear since it is so close to such a bright star.

Image 6 of Figure 4.2 shows an object with an interesting peculiarity. This object consists of a small bright spot of less than 1″ in size at the center of a low surface brightness halo of 2″ in diameter. It has the apperance of a bright star surrounded by a faint halo. Such an object may be a planetary nebula rather than a galaxy, but the central bright spot has an extended radial light profile which may be identified more with a spiral galaxy than with a star. Therefore, the nature of this object cannot be determined with the resolution of this image.

The existing shallow surveys in the $I$, $J$ and $K$-bands such as DENIS do not have enough resolution to detect these small and faint objects. Therefore, deeper NIR

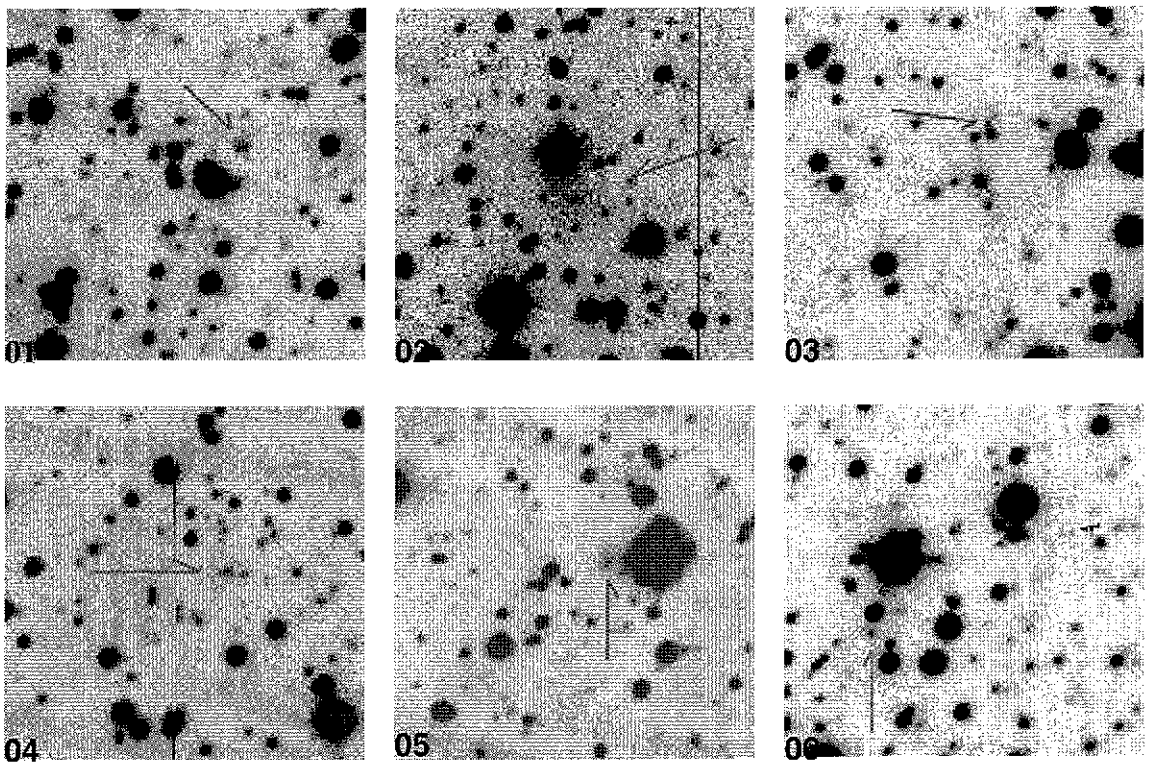


Figure 4.2: The images of seven uncertain galaxy candidates. Images are about 36″x 36″. RA increases horizontally to the left while Dec decreases vertically downwards.

observations are required in order to unveil the nature of these seven objects. Deep observations in the near and far infrared would confirm whether or not they are of extragalactic origin.

## 4.4 Cross-Identification with Known Objects

For the search of counterparts I made use of the following two databases: The CATS database (http://cats.sao.ru, Verkhodanov et al. 1997) and the NASA/IPAC Extragalactic Database (NED, http://nedwww.ipac.caltech.edu). Only 14 galaxy candidates of the 55 candidates listed in Tables 4.1 and 4.3 have one counterpart in either the near infrared (DENIS), far infrared (IRAS), radio and/or X-rays.

The IRAS SSSC and IRAS PSC (Joint *IRAS* Science Working Group 1998) were searched for IRAS counterparts of the here discovered galaxies presented in Table 4.1 and Table 4.3. IRAS counterparts were searched for within a radius of 2′ from the positions as determined from their $I$-band images. IRAS positions have elliptical un-

certainties. The semimajor (smj) and semiminor (smn) axes in arcsec determine the size of the uncertainty ellipse. IRAS flux densities are given in Jansky for the wavelenghts of 12 $\mu$m, 25 $\mu$m, 60 $\mu$m and 100 $\mu$m. The possible IRAS counterparts were investigated individually for a match taking the following criteria into consideration.

**a** IRAS positional uncertainty ellipses and the positional offset between a candidate and its possible IRAS counterpart.

**b** The color defined with the IRAS different wavebands (12 $\mu$m, 25 $\mu$m, 60 $\mu$m and 100 $\mu$m) as $col_1 = f_{12} \cdot f_{25}/(f_{60})^2$ (Yamada et al. 1993), where $col_1 < 1$ indicates that the IRAS source could be a galaxy.

**c** Possible coincidences with other astronomical objects detected in the near infrared, at radio wavelenghts and/or in X-rays.

Possible concidences with some DENIS galaxies whose positions have not been published yet and were provided by Anja Schröder were also investigated for a match. These unpublished DENIS positions are expected to have uncertainties of few arcsec due to inaccurate information in the headers of the respective DENIS images (strips).

### Galaxy Candidate 9

IRAS PSC: 13367−5858
RA & Dec : $13^h\,40^m04\overset{s}{.}2$ $-59°\,13'58''$ (J2000)
Uncertainty Ellipse: smj = $48''$ and smn = $12''$ at p.a. = $133°$
Flux Densities: $f_{12} = 0.48$, $f_{25} < 0.25$, $f_{60} < 3.36$ and $f_{100} < 27.75$ Jy
Discussion: Galaxy candidate 9 appears as a small, low surface brightness spot surrounded by a faint, fuzzy halo. It is a candidate for a spiral galaxy visually determined from its I-band image. Flux densities of the IRAS PSC counterpart give a color $col_1 < 1$ which indicates that IRAS 13367−5858 may be a spiral galaxy. Galaxy 9 is about $116''$ away from the IRAS position and hence, outside of the uncertainty ellipse. This IRAS source could also indicate the existence of a spiral galaxy near to galaxy candidate 9.

IRAS SSSC: X1336−589
RA & Dec : $13^h\,39^m47\overset{s}{.}5$ $-59°\,13'37''$ (J2000)
Flux Density: $f_{60} = 5$ Jy
Discussion: This IRAS SSSC source is $33''$ away but I am not sure if it is related

to galaxy candidate 9. There are no errors or sizes available for IRAS extended sources.

### Galaxy Candidate 15

H-I Blind Survey of HI-Bright Galaxies in the Southern ZOA[2]: HIZSS 082
RA & Dec : $13^h\,42^m14\overset{s}{.}0$ $-61°\,04'58''$ (J2000)
Uncertainty Ellipse: smj = 300″, smn = 300″ at p.a. = 0°
Discussion: HIZSS 082 is 203″ from galaxy candidate 15 and is charted as a galaxy. The position of galaxy candidate 15 position is within the uncertainty ellipse. Despite the large positional offset, it is highly possible that galaxy candidate 15 could be the optical counterpart of HIZSS 082. Galaxy candidate 15 appears as a spiral in the I-band image of the WFI.

DENIS:
RA & Dec : $13^h\,42^m09\overset{s}{.}7$ $-60°\,08'20''$ (J2000)
Comment: This position has been provided by Anja Schröder. It is only detected in the K-band of DENIS.

Summary: It is high likely that the galaxy candidate 15 is the optical counterpart of HIZSS 082.

### Galaxy Candidate 20

DENIS: P J134403.3−601936
RA & Dec : $13^h\,44^m03\overset{s}{.}3$ $-60°\,19''36'$ (J2000) (Rousseau et al. 2000)
Uncertainty: 5″ in RA and Dec
Discussion: It is seen in the I, J and K-band of DENIS. It has an I-band magnitude of $16\overset{m}{.}87$ (provided by Anja Schröder). This DENIS galaxy likely coincides with galaxy candidate 20, a big elliptical, possibly an E2.

### Galaxy Candidate 32

IRAS PSC: 13430−6008
RA & Dec : $13^h\,46^m29\overset{s}{.}5$ $-60°\,23'32''$ (J2000)
Uncertainty Ellipse: smj = 26″ and smn = 6″ at p.a. 130°
Flux Densities: $f_{12} = 0.92$, $f_{25} = 0.56$, $F_{60} < 3.10$ and $f_{100} < 36.64$ Jy
Discussion: Galaxy Candidate 32 is seen as a faint, tiny spiral in its I-band image. A color $col_1 < 1$ indicates that 13430−6008 may be a galaxy. This IRAS point source is at 84″ from galaxy candidate 32, thus an unlikely match.

[2]Henning P. A. et al. 2000

**Galaxy Candidate 33**

PKSCAT90[3]: PKS 1343−601
RA & Dec : $13^h\,46^m57^s.6$ $-60°\,22'59''$ (J2000)
Flux Densities: $f_{1410MHz} = 79$ Jy, $f_{2700MHz} = 29$ Jy and $f_{5GHz} = 27.1$ Jy
Comment: PKS 1343-601 was detected for the first time in radio. It is the second brightest extragalactic radio source in the southern sky (MacAdam 1991 and references therein). This radio galaxy also has an active galactic nucleus (AGN).

West & Tarenghi (1989): Optical Counterpart of PKS 1343−601
RA & Dec : $13^h\,46^m48^s.95$ $-60°\,24'29''.7$ (J2000)
Uncertainty: $\pm$ 3″ in both RA and Dec
Discussion: Galaxy candidate 33 is .15″ in RA and 0.3″ in Dec away from the position given in West & Tarenghi. The optical image of PKS 1343−601 is that of a typical elliptical galaxy, *i.e.* E0.

The Einstein Observatory: 2E1343.4−6009
RA & Dec : $13^h\,43^m25^s$ $-60^h\,09'26''$ (B1950) or $13^h\,46^m50^s.6$ $-60°\,24'25''$ (J2000)
Flux Density: 2.5 x $10^{-15}$ W $m^{-2}$ at 0.16-3.5 KeV
Comment: This X-ray point source is within 15 arcsec of the PKS 1343-601 galactic core (McAdam 1991). Hence, it is a certain match.

ASCA[4]: 2E 1343.4−6009 or PKS 1343−601
RA & Dec : $13^h\,46^m49^s$ $-60°\,24'46''$ (J2000)
Uncertainty: Position accuracy determination of 40″
Flux Density: Core emission of $f = (6.4 \pm 0.2)$ x $10^{-14}$ $Wm^{-2}$ at 2-10 keV or 2.6 x $10^{-14}$ W $m^{-2}$ at 0.16-3.5 keV.
Comment: The ASCA satellite detected an X-ray source located at $(\alpha, \delta)_{J2000} = (13^h\,46^m49^s, -60°\,24'46'')$ which coincides with the position of the radio core of PKS 1343−601.

DENIS[5]
RA & Dec Coords: $13^h\,46^m49^s.3$ $-60°\,24'31''$ (J2000)
Comment: It is seen in the I, J, and K-band of DENIS. Its I-band magnitude

[3]PKSCAT90: The Southern Radio Source Database (Otrupcek & Wright 1991).
[4]*Tashiro M. et al. 1998.*
[5]Data provided by Anja Schröder.

is about $16^m$.

Summary: There is enough evidence to confirm the existence of galaxy candidate 33 as the giant elliptical galaxy (E0) as PKS 1343−601.

**Galaxy Candidate 34**

IRAS PSC: 13441−6019
RA & Dec: $13^h\,47^m33^s.1$ $-60°\,34'16''$ (J2000)
Uncertainty Ellipse: smj = $52''$ and smn = $9''$ at $\theta = 131°$
Flux Densities: $f_{12} = 0.61$, $f_{25} = 0.30$, $f_{60} < 5.06$, and $f_{100} < 52.31$ Jy
Discussion: Galaxy candidate 34 is seen as a faint, small face-on spiral. It could be interacting with the certain galaxy candidate 5 which seems to be another spiral. IRAS PSC 13441−6019 lies $109''$ from galaxy candidate 39 and has $col_1 < 1$ for its fluxes. Thus 13441−6019 has a color indicative of a galaxy, but it is far from the galaxy candidate 39.

DENIS
RA & Dec : $13^h\,47^m18^s.9$ $-60°\,34'15''$ (J2000)
Comment: This position has an uncertainty of several arcsec. It is only seen in the J and K-band of DENIS (from Anja Schröder).

**Galaxy Candidate 37**

IRAS PSC: 13442−6022
RA & Dec: $13^h\,47^m39^s.1$ -60° 37′21″ (J2000)
Uncertainty Ellipse: smj = $21''$ and smn = $8''$ at $\theta = 127°$
Flux Densities: $f_{12} = 0.36$, $f_{25} = 0.88$, $f_{60} = 3.70$, and $f_{100} = 18.17$ Jy
Discussion: This IRAS point source is $29''$ from galaxy candidate 37 which is not within the uncertainty ellipse. Flux densities give a color $col_1 < 1$. With such fluxes and small offset, this IRAS emission could be associated with galaxy candidate 37 .

The Einstein Observatory: 2E 1344.1−6022
RA & Dec : $13^h\,44^m11^s$ $-60°\,22'11''$ (B1950) or $13^h\,47^m37^s.4$ $-60°\,37'08''$ (J2000)
Comment: This X-ray source with 182 counts is much stronger than its neighbor galaxy candidate 33 wich has $\sim$ 48 counts. The radio emission detected

from 2E 1344.1−6022 is less than 5mJy at 843 MHz (McAdam 1991). Galaxy candidate 37 is likely to be the optical counterpart of 2E 1344.1-6022. In the I-band image, galaxy candidate 37 appears as a big elliptical galaxy.

ASCA[6]: 1H 1338−604, 3A 1344−602, or 4U 1344−60
RA & Dec: $13^h\,47^m37^s$ $-60°\,37'46''$ (J2000)
Uncertainty: An accuracy of $40''$
Flux density: A counting rate of 0.20 counts $s^{-1}$ at 0.17-10 keV while its neighbor PKS 1343-601 (galaxy candidate 33) has 0.13 counts $s^{-1}$ (Tashiro et al. 1998).
Discussion: This X-ray source is $15'$ to the southeast from PKS 1343-601 (Tashiro et al. 1998) while galaxy candidate 37 is $14'$ to the southeast from galaxy candidate 33 (PKS 1343-601) Lying within the positional uncertainty ($40''$) of ASCA, galaxy candidate 37 is a possible optical counterpart of this second X-ray source.

### Galaxy Candidate 40

IRAS PSC: 13449−5956
RA & Dec : $13^h\,48^m24\overset{s}{.}7$ $-60°\,11'14''$ (J2000)
Uncertainty Ellipse: smj = $61''$ and smn = $12''$ at $\theta = 138°$
Flux Densities: $f_{12} < 0.53$, $f_{25} < 0.62$, $f_{60} = 1.82$ and $f_{100} < 56.63$ Jy
Discussion: The galaxy candidate 40 is $34''$ from this IRAS point source, but it is not within the uncertainty ellipse. Galaxy candidate 40 is seen as a bright elliptical galaxy in the I-band. With $col_1 < 1$ and small positional offset, 13449-5956 is likely to be the IRAS counterpart of galaxy candidate 40.

DENIS
RA & Dec : $13^h\,48^m27\overset{s}{.}8$ $-60°\,11'44''$ (J2000)
Comment: It was also detected in DENIS I, J and K-band images by Anja Schröder. Its I-band magnitude is $16\overset{m}{.}27$.

[6]Tashiro M et al. 1998

### Galaxy Candidate 44

PMN[7]: PMN J1350−6020
RA & Dec : $13^h\,50^m40^s.9$ $-60°\,20'42''$ (J2000)
Uncertainty Ellipse: smj = 78″, smn = 66″, and $\theta = 90°$
Discussion: Galaxy candidate 44 is 96″ from the radio source PMN J1350-6020. Even though the PMN J1350-6020 position has large uncertainties, the position of galaxy 44 is not within the uncertainty ellipse. The galaxy 48 I-band image seems to be that of an early type galaxy, possibly E2. Galaxy 44 may be the optical counterpart of this radio source despite the large positional offset.

### Galaxy Candidate 47

IRAS SSSC: X1348−592
RA & Dec : $13^h\,52^m04^s.0$ $-59°\,32'00''$ (J2000)
Flux Density: $f_{12} = 8$ Jy
Discussion: The IRAS SSSC does not list a counterpart for X1348−592. Galaxy candidate 47 is 59″ away from X1348−592 and appears as a faint spiral in the I-band. It could be its counterpart since extinction is quite high.

### Galaxy Candidate 48

IRAS PSC: 13488−5803
RA & Dec : $13^h\,52^m19^s.2$ $-59°\,18'03''$ (J2000)
Uncertainty Ellipse: smj = 25″ and smn = 10″ at $\theta = 127°$
Flux Densities: $f_{12} = 0.73$, $f_{25} = 0.44$, $f_{60} < 3.35$ and $f_{100} < 27.61$ Jy
Discussion: 13488−5803 could be a galaxy since $col_1 < 1$, but it is far (67″) from galaxy candidate 48 which is visible as a small, low surface brightness spiral in the I-band. If 13488−5803 is not the IRAS counterpart of galaxy candidate 48, it could be another galaxy in the vicinity of galaxy candidate 48.

Seven galaxy candidates have a possible match with IRAS sources; five of them (9, 32, 24, 47 and 48) are listed as spiral and two (37 and 40) as elliptical galaxy in Table 4.1. Another 4 galaxy candidates have cross-identifications with DENIS positions provided by Anja Schröder and one with a DENIS published position. Two galaxy candidates (33 and 37) have X-ray counterparts; both are elliptical and one of

[7]The Parkes-MIT-NRAO (PMN) surveys (Griffith & Wright 1993).

them is the radio galaxy PKS 1343−601. Four have radio counterparts; the galaxies 3, 15, 20 and 49 have counterparts from deep multibeam H I-survey. An comnination of $I$, $J$ and $K$-band images covering partly the central field PF01 have retrieved galaxies 29, 30, 33, 32, 34, 37 and 40 (provided by Takahiro Nagayama & Shuji Sato from Nagoya University). Nagayama and Sato detected further 5 galaxies with the central field PF01 not visible in the images analyzed in this thesis. These galaxies are too faint to be uncovered in the $I$-band images reduced in this thesis. No counterparts were found for the uncertain galaxy candidates.

# Chapter 5

# Analysis of the Distribution of the Unveiled Galaxies

## 5.1 Introduction

The distribution of the unveiled galaxies shown in chapter 4 is presented and analyzed in this chapter. Also, the results of a simulation of how the well-known Coma cluster of galaxies would appear in the $I$-band if it were located at the redshift and position of PKS 1343−601 deep in the ZOA. The simulated distribution of the Coma galaxies is compared to the distribution of the unveiled galaxies.

## 5.2 The Distribution of the Unveiled Galaxies

The distribution in Galactic coordinates of the galaxy candidates uncovered in the $I$-band imaged region of about $2^\circ \times 2^\circ$ around the source PKS 1343−601 presented in Tables 4.1 and 4.3 of Chapter 4 is shown in Fig. 5.1. The filled circles in Fig. 5.1 correspond to galaxies classified as early type. Crossed circles represent galaxy candidates with a spiral morphology. The empty circles shown the uncertain galaxy candidates for which no morphology could be proposed since the nature of these objects is uncertain. It should be noted that these unveiled galaxies are observed through high extinction in the $I$-band. It is therefore very difficult to classify their morphology. The assigned morphological type is a suggestion only. The contours correspond to the extinction levels (from top to bottom) in $A_I = 2^{\rm m}$ (yellow) , $3^{\rm m}$, $4^{\rm m}$, $5^{\rm m}$, $6^{\rm m}$, $7.5^{\rm m}$, and $10^{\rm m}$ (dashed black) according to the DIRBE dust extinction maps (Schlegel et al. 1998). The outline of the observed field is also shown as a black squared outline.

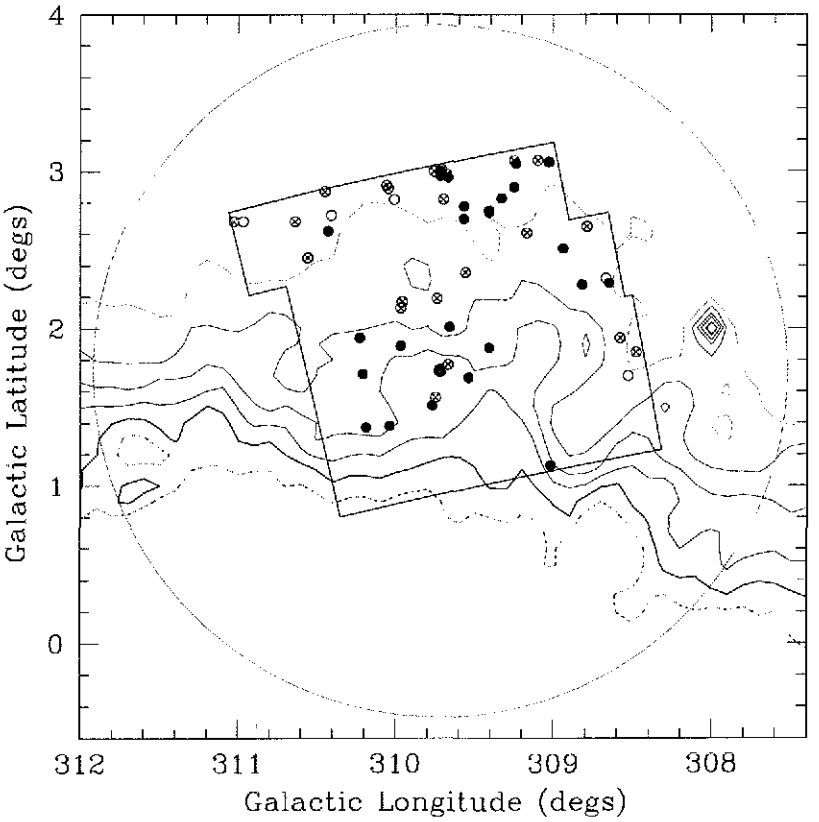


Figure 5.1: The distribution in Galactic coordinates of the galaxies unveiled in the vicinity of the strong southern radio source PKS 1343−601 (big red dot) and presented in Chapter 4. The large green circle marks the Abell radius ($R_A = 2.^\circ 2 = 3\,h_{50}^{-1}$ Mpc) assuming a rich cluster at the redshift distance of PKS 1343−601 (cz=3872 km s$^{-1}$, West & Tarenghi 1989). The squared outlined region (in black) indicates the area imaged with the WFI in the $I$-band (16 fields of $34' \times 33'$ each) around PKS 1343−601. The filled circles mark eliptical galaxies (25), the crossed circles represent spirals (24) and the open circles show the uncertain candidates (6). The contours are equivalent to the extinction levels in the $I$-band of $A_I = 2^{\rm m}$ (yellow), $3^{\rm m}$, $4^{\rm m}$, $5^{\rm m}$, $6^{\rm m}$, $7.5^{\rm m}$ (solid black line), y $10^{\rm m}$ (dashed black line) (Schlegel et al. 1998).

The big red dot marks the position of PKS 1343−601. The large green circle corresponds to the Abell radius for a rich cluster of galaxies which is $2.^\circ 2$ at the distance of PKS 1343−601.

It can be seen that ellipticals are found mainly at higher extinction levels while at lower extinction levels spirals predominate. The cores of ellipticals and bulges of

spirals contain mainly red old star population and are expected to be visible up to higher extinction levels. As expected, late-type spirals galaxies are not detected at extinction levels higher than $A_I = 6^{\rm m}$.

The distribution of galaxies is modulated by the strong extinction gradient in this region, see Fig. 5.1. Hence, a concentration of galaxies towards the radio galaxy PKS 1343−601 is not observed and this was expected, but this should be modelled in the next section.

## 5.3 Completeness of this Optical Search of Galaxies

In order to compare the distribution of galaxies presented in Fig 5.1 with the simulated distribution of the Coma cluster of galaxies located at the PKS 1343−601 position, it is important to have some idea about the magnitude limit to which galaxies were detected in this search. To assess the magnitude limit for this search, the characteristics of the chosen $I$-band filter have to be taken into account. The selected filter was a narrow $I$-band filter (n816) instead of the standard $I$ passband filter. The n816 filter has a FWHM[1] of only 20.9nm at a central wavelength of $\lambda_c = 815.9$nm.

With a 30 minutes exposure at the MPG-ESO 2.2-m telescope with the WFI camera, a surface brightness limit of $I_{n816} = 23.5$ mag arcsec$^{-2}$ with a signal-to-noise ratio of about 3 was expected (Observation proposal - P. A. Woudt). For the applied exposures times of 1,500 and 600 seconds, this relates to a surface brightness limit of:

$$SB_{I_{\rm n816}} = 23.4 \text{ mag arcsec}^{-2} \qquad \text{(for 1,500 sec)} \qquad (5.1)$$

$$SB_{I_{\rm n816}} = 22.9 \text{ mag arcsec}^{-2} \qquad \text{(for 600 sec)} \qquad (5.2)$$

Typically, objects (galaxies) that are 10% brighter than the sky can be detected. Hence, the surface brightness limit of a galaxy still visible on my images is of the order of:

$$SB_{I_{\rm n816}}(galaxy) = 21.1 \text{ mag arcsec}^{-2} \qquad \text{(for 1,500 sec)} \qquad (5.3)$$

$$SB_{I_{\rm n816}}(galaxy) = 20.6 \text{ mag arcsec}^{-2} \qquad \text{(for 600 sec)} \qquad (5.4)$$

[1]Full width at half maximum

The smallest galaxies detected in this survey have semi-major (D) and minor (d) diameters of $2\farcs5 \times 2\farcs5$, this translates to a magnitude limit of about:

$$I_{\rm n816}^{limit}(galaxy) = SB_{I_{\rm n816}}^{limit}(galaxy) - 2.5 log(\pi \times \frac{D''}{2} \times \frac{d''}{2}) = 19\fm3 \qquad (5.5)$$

Since the $I$-band magnitudes of the Coma galaxies calculated in the simulation correspond to the standard $I$-band filter, the above magnitude limit obtained with the special filter have to be converted to the standard $I$-band. I estimate that the $I_{n816}$ filter covers approximately a factor of 5 less under the transmission curve than the standard $I$-band filter ($I_{\rm std}$). The above limit (eq. 5.5) is equivalent to the $I_{\rm std}$ filter to a $\triangle$m $= 2.5log(5) = 1\fm75$ brighter magnitude limit. Hence, the magnitude limit of a standard $I$-band would be:

$$I_{\rm std}^{limit}(galaxy) \simeq 17\fm5 \qquad (5.6)$$

This is the magnitude limit applied to the plots made from the simulation and presented in this Chapter.

## 5.4 A Comparison with the Coma Cluster at the Position of PKS 1343−601

In order to know whether the observed distribution of galaxies in Fig 5.1 matches the expectation of a rich cluster of galaxies at high extinction, I made some simulations using the well-studied Coma cluster of galaxies as a reference. I simulated how a rich cluster would appear in the $I$-band at the distance and position of PKS 1343−601, and under the same extinction. For this I used the deep Coma galaxies catalogue of Godwin et al. (1983). This catalogue lists 6,724 galaxies in a field of 2.63 square degrees (6 $h_{50}^{-1}$ Mpc radius) to a magnitude limit of $b_{26.5} = 21$. The $b$-band defined in this catalogue is standarized to the international Johnson-Morgan $B$-band filter without color-dependent transformations (Godwin & Peach 1982). The simulation program and the program to calculate the $I$-band extinction ($A_I$) at each galaxy position are presented in the Appendix A.

From this catalogue, the X and Y positions of each of the 6,724 Coma galaxies relative to the cluster center and their magnitude in $b$ are used for the simulation. In this simulation the galaxies of Coma are put at the same redshift distance and position

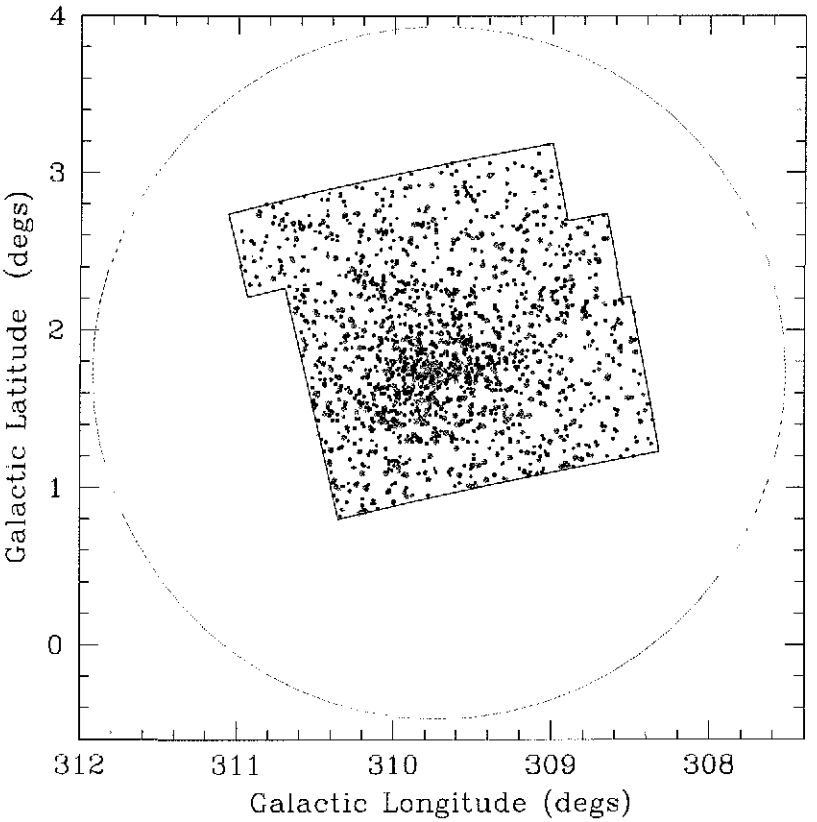




Figure 5.2: The distribution of 1979 galaxies of the Coma clusters put at the positon and distance of PKS 1343−601 without extinction.

of the radio galaxy PKS 1343−601, at $(l, b, v) = (309.^\circ7,\ 1.^\circ8,\ 3,872\ \mathrm{km\ s^{-1}})$ (West & Tarenghi 1989, Woudt 1998, Kraan-Korteweg & Woudt 1999). The velocity used for the Coma cluster centered on NGC 4874 is $v = 6,853\ \mathrm{km\ s^{-1}}$ (Colless & Dunn 1996). By setting the Coma galaxies at the PKS 1343−601 position and distance, their X and Y offsets increase by a factor of $v_{\mathrm{Coma}}/v_{\mathrm{PKS1343-601}} = 6853/3872 = 1.77$. Bringing the Coma cluster galaxies closer implies an increase in their brightness of $\Delta\mathrm{m} = 1.^{\mathrm{m}}24$.

Since the observations presented in this thesis are in the $I$-band, thus $I$-band magnitudes would be ideal for the galaxies of the Coma cluster. As these were not available, I therefore used the color terms $(B\text{-}I) = 2.^{\mathrm{m}}0$ for ellipticals and $(B\text{-}I) = 1.^{\mathrm{m}}5$ for spirals to transform the $b$ magnitudes of the Coma galaxies to $I$-band magnitudes (Buta & Williams 1995; Buta et al. 1994). Figure 5.2 shows the distribution of 1979 Coma galaxies without extinction that would fall within the $I$-band imaged

region around PKS 1343−601 at the distance and position of PKS 1343−601. This distribution plot contains galaxies with $I$-band magnitudes $\leq 17\overset{m}{.}5$, since this is the magnitude limit of my search. The largest (green) dots represent galaxies with $I$-band magnitudes between $17\overset{m}{.}0 < I \leq 17\overset{m}{.}5$. Medium size (cyan) dots show galaxies with I magnitudes in the range $16\overset{m}{.}0 < I \leq 17\overset{m}{.}0$. The small (blue) dot marks galaxies with magnitudes in the interval $15\overset{m}{.}0 < I \leq 16\overset{m}{.}0$, while the smallest (black) dots in Fig. 5.2 correspond to galaxies with $I \leq 15\overset{m}{.}0$. Galaxies with $I$-band magnitudes fainter than $17\overset{m}{.}5$ are not plotted in Fig. 5.2 because the magnitude limit of my search, see Section 5.3. Hence, they would not be visible in the $I$-band images presented here. A distinct concentration of galaxies towards the cluster center is seen in Fig. 5.2, but note that the extinction around PKS 1343−601 was not applied. The large green circle again marks the Abell radius (RA = 2°.2) for a rich cluster at the PKS 1343−601 distance.

For all 1979 galaxies shown in Fig. 5.2, an extinction value $A_I$ was determined using the DIRBE dust extinction maps (Schlegel et al. 1998) according to their Galactic coordinates, $\ell$ and $b$. The determined $I$-band magnitudes are then absorbed according to the laws of Cameron (1990). The magnitude reduction factors due to absorption are morphology-dependent. Since the Coma galaxy catalogue of Godwin et al. 1983 does not include morphological types, I assumed two extreme cases. First, it was asumed that all Coma galaxies are ellipticals or lenticulars. In the second case, I consider all Coma galaxies as spirals. Since a major fraction of the galaxies in the central region of a rich cluster are ellipticals, I expect to see mainly the cores of ellipticals and some bulges of spirals. Therefore, the case for assuming all galaxies as early type is more realistic.

After the $I$-band magnitudes of the 1979 Coma galaxies were artificially absorbed, 54 galaxies were left with magnitudes $I \leq 17\overset{m}{.}5$. The distribution of these remaining 54 Coma galaxies are displayed in Fig. 5.3. The sizes of the dots correpond to the magnitude ranges: $I \leq 15\overset{m}{.}0$, $15\overset{m}{.}0 < I \leq 16\overset{m}{.}0$, $16\overset{m}{.}0 < I \leq 17\overset{m}{.}0$, and $17\overset{m}{.}0 < I \leq 17\overset{m}{.}5$. The largest dots represent galaxies with magnitudes $17\overset{m}{.}0 < I \leq 17\overset{m}{.}5$ while the smallest dots correspond to galaxies with magnitudes $I \leq 15\overset{m}{.}0$. In Fig. 5.3, I plotted fainter galaxies up to $17\overset{m}{.}5$ because this is close the magnitude limit of my observations. I am not expecting to see fainter galaxies than $17\overset{m}{.}5$ in the $I$-band. The $I$-band magnitude for the faintest unveiled galaxy (galaxy 20) is $16\overset{m}{.}87$ (Anja Schröder, private communication). Based on the size and surface brightness of the galaxies identified in this thesis, I estimated the faintest galaxy to have a magnitude of the order of approximately $17\overset{m}{.}5$ uncorrected for extinction. In my simulation plots I therefore set the $I$-band magnitude limit to $17\overset{m}{.}5$. The radio galaxy PKS 1343−601

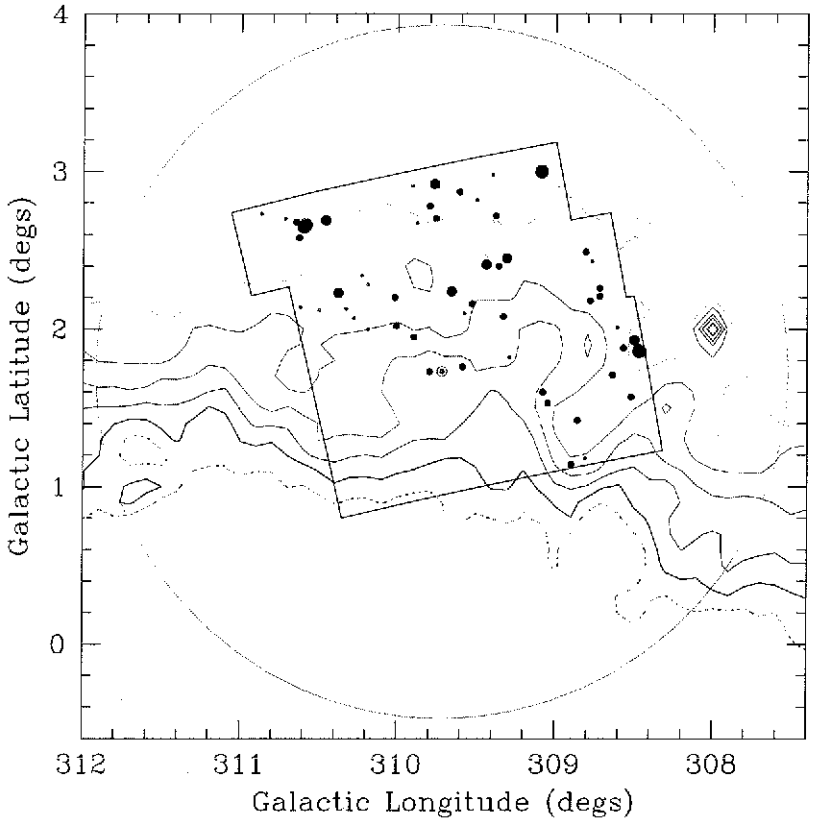




Figure 5.3: The distribution of the 54 galaxies of the Coma clusters that remain after $I$-band magnitudes were subjected to extinction. The contour levels in Fig. 5.3 are the same as those in Fig. 5.1.

is shown as a (red) circle with a central dot in these plots. The distribution of Coma galaxies shown in Fig. 5.3 is very similar to that shown in Fig. 5.1 for the unveiled galaxies presented in Chapter 4. The distribution in Fig. 5.3 is modulated by the extinction gradient as in the Fig. 5.1. As expected, at higher extinction levels fewer galaxies are seen.

In Fig 5.4, I furthermore present the distribution of the Coma galaxies assuming all galaxies to be spirals and with a magnitude limit $I = 17\overset{m}{.}5$. The dots are magnitude-coded and represent the same range of $I$-band magnitudes as in the previous figure. In Fig 5.4, it is observed that spirals are confined to lower extinction regions. Spirals are lost at higher extinction because of their low surface brightness and narrower surface brightness profile than early type ones. This distribution is consistent with the distribution of spirals shown in Fig 5.1. Few or no spirals are expected to be

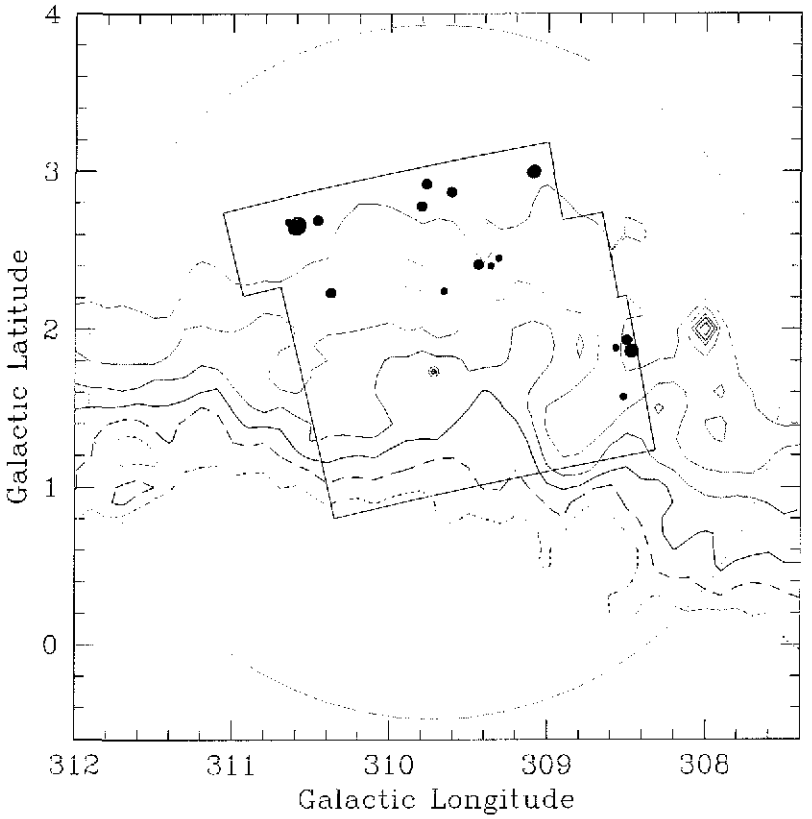


Figure 5.4: This plot resulsts if the Coma galaxies are considered as spirals. The distribution of the 17 galaxies of the Coma cluster that are left if extinction is included and with a magnitude limit $I = 17\overset{m}{.}5$.

found in regions of high extinction.

The simulation shows that the distribution of galaxies of the Coma cluster (Fig. 5.3) within the field of view and at the distance and position of PKS 1343−601 is comparable to the distribution presented in Fig. 5.1. Hence, the observed distribution of the unveiled galaxies around the radio galaxy PKS 1343−601 is consistent with the presence of a rich cluster of galaxies highly obscured in the $I$-band.

# Chapter 6

# Conclusions and Future Plans

The objective of this thesis has been the search of galaxies around the radio galaxy PKS 1343−601 to investigate if this object marks the center of another rich cluster of galaxies in the GA region. To accomplish this, a field of about $2^\circ \times 2^\circ$ around PKS 1343−601 was imaged in the $I$-band with the MPG-ESO 2.2-m telescope and the WFI camera at the La Silla Observatory. 128 $I$-band images of 1,500 and 600 sec exposures were obtained. My search was complete up to an $I$-band magnitude limit of $I_{\rm n816} = 19\overset{\rm m}{.}3$ in the narrow filter chosen for the observations which compares to $I_{\rm std} \simeq 17\overset{\rm m}{.}5$ of the standard $I$-band filter. On this images, 55 galaxy candidates were discovered through careful visual examination down to extinction levels of up to $A_I = 5\overset{\rm m}{.}5$ according to the DIRBE extinction dust maps. The distribution of these galaxy candidates was compared to the distribution of the well-known Coma cluster of galaxies as it would appear if centered at the position of the radio galaxy PKS 1343−601. If Coma would lie at distance and low Galactic latitude of PKS 1343−601 and would have been observed under same conditions as in our survey, only 54 of the 6724 galaxies of the Coma catalogue would remain visible. The distribution in Galactic coordinates of these 54 remaining Coma galaxies is similar to that of the 55 galaxy candidates actually found. In both distributions, ellipticals (and/or lenticulars) predominate at extinction levels of $A_I \geq 3\overset{\rm m}{.}8$ while spirals are more visible at $A_I \leq 3\overset{\rm m}{.}8$. The distribution of galaxies, in both distributions, is modulated by the extinction gradient in this region. Based on the above results, there is evidence that PKS 1343−601 marks the bottom of the gravitational potential well of a rich cluster of galaxies.

The distributions of galaxies behind the southern Milky Way around the radio galaxy PKS 1343−601 indicates the presence of a rich cluster in the central region

of the Great Attractor (GA). The existence of another rich cluster of galaxies similar to the Norma cluster in the inner region of the Great Attractor will help to explain the observed velocity flow in the local universe. Moreover, the existence of a second massive cluster at the core of the GA will support the existence of the GA overdensity and encourage us to continue searching for the rest of the GA mass hidden behind the southern Milky Way.

The above results were a motivation to continue the research of this prospective cluster of galaxies with deep near-infrared observations to unveil fainter galaxies that were not detectable in my search. The mapping of this cluster in the near-infrared is in progress using the the Japanese-South African Infrared Survey Facility (IRSF). This survey is conducted with a 1.4-m telescope with a simultaneous 3-channel imager camera in the infrared $J$, $H$ and $K$-band and it is in collaboration with T. Nagayama and S. Sato. A preliminary imaging of the central field of this cluster has confirmed all the detections of galaxies in this field presented in this thesis, *i.e.* the galaxies (29), (30), (32), (33), (34), (37) and (40). Nagayama and Sato have uncovered on additional five galaxies that were not detected in the present work because their survey is deeper. This new near-infrared data, still in progress, promise to unveil more cluster members to confirm the extent and richness of this obscured cluster.

$K$-band photometry of the prospective cluster members will be of particular interest because it is the least affected by extinction. The $K$-band luminosity function of the PKS 1343−601 cluster can then be compared with the $K$-band bright end of the luminosity function of the Coma cluster and lead to an estimation of its mass.

Most of these galaxies are invisible in the optical and too faint for optical spectroscopy. Observations in H I of the suspected optical cluster members would be more helpful to determine radial velocities and thus cluster membership. This will give us an indication of its virial mass from the velocity dispersion of the cluster members.

Finally, deep X-ray observations around PKS 1343−601 could determine if the X-ray emission from this area is due to thermal emission from the hot intercluster gas of this cluster and not to the inverse Compton effect, the scattering of the cosmic microwave background photons caused by relativistic electrons of the radio galaxy.

# Appendix A

# The $A_I$ and Simulation Programs

## A.1 The $A_I$ - Program

The program shown in the Fig. A.1 was used to calculate the $I$-band extinction ($A_I$) at the position of each galaxy candidate. The input data files for this program are gpcgd.dat and DIRBEpks.dat. The first one contains the positions in Galactic coordinates of the 49 galaxy candidates. The second one has three columns and was obtained from the DIRBE extinction dust maps (Schlegel et al 1998) where the first two columns contain the Galactic longitude and latitude $(\ell, b)$. The corresponding *color excess* $E(B-V)$ at this position is given in the third column. The table DIRBEpks.dat gives the extinction values for $307.^{\circ}0 \leq \ell \leq 313.^{\circ}0$ and $-1.^{\circ}0 \leq b \leq 5.^{\circ}0$ in increments of $0.^{\circ}1$ for both coordinates. First, $\ell$ goes from $\ell = 307.^{\circ}000$ to $\ell = 313.^{\circ}000$ by increments of $+0.^{\circ}1$ while $b$ is fixed starting at $b = -1.^{\circ}000$, and subsequentially increases to cover the latitude interval in increments of $0.^{\circ}1$.

The program determines the $I$-band extinction at the position of each galaxy candidate with the following loops. First, the program finds a Galactic latitude value $bh$ in the file DIRBEpks.dat for the Galactic latitude coordinate $b$ of a galaxy candidate position with $|b - bh| \leq 0.^{\circ}05$. Then, the program does the same calculation for the Galactic longitude coordinate $\ell$ so that $|\ell - \ell h| \leq 0.^{\circ}05$. The *color excess* $E(B-V)$ for the coordinates $(\ell h, bh)$ is assigned to the galaxy cadindate's position $(\ell, b)$. The $I$-band extinction for $(\ell, b)$ is obtained from the *color excess* according to $A_I$=$1.86E(B-V)$ (Cardelli et al. 1989). For example, galaxy candidate 2 has the coordinates $\ell = 308.^{\circ}58$ and $b = 1.^{\circ}94$. For these coordinates, the program finds $\ell h = 308.^{\circ}600$ and $bh = 1.^{\circ}900$ with $E(B-V) = 1.87$. The $I$-band extinction at the position of galaxy 2 is $A_I = 1.86 \times 1.^{m}87 = 3.^{m}5$. The same procedure was used to

*determine the I-band extinction at the positions of the uncertain galaxy candidates.*

```
c ------------------------------------------------------------------
c    Determination of A_I Values at Each Galaxy Candidate Position
c ------------------------------------------------------------------

      IMPLICIT DOUBLE PRECISION(A-Z)
      CHARACTER line*46

      OPEN(10,FILE='/cosa_3/thesis/mochoa/a_i/data/gpegd.dat',
     *          STATUS='old',ERR=9000)
      OPEN(11,FILE='/cosa_3/thesis/mochoa/a_i/data/DIRBEpks.dat',
     *          STATUS='old',ERR=9100)
      OPEN(12,FILE='ai.cat',STATUS='old',ERR=9200)

c --- Set Line Number Equal to Zero ------------------------------

      ln = 0

c --- Read Galactic Coordinates of Galaxy Candidates -------------

50    read(10,100,END=1000) line,l,b
100   format(A46,T30,F6.3,1x,F6.3)

c --- Reading Test -----------------------------------------------
c      print*, l,b

c --- Line Number ------------------------------------------------
      ln = ln + 1

c --- Determination of E(B-V) from DIRBE Data --------------------

      rewind 11
200   continue
      read (11,300,end=9400) lh,bh,EBV
300   format(2x,F7.3,2x,F6.3,5X,F8.3)
      difb=dabs(b-bh)
      if(difb.gt..051d0) go to 200
      difl=dabs(l-lh)
      if(difl.gt..051d0) go to 200

c --- Determination of A_B and A_I -------------------------------

350   continue
      AB=4.14d0*EBV
      AI=1.86d0*EBV

c --- Write on the Screen the Values: ln, l, b, E(B-V), A_B, A_I -----
c      PRINT*, ln,l,b,ebv,ab,ai

c --- Write data to file ai.dat ----------------------------------

      WRITE(12,500) ln,l,b,EBV,AB,AI
500   FORMAT(F5.0,2x,2(F8.3),2x,F8.3,2x,F6.2,2x,F6.2)

c --- Go to Get the Next Galaxy Candidate l & b Values -----------

      go to 50

1000   CONTINUE
       CLOSE (10,STATUS='KEEP')
       CLOSE (11,STATUS='KEEP')
       CLOSE (12,STATUS='KEEP')

c --- Stop the Program if it Works! ------------------------------
       STOP

9000   STOP 'ERROR IN READING gpegd.cat'
9100   STOP 'ERROR IN READING DIRBEpks.dat'
9200   STOP 'ERROR IN WRITING ai.cat'
9400   Print*, l,b
       STOP 'ERROR : no extinction value found in DIRBEpks.dat for
     *           the above l and b'
       END
```



Figure A.1: The program that calculates the $I$-band extinction ($A_I$) at the galaxy candidates' positions.

## A.2 The Simulation Program

The program shown in Fig A.2 was used to compare the Coma cluster of galaxies when located at the position of PKS 1343−601 with the actually obtained distribution presented in Fig. 5.1 of Chapter 5. The basis for this comparison is the catalogue of 6724 galaxies with $b_{26.5} < 21\overset{m}{.}0$ in a field of 2 63 squared degrees centered on the Coma cluster (Godwin et al. 1983) and the dust infrared emission maps of DIRBE (Schlegel et al. 1998). The program makes use of two data files. The file 'coma.dat', that has the data of the 6724 galaxies of the Coma cluster, contains the galaxy position (X and Y) relative to the center of the cluster ($\alpha$ =12$^h$ 57$\overset{m}{.}$3, $\delta$ = +28° 14′4 (1950.0)), the $b$-band magnitude, and other properties. The difference between the photographic ($b$) passband and the standard $B$-band does not exceed $\approx 0\overset{m}{.}05$ (Godwin et al. 1983). The second data file used by this program is the DIRBE extinction grid (DIRBEpks.dat) mentioned in Section A.1.

I basically used this same program (Fig A.2) with some modifications to produce the plots presented in the Chapter 5. In a first step, the effects for the difference in distance are determined. The positions and magnitudes are adjusted to the PKS 1343−601 distance at the location $\ell = 309\overset{\circ}{.}74$ and $b = 1\overset{\circ}{.}75$. Since the radio galaxy PKS 1343−601 is closer than the Coma cluster, the relative galaxy positions X and Y need to be increased by a factor of $v_{\rm Coma}/v_{\rm PKS1343-601} = 6853/3872 = 1.77$ and apparent magnitudes become brighter by $\Delta$m = $1\overset{m}{.}24$. Then, the $I$-band magnitudes are determined using distance corrected magnitudes and the color term $(B-I) = 2.0$ for ellipticals and lenticulars (Buta et al. 1994 & 1995) . The data for the plot in Fig. 5.3 were generated with this program taking all Coma galaxies as ellipticals and lenticulars. In the simulation all galaxies are treated as early type galaxies as they are the most likely ones because of their high surface brightness to be detectable through the foreground dust layer.

Thirdly, the $I$-band ($A_I$) extinction is determined for each Coma galaxy as it were centered on PKS 1343−601 with the relative position already enlarged by the factor 1.77. Then, the dimming due to the foreground absorption is determined according to Cameron (1990). Fourth, the extinction is applied to magnitudes using Cameron's formulae. Fifth, the Galactic coordinates are transformed to equatorial coordiantes to determine which galaxies fall within the field of view observed around PKS 1343−601. Finally, the positions and magnitudes corrected by distance and extinction of those galaxies than are within the field of view of the observations around PKS 1343−601 are recorded. These are the data used to make the plot presented in Fig. 5.3.

```
c ------------------------------------------------------------------------------
c   The Simulation Program (Elliptical Case)
c ------------------------------------------------------------------------------
      IMPLICIT DOUBLE PRECISION(A-Z)
      Integer id,gx,gy,nr,nb

      OPEN(10,FILE='/coma_3/thesis/mochoa/sim_coma/data/coma.dat',
     &     STATUS='OLD',ERR=9000)
      OPEN(11,FILE='/coma_3/thesis/mochoa/sim_coma/data/DIRBEpks.dat',
     &     STATUS='old',ERR=9100)
      OPEN(unit=12,FILE='ecoma.dat',STATUS='old',ERR=9200)

c ---- Number of entries for B-mag (nb) and R-mag nonzero (nr) ----------------
      nr=0
      nb=0
      bsum=0.D0
      rsum=0.D0

c ---- Read data from coma.dat, Coma data from Godwin et al. 1983 -------------
50    READ(10,100,END=1000) id,gx,gy,mB,dB,mR,dR,color
100   FORMAT(1x,I4,2x,I5,1x,I5,2x,F5.2,2x,F5.1,2x,F5.2,2x,F5.1,1x,F6.2)

c ---- Corrections for magnitude, positions and diameters due to distance ------
c     Distance in x and y positions centered at PKS 1343 position:
c       F=6853/3872=1.77 -> dm(magnitude)=1.24.
c     Transformation of the B and R magnitudes to the I-band magnitude:
c       The colorterms: B-I=2.0 and R-I=0.6 have been adopted for ellipticals
c       and Lenticulars
c     NOTE: mR is incomplete!!! Therefore, only mB is used to make the plots.
c     Notation:
c     li, bi = Galactic coordinates
c     mIB - I mag determined from the B-band
c     mIR - I mag determined from the R-band
c     dBc - Distance corrected diameter determined from B
c     dRc - Distance orrected diameter determined from R
c     PRINT*, gx,gy
      li=(1.77D0*gx/3600.D0) + 309.74D0
      bi=(1.77D0*gy/3600.D0) + 1.75D0
      mIB=mB-1.24D0-2.0D0
      mIR=0
      IF(mR.GE.0.D0) mIR=mR-1.24D0-0.6D0
      dBc=1.77*dB
      dRc=1.77*dR

c ---- Determination of E(B-V) from DIRBE data --------------------------------
      rewind 11
200   continue
      read(11,300,end=9400) lh,bh,EBV
300   format(1x,F7.3,2x,F6.3,4x,F9.6)
      difb=dabs(bi-bh)
        if(difb.gt..051d0) go to 200
      difl=dabs(li-lh)
        if(difl.gt..051d0) go to 200
350   continue

c ---- Print values so far calculated -----------------------------------------
c      print*, id,li,bi,difl,difb,EBV

c ---- Determination of I-band extinction (A_I) for l and b positions ----------
      AI=1.86d0*EBV
        IF (AI.GT.6.D0) AI=6.D0

c ---- Determination of reduction factors due to extinction (Cameron 1990) -----
c     NOTE: Only Ef and Edelta are used for the plots since the values
c           adopted for B-I and R-I are for ellipticals and lenticulars.
      Sf    = 10.D0**(.1D0*(AI**1.7D0))
      Sdelta= .07D0*(AI**2.5D0)
      Ef    = 10.D0**(.13D0*(AI**1.3D0))
      Edelta= .08D0*(AI**1.8D0)

c ---- Determination of diameters and magnitudes with extinction for ----------
c     for spirals and ellipticals (Cameron 1990).
c     NOTATION:
c     SdBc - Extinction applied diameter determined from B for spiral
c     SmIB - Extinction applied I mag. determined from the B-band for spiral
c     EdBc - Extinction applied diameter determined from B for elliptical
```

Figure A.2: The simulation program

```
c       EmIB -  Extinction applied I mag, determined from the B-band for ellipti
        SdBc = (dBc*Sf)
        SdRc = (dRc*Sf)
        EdBc = (dBc*Ef)
        EdRc = (dRc*Ef)

        SmIB = mIB + AI + Sdelta
        SmIR = 0.D0
          if (mIR.GT.0.D0) SmIR = mIR + AI + Sdelta
        EmIB = mIB + AI + Edelta
        EmIR = 0.D0
          if (mIR.GT.0.D0) EmIR = mIR + AI + Edelta

c ---- Determination of RA and Dec (for negative dec only) ------------------
        pi = 3.1415926536D0
        l = (pi/180.D0)*li
        b = (pi/180.D0)*bi
        c=(pi/180.D0)*62.6D0
        c1=DSIN(c)
        c2=DCOS(c)

c       Declination
        dec = DASIN(c1*DCOS(b)*Dsin(l-((pi/180.D0)*33.D0)) - c2*DSIN(b))
        ddec = DMOD((180.D0/pi)*dec,360.D0)

c       Right Ascension
        c3=(pi/180.D0)*(282.25D0)
        c4=(pi/180.D0)*(33.D0)
        c5 = ( DCOS(b)*DCOS(l-c4) ) / DCOS(dec)
        ra = DACOS(c5) + c3
        TEST = (C2*DCOS(b)*DSIN(l-C4) - C1*DSIN(b)) / DCOS(dec)
          if (TEST.LT.0.D0) ra = 2.D0*PI + 2.D0*C3 - ra
        dra = DMOD((180.D0/pi)*ra,360.D0)

c ---- To test if it lies in WFI fields and writting the outputs ------------
        if(dra.lt.207.98d0.and.dra.gt.203.89d0.and.
     &     ddec.lt.-58.87d0.and.ddec.gt.-59.37d0) go to 499
        if(dra.lt.207.50d0.and.dra.gt.203.38d0.and.
     &     ddec.lt.-59.37d0.and.ddec.gt.-59.92d0) go to 499
        if(dra.lt.207.52d0.and.dra.gt.203.25d0.and.
     &     ddec.lt.-59.92d0.and.ddec.gt.-60.92d0) go to 499
        go to 50

c ---- The output of this program (with extinction):
c       id - Coma galaxy number
c       li and bi galaxy Galactic coordinates
c       AI - Extinction in the I-band from DIRBE
c       EmIB, EmIR I-band mag. for ellipticals determined from B and R-band
c       EdBc, EdRc diameters for ellipticals determined from B and R-band
c       Simaliar notation for spiral -----------------------------------------
499     write(12,500) id,li,bi,AI,
     &                EmIB,EdBc,EmIR,EdRc
c      *                SmIB,SdBc,SmIR,SdRc
500     format(1x,I4,2x,F6.2,2x,F6.2,2x,F6.2,2x,F6.2,2x,
     &       2(F4.1,2x,F5.2,2x),2(F4.1,2x,F5.2,2x))

c ---- Go to get the next entry (galaxy) ------------------------------------
        go to 50

1000    CONTINUE
        print*, id,li,bi,AI,EmIB,EdBc,EmIR,EdRc,SmIB,SdBc,SmIR,SdRc
        CLOSE (UNIT=10,STATUS='KEEP')
        CLOSE (UNIT=11,STATUS='KEEP')
        CLOSE (UNIT=12,STATUS='KEEP')
c ---- End the program ------------------------------------------------------
        stop

c ---- If there are errors --------------------------------------------------
9000    STOP 'ERROR IN READING COMA.DAT'
9100    STOP 'ERROR IN READING DIRBE.dat'
9200    STOP 'ERROR IN WRITING COMA_SIM.dat'
9400    Print*, n,l,b
        STOP 'ERROR : no extinction value found in nlext.dat for
     &                the above l and b'
        END
```

Figure A.2: continued

# Bibliography


[1] Abell G.O. 1958, ApJSS, **3**, 211

[2] Abell G.O., Corwin H.G.Jr. & Olowin R.P. 1989, ApJSS, **70**, 1

[3] Andernach H. 1999, *Internet Services for Professional Astronomy*, in *Internet Resources for Professional Astronomy*, eds. M. Kidger, I. Pérez-Fournon & F. Sánchez, Cambridge University Press, 1−28

[4] Bertschinger E., & Dekel A. 1989, ApJ, **336**, L5

[5] Böhringer H., Neumann D.M., Schindler S. & Kraan-Korteweg R.C. 1996, ApJ, **467**, 168

[6] Burstein D., Faber S.M. & Dressler A. 1990, ApJ, **354**, 18

[7] Buta R. & Williams K.L. 1995, AJ, **109**, 543

[8] Buta R., Mitra S., De Vaucouleurs G. and Corwin H.G. Jr. 1994, AJ, **107**, 118

[9] Cameron L.M. 1990, A&A, **233**, 16

[10] Cardelli J. A., Clayton G.C. & Mathis J.S. 1989, ApJ, **345**, 245

[11] Colless M., & Dunn A.M. 1996, ApJ, **458**, 435

[12] Dekel A. 1994, ARA&A, **32**, 371

[13] Dekel A. 1995, in *Clustering in the Universe*. eds. S. Maurogordato, C. Balkowski, C. Tao & J. Trân Thanh Vân, XXXth Rencontres de Moriond, Series: Moriond Astrophysics Meetings, 89

[14] Dressler A. 1991, in *Large-Scale Structures and Peculiar Motions in the Universe*, eds. D.W. Latham and L.N. da Costa, ASP Conf. Ser. **15**, 19

[15] Dressler A. & Faber S.M. 1990a, ApJ, **354**, 13

[16] Dressler A. & Faber S.M. 1990b, ApJ, **354**, L45

[17] Drinkwater M.J., Barnes D.G. & Ellison S.L. 1995, PASA, **12**, 248

[18] Fairall A. 1998, *Large-Scale Structure in the Universe*, John Wiley & Sons Ltd, 73

[19] Godwin J.G., Metcalfe N. & Peach J.V. 1983, MNRAS, **202**, 113

[20] Godwin J.G. & Peach J.V. 1982, MNRAS, **200**, 733

[21] Griffith M.R. & Wright A.E. 1993, AJ, **105**, 1666

[22] Henning P.A., Staveley-Smith L., Ekers D.R., Green A.J., Haynes R. F., et al. 2000, AJ, **119**, 2686

[23] Henning P.A., Staveley-Smith L., Kraan-Korteweg R.C. & Sadler E.M. 1999, PASA **16**, 35

[24] Herschel J. 1847, *Results of astronomical observations made during the years 1834-1838 at the Cape of Good Hope*. London: Smith, Elder and Co.

[25] Herschel J. 1864, *Philosophical Transactions*

[26] Hubble E.P., 1936, *The Realm of the Nebulae*

[27] Hudson M.J., & Lynden-Bell, D. 1991, MNRAS, **252**, 219

[28] Joint *IRAS* Science Working Group 1988, *IRAS* Small Scale Structure Catalog, Version 2, Washington: US Government Printing Office, IRAS SSSC

[29] Joint *IRAS* Science Working Group 1988, *IRAS* Point Source Catalog, Version 2, Washington: US Government Printing Office, IRAS PSC

[30] Kolatt T., Dekel A. & Lahav O. 1995, MNRAS, **275**, 797

[31] Kogut A., Lineweaver C., Smoot G.F., et al. 1993, ApJ, **419**, 1

[32] Kraan-Korteweg R.C. 2000a, A&AS, **141**, 123

[33] Kraan-Korteweg R.C. 2000b, in *From the Sun to the Great Attractor, 1999 Guanajuato Lectures on Astrophysics*, Lecture Notes in Physics, eds. D. Page & J.G. Hirsch, **556**, 301

[34] Kraan-Korteweg R.C. & Lahav O. 2000, A&ARv **10**, 211

[35] Kraan-Korteweg R.C. & Woudt P.A. 1999, PASA, **16**, 53

[36] Kraan-Korteweg R.C., Woudt P.A., Cayatte V., Fairall A.P., Balkowski C. & Henning P.A. 1996, Nature, **379**, 519

[37] Lahav O. 1987, MNRAS, **225**, 213

[38] Lauberts A. 1982, *The ESO-Uppsala Survey of the ESO (B) Atlas*, (Garching: ESO)

[39] Lewis G. & Irwin M. 1996, Spectrum, Newsletters of the Royal Observatories, **12**, 22

[40] Lynden-Bell D., Faber S.M., Burstein D., Davies R.L., Dressler A., Terlevich R.J. & Wegner G. 1988, ApJ, **326**, 19

[41] McAdam W.B. 1991, PASA, **9**, 255

[42] Naim A. 1995, Ph.D. Thesis, Univ. of Cambridge

[43] Nilson P. 1973, *Uppsala General Catalog of Galaxies*, (Uppsala: University of Uppsala)

[44] Ohanian H. & Ruffini R., *Gravitation and Spacetime*, (W.W. Norton & Company), 529

[45] Otrupcek R.E. & Wright A.E. 1991, PASA, **9**, 170

[46] Padmanabhan T. 1993, *Structure Formation in the Universe*, (Cambridge University Press), 203 & 259

[47] Peacock J. A. 1999, *Cosmological Physics*, (Cambridge University Press), 501

[48] Proctor R. 1878, *The Universe of Stars*, (London: Longmans, Green & Co.), 41

[49] Rousseau J., Paturel G., Vauglin I., Schröder A., et al. 2000, A&A, **363**, 62

[50] Schlegel D.J., Finkbeiner D.P. & Davis M. 1998, ApJ, **500**, 525

[51] Shane C.D. & Wirtanen C.A. 1967, *Publ. Lick Obs.*, XXII, Pt I

[52] Shapley H. 1961, in Galaxies, Cambridge: Harvard University Press, 159

[53] Tashiro M., Kaneda H., Makishima K., et al. 1998, Ap.J., **499**, 713

[54] Verkhodanov O.V., Trushkin S.A., Andernach H. & Chernenkov V.N. 1997, The CATS Database, in *Astronomical Data Analysis Software and Systems VI*, eds. G. Hunt and H.E. Payne, ASP Conf. Ser. **125**, 322

[55] Vorontsov-Velyaminov B. & Archipova V. 1963-74, *Morphological Catalog of Galaxies*, Parts 2-5, (Moscow: Moscow University)

[56] West R.M. & Tarenghi M. 1989, A&A, **223**, 61

[57] Willick J.A., Courteau S., Faber S. M., Burstein D. & Dekel A. 1995, ApJ, **446**, 12

[58] Willick J.A., Courteau S., Faber S. M., Burstein D., Dekel A. & Kolatt T. 1996, ApJ, **457**, 460

[59] Willick J.A., Courteau S., Faber S. M., Burstein D., Dekel A. & Strauss M. A. 1997, ApJSS, **109**, 333

[60] Woudt P.A. & Kraan-Korteweg R.C. 2001, A&A, **380**, 441

[61] Woudt P.A., Kraan-Korteweg R. C. & Fairall A. P., et al. 2000a, in *Towards an Understanding of Large-Scale Structure*, eds. S. Courteau, M.A. Strauss & J.A. Willick, ASP Conf. Ser. **201**, 88

[62] Woudt P.A., Kraan-Korteweg R. C. & Fairall A. P., et al. 2000b, in *Mapping the Hidden Universe: The Universe Behind the Milky Way - The Universe in HI*, eds. R. C. Kraan-Korteweg, P. A. Henning & H. Andernach, ASP Conf. Ser. **218**, 203

[63] Woudt P.A. 1998, Ph.D. Thesis, Univ. of Cape Town

[64] Yamada T., Takata T., Djamaluddin T., et al. 1993, ApJSS, **89**, 57